



Long-Term Morphological Modelling of Tidal Inlet Systems:

Implementing Salt Marshes in ASMITA

Marloes Bonenkamp

Long-Term Morphological Modelling of Tidal Inlet Systems:

Implementing Salt Marshes in ASMITA

by

Marloes Bonenkamp

to obtain the degree

Master of Science

at Delft University of Technology (TU Delft)

to be defended publicly on June 12, 2023

<i>Student number</i>	4585631	
<i>Date</i>	June 12, 2023	
<i>Chair committee</i>	Prof. dr. ir. Z.B. Wang	Delft University of Technology & Deltares
<i>Thesis committee</i>	Dr. Y. Huisman	Delft University of Technology & Deltares
	Prof. dr. P.M.J. Herman	Delft University of Technology & Deltares
	Dr. J.T. Dijkstra	Deltares
	Drs. Q.J. Lodder	Delft University of Technology & Rijkswaterstaat
<i>Project duration</i>	September 2022 - June 2023	

Cover: Salt marsh on Schiermonnikoog, NL (Kers, 2012).

An electronic version of this thesis is available at <http://repository.tudelft.nl/>.



Acknowledgements

This report presents my thesis on implementing salt marshes in the long-term morphological model ASMITA. The research was conducted to obtain my master's degree in Hydraulic Engineering at Delft University of Technology. It is a collaboration between Delft University of Technology and Deltares.

First, I would like to express my gratitude to those who helped me shape this research. I was lucky enough to work with an outstanding graduation committee. Zheng Bing, thank you for trusting me to work on this topic, always being available for questions and providing valuable feedback and ideas. I am very grateful for the opportunity you gave me to present this work at the NCK days. Ymkje, thank you for your enthusiasm, trust and patience while answering my questions repeatedly. Your positivity and sharp remarks ensured I was able to enjoy the process and kept me on track at the same time. Peter, I really enjoyed our fruitful discussions in which I learned so much about the beautiful salt marshes. Thank you for being so engaged in this project. Jasper, thank you for your critical questions and for making sure I did not lose the bigger picture out of sight. Quirijn, thank you for the new insights you gave me for examining the model outcomes.

I would also like to thank Marinka van Puijenbroek, Han van Dobben and Alma de Groot for providing me with data and for answering my many questions. Thank you for your availability and involvement in this research.

Moreover, I am incredibly thankful for the inspiring and open working environment at Deltares. Thank you to everyone who helped me during this research with brainstorming sessions, feedback and genuine interest. I felt very welcome and really enjoyed learning from all your expertise. A special thanks goes to my fellow interns, the past months would not have been as enjoyable if it weren't for all of you. Koen, your presence from the beginning till the end enabled me to make the most of this period.

Last but definitely not least, I could not have achieved this without the endless support of my family and friends. Pap, Mam, Niek & Esther, thank you for always believing in me and for your unconditional support throughout my entire study. My roommates and personal cheerleaders, Lin, Car, Skip & Mau, thank you for being there during the highs and lows of this project. I am grateful for many more people who supported me during this thesis and made my years in Delft an unforgettable experience, thanks to all of you!

*Marloes Bonenkamp
Delft, June 2023*

Summary

A rise in the global mean temperature induced by climate change is expected to have a large impact on ecosystems in all regions of the world. One of the threats is accelerated sea level rise (SLR). This may induce the loss of intertidal areas in tidal inlet systems, which is alarming due to their crucial role in coastal protection and their ecological importance. The long-term morphological response of tidal inlet systems can be modelled using the reduced complexity model ASMITA (Aggregated Scale Morphological Interaction between Tidal inlets and the Adjacent coast). The ASMITA model simulates morphological development on an aggregated spatial and temporal scale by imposing a morphological equilibrium condition. As such the model is fast, allowing for multiple long-term simulations. The model is physics-based and the parameters can be related to field values.

Currently, salt marshes are not implemented in ASMITA. However, salt marshes could be of importance to the morphological development in tidal inlet systems. Moreover, it is relevant to assess the resilience of the ecologically important salt marshes by themselves. The aim of this research is to implement salt marshes in ASMITA to assess their influence on the rest of the tidal inlet system and to gain insight into the long-term morphological response of salt marshes to accelerated SLR.

Salt marsh development is governed by a number of horizontal and vertical processes. The marsh height increases by capturing mineral sediment and by the accumulation of plant biomass. Autocompaction and deep subsidence lead to a decrease in marsh height. The implementation of salt marshes in ASMITA relies solely on the input of mineral sediment, as the research areas in this study are located in the Dutch Wadden Sea where mineral sedimentation prevails. At the marsh edge, generally, a cyclic behaviour of sedimentation and cliff erosion occurs. Due to the high degree of spatial aggregation, cliff erosion is excluded from the model extension. The governing processes for salt marsh development in the ASMITA model extension are mineral sedimentation, sediment availability and relative sea level rise (rSLR), which includes deep subsidence and SLR.

The spatial and temporal aggregation of governing processes for salt marsh development are included in the aggregated advection-diffusion equation and model parameters for the horizontal & vertical exchange of sediment, and sediment availability. Data analysis on hydrodynamic conditions and salt marsh development was conducted for the derivation and calibration of these model parameters. To verify the salt marsh implementation, three ASMITA models were created. A one-element salt marsh model consisting of only a salt marsh element, and two different multiple elements models, which contain all tidal inlet system elements: the ebb-tidal delta, channels, tidal flats and salt marshes.

The modelled salt marsh sedimentation rates are calibrated against field data, which means that a hindcast can be realized by varying the model parameters within the physically plausible range. The impact of salt marshes on the other tidal inlet system components largely depends on the size of the salt marsh. In cases where the salt marsh size is an order of magnitude smaller than the other tidal inlet components, the impact is limited to slightly affecting the sand-mud distribution on the tidal flats. For a larger salt marsh element, the evolution of the remaining elements is affected by the prevailing model assumption that assigns dominance to the sediment demand of the salt marsh over that of the rest of the tidal inlet system. Moreover, the sand-mud distribution in both the channel and tidal flat element is altered.

It can be concluded that ASMITA is capable of modelling the mineral sedimentation on a salt marsh but depicts a large sensitivity to the parameter setting, particularly for the sediment concentration. Based on the chosen parameter configuration, the Oosterkwelder salt marsh is preserved when subjected to SLR rates below 16 mm/year. Organic processes, autocompaction and cliff erosion are excluded from the model formulations due to their smaller contribution to salt marsh development compared to mineral sedimentation.

The ASMITA salt marsh extension can be employed to obtain an expeditious first impression of long-term morphological salt marsh development. However, due to the lack of incorporation of detailed processes, the model should not be employed for in-depth analyses of salt marsh development. The interaction between the salt marsh element and the remaining tidal inlet system components requires further model improvements.

Table of Contents

Acknowledgements	i
Summary	ii
Abbreviations	vi
Symbols	vii
1 Introduction	1
1.1 Background	1
1.2 Problem Description	1
1.3 Research Objective	2
1.4 Research Methodology	2
1.5 Thesis Outline	2
2 Dynamics of Tidal Inlet Systems and Salt Marshes	4
2.1 Tidal Inlet System Components	4
2.2 Hydrodynamics	5
2.3 An Introduction to Salt Marshes	6
2.4 Sediment Dynamics	7
2.5 Vegetation Establishment	10
2.6 Autocompaction and Subsidence	11
2.7 Effect of Accelerated SLR	11
2.8 Salt Marsh Extent in Literature	12
2.9 Salt Marsh Accretion Rates	15
3 Long-Term Morphological Modelling in ASMITA	18
3.1 Relevance of Reduced Complexity Modelling	18
3.2 Physics	19
3.3 Aggregation	20
3.4 Element Definitions	22
3.5 Morphological Equilibrium & Computational Procedure	23
3.6 Parameter Setting	25
3.7 Multiple Elements Schematisation	27
4 Study Areas	29
4.1 Requirements	29
4.2 The Dutch Wadden Sea	29
4.3 Salt Marshes on Ameland	30
4.3.1 Neerlandsreid	30
4.3.2 De Hon	32
4.4 Salt Marshes on Schiermonnikoog	33
4.4.1 Het Rif	33
4.4.2 Oosterkwelder	33
5 Data Analysis	34
5.1 Hydrodynamic Data Analysis	34
5.2 Vegetation Zonation	36
5.3 Salt Marsh Extent	37
5.4 Subsidence	38
5.5 Historical Salt Marsh Development	39
5.5.1 Digital Terrain Models	39
5.5.2 Local Measurements: SEBs	44

5.5.3	Comparison between Digital Terrain Models and Local Measurements	55
5.5.4	Salt Marsh Hypsometry Correction	59
6	Extending ASMITA	60
6.1	Governing Processes for Salt Marsh Implementation	60
6.2	Computational Procedure Salt Marsh Element	61
6.3	One-Element Salt Marsh Model	61
6.4	Derivation of Horizontal Exchange Coefficient δ	65
6.5	Derivation of Vertical Exchange Coefficient w_s	66
6.6	Derivation of Global Equilibrium Concentration c_E	67
6.7	Four Elements Model: Implementation of Salt Marshes	68
6.8	Initial Parameter Setting	69
7	Results	70
7.1	One-Element Model: Zero SLR	70
7.2	One-Element Model: SLR	74
7.3	Sensitivity Analysis	78
7.4	Four Elements Model: Zero SLR	81
7.5	Three + One Elements Model	84
7.6	Salt Marsh Development for Different Rates of SLR	87
7.6.1	One-Element Model	87
7.6.2	3 + 1 Elements Model	87
7.7	3 + 1 Model: Sand-Mud Distribution	89
8	Discussion	91
8.1	Salt Marsh Implementation in ASMITA	91
8.2	ASMITA Model Results	94
8.3	Implications for Management Strategies	98
9	Conclusions & Recommendations	99
9.1	Conclusions	99
9.2	Recommendations	102
	References	104
A	AHN Hypsometric Curves without Correction for rSLR	109
B	AHN Sampled at Locations of SEBs	111
C	One-Element Results for Remaining Salt Marshes	114
D	Four Elements Model: SLR	116
E	3 + 1 Model: Element Volumes for SLR	118

Abbreviations

Abbreviation	Definition
0D	Zero-Dimensional
1D	One-Dimensional
2D	Two-Dimensional
3D	Three-Dimensional
AHN	Actueel Hoogtebestand Nederland
ASMITA	Aggregated Scale Morphological Interaction between Tidal Inlets and the Adjacent coast
DSM	Digital Surface Model
DTM	Digital Terrain Model
LiDAR	Laser image Detection And Ranging
MHW	Mean High Water
MHWS	Mean High Water Spring
MLW	Mean Low Water
NAP	Normaal Amsterdams Peil
rSLR	relative Sea Level Rise
SEB	Sedimentation Erosion Bar
SLR	Sea Level Rise
SSC	Suspended Sediment Concentration

Symbols

Symbol	Definition	Unit
A	area	[L ²]
α	vertical shape coefficient	[-]
β	proportionality constant	[-]
c_E	global equilibrium concentration	[-]
c_e	local equilibrium concentration	[-]
c	actual sediment concentration	[-]
D	dispersion coefficient	[L ² T ⁻¹]
δ	horizontal exchange coefficient	[m ³ /s]
ϵ	turbulent diffusion coefficient	[L ² T ⁻¹]
f_{area}	salt marsh area magnification factor	[-]
f_b	sediment flux between water column & bed	[LT ⁻¹]
h	water depth <i>or</i> tidal range <i>or</i> marsh height	[L]
n	porosity	[-]
P	tidal prism	[m ³]
ρ	density	[kg/m ³]
s	suspended sediment transport rate	[L ² T ⁻¹]
t	time	[T]
u, v	horizontal flow velocity components	[LT ⁻¹]
$V_{channel}$	wet volume channel	[m ³]
V_{delta}	sediment volume ebb-tidal delta	[m ³]
V_{flat}	sediment volume tidal flat	[m ³]
V_{marsh}	sediment volume marsh	[m ³]
w_s	vertical exchange coefficient	[m/s]
x, y	horizontal coordinates	[L]
z	vertical coordinate	[L]

Introduction

1.1 Background

A rise in the global mean temperature induced by climate change is expected to have a large effect on ecosystems in all regions of the world (Warren et al., 2011). One of the threats is the predicted accelerated sea level rise (SLR) (IPCC, 2023), which may cause a partial loss of intertidal areas. This is alarming, as intertidal areas serve not only as important coastal protection from storm impact and erosion for residential areas but also accommodate ecologically important tidal flats and salt marshes (FitzGerald et al., 2008). The survival of tidal flats and salt marshes essentially depends on the balance between sediment accumulation and SLR (Temmerman et al., 2004). Tidal flats and salt marshes may become fully inundated if their ability to keep up with SLR is insufficient (Elschot, 2015). A higher sea level implies more accommodation space for sediment, causing an increase in sediment demand (Beets & van der Spek, 2000). However, a study by Huismans et al. (2022) found that it takes time for the sediment import rates in a tidal inlet system to increase. Consequently, the intertidal area cannot directly adjust to the rising sea level and severe losses could occur, depending on the rate of SLR. This has significant ecological consequences. Intertidal flats and in particular salt marshes provide a home to numerous animals including birds, rabbits, hares, geese, many invertebrates and (micro)benthos. Salt marshes also contain a large variety of plant species (Bakker, 2014; Olf et al., 1997). Due to a large amount of vegetation, salt marshes act as an important coastal protection against waves and storm surge to prevent coastal erosion (Barbier et al., 2011; Reed et al., 2018). Additionally, salt marshes play a significant role in carbon sequestering (McLeod et al., 2011).

Several researchers discovered that some salt marshes are more prone to drowning as a result of accelerated SLR than others, depending on the marsh accretion rates (Elschot, 2015; Bakker et al., 1993; Van Wijnen and Bakker, 2001; Temmerman et al., 2004). The interaction between the different components within a coastal ecosystem determines the extent of marsh accretion and thus the vulnerability of a salt marsh. Next to the salt marshes important components in a tidal inlet system, such as the Dutch Wadden Sea, are the ebb-tidal delta, tidal channels and the earlier-mentioned tidal flats.

It is possible to simulate the interaction between these different components and thus the morphological system development using the reduced complexity model ASMITA: Aggregated Scale Morphological Interaction between Tidal Inlets and the Adjacent coast (Stive et al., 1998; Stive and Wang, 2003; Townend et al., 2016a, 2016b). The ASMITA model simulates morphological development on an aggregated spatial and temporal scale by imposing a morphological equilibrium condition. As such the model is fast, allowing for multiple long-term simulations. The model still represents real-world processes and the model parameters can be related to field values (Wang et al., 2008).

1.2 Problem Description

Currently, salt marshes are not implemented in ASMITA. However, it was found that salt marshes may be of importance to the morphological development in tidal inlet systems and estuaries (Wang & Lodder, 2019). This could be especially true when considering accelerated SLR, as salt marshes will be inundated more frequently and are thus expected to have more sediment exchange with the other system components. Moreover, it is relevant to assess the resilience of the ecologically important salt marshes by itself. Previous research states that a 20 - 50% loss of salt marshes could occur in the next century (Kirwan et al., 2016). Therefore, this thesis will focus on implementing salt marshes in ASMITA to assess their influence on the rest of the tidal inlet system and to gain insight into the long-term morphological response of salt marshes to accelerated SLR.

1.3 Research Objective

The aim of this research is to implement salt marshes in ASMITA for assessing how salt marshes influence the tidal inlet system and to gain insight into the long-term morphological response of salt marshes to accelerated SLR. The challenge with respect to implementing salt marshes is mainly found in translating the physical development of salt marshes into aggregated model parameters. As described by Wang et al. (2008), the aggregated model parameters that are currently present in ASMITA can be related to measurable physical quantities. The same must hold for the salt marshes. Therefore, it is important to have a thorough understanding of the physical processes that govern salt marsh development. Subsequently, the translation from physical processes into aggregated model parameters should be made. The research goals are captured in the research questions below. The final objective of this thesis is to simulate the morphological development and behaviour of a tidal inlet system where salt marshes interact with other tidal inlet system components.

The main research question is:

How can long-term salt marsh development be modelled on a temporally and spatially aggregated scale?

The sub-questions are:

1. What are the governing processes for salt marsh development?
2. How can these processes be captured in a temporally and spatially aggregated way to implement them in the ASMITA model?
3. To what extent can salt marsh development be modelled by ASMITA?
4. How do salt marshes interact with the other components of a tidal inlet system?
5. How do salt marshes respond to accelerated SLR?

1.4 Research Methodology

The research methodology is shown in Figure 1.1. These four stages are conducted sequentially in order to find answers to the research questions that were posed.

1.5 Thesis Outline

The outline of this thesis follows the same four-stage structure as that of the research methodology.

A literature review on the system dynamics of tidal inlets and salt marshes is conducted in Chapter 2. Accordingly, the governing processes of salt marsh development can be identified. Chapter 3 elaborates on the long-term morphological ASMITA model. The existing formulations, concepts and elements are discussed to gain insight into the aggregated modelling approach and the derivation of model parameters.

For the data analysis that is performed, the study areas are introduced in Chapter 4. Hereafter, the data analysis on hydrodynamics, vegetation, subsidence and accretion is elaborated on in Chapter 5.

The ASMITA model extension for salt marshes is explained in Chapter 6. The governing processes are captured in formulations and in the derived model parameters.

Chapter 7 depicts the results of different model simulations. Three different models were created to verify the salt marsh implementation. Scenarios with and without SLR are assessed, and the interaction between salt marshes with the other tidal inlet system components is studied.

Hereafter, a discussion on the research is given in Chapter 8. Finally, conclusions are presented by answering the research questions in Chapter 9, along with recommendations for further research.

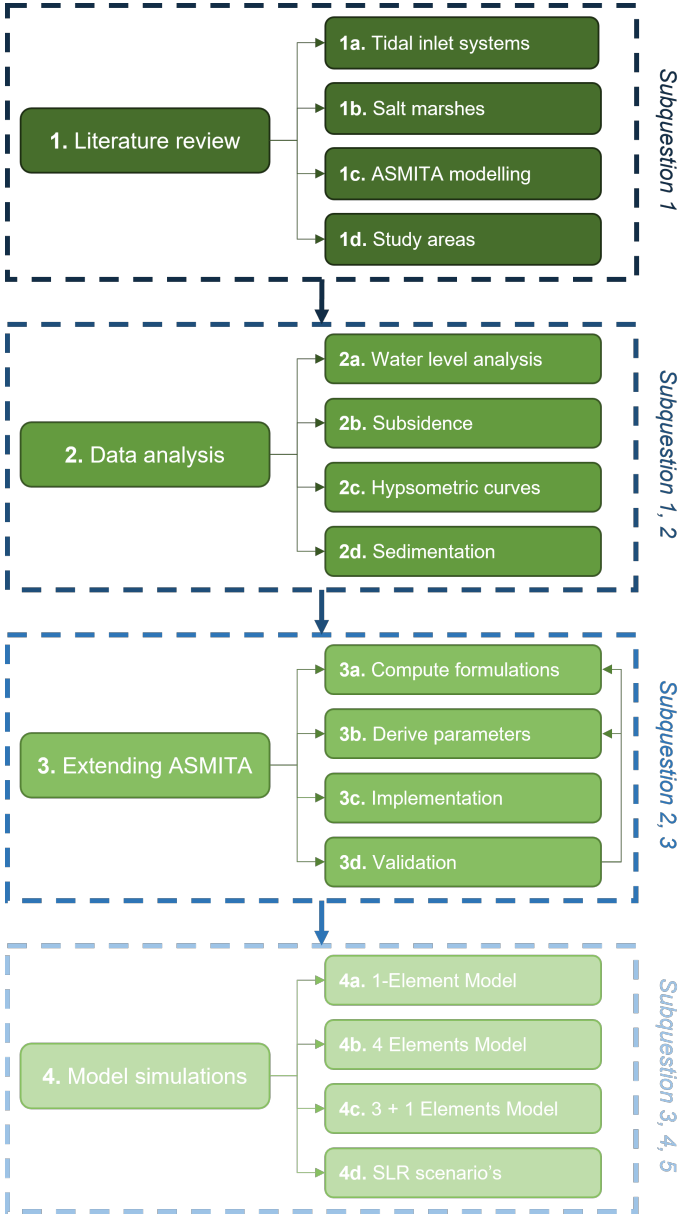


Figure 1.1: Flowchart of the methodology for this thesis.

Dynamics of Tidal Inlet Systems and Salt Marshes

This chapter introduces the components of a tidal inlet system in section 2.1. The hydrodynamics are elaborated upon in section 2.2, after which the salt marsh is explained more extensively in section 2.3. More information on sediment dynamics, organic processes and autocompaction is given in respectively section 2.4 up to and including 2.6. The expected effect of accelerated SLR on tidal inlet systems is presented in section 2.7. The numerous definitions of a salt marsh in literature are discussed in section 2.8. Finally, section 2.9 elaborates on characteristic salt marsh accretion rates.

2.1 Tidal Inlet System Components

The development of tidal inlets started during the Holocene. After the last glacial period, a significant global SLR rate led to an increase of marine influences. As a result, breakthroughs and floods of low-lying inland zones occurred and they were covered by marine sediments. Freshwater marshes were transformed into tidal salt marshes and mudflats (Bakker, 2014). Additionally, tectonic subsidence, fluvial erosion, glacial action and bottom subsidence due to human interference led to a reinforcement of the tidal inlet development (Bosboom & Stive, 2021).

For this research, one type of tidal inlet is considered: the tidal lagoon. This type of tidal inlet is characterized by the presence of coastal barrier islands. The tidal inlet experiences water inflow through the inlets during flood and outflow during ebb. A tidal inlet consists of three main components: the ebb-tidal delta, tidal channels and intertidal zone, see Figure 2.1. The intertidal zone is the area that is alternately wet and dry. It consists of intertidal flats, or mudflats, and supra tidal flats, or salt marshes. The intertidal flats will be abbreviated to tidal flats from now on. The supra tidal flats are referred to as salt marshes. Tidal flats are frequently inundated: they fall dry and wet twice a day in a semi-diurnal tidal environment. Salt marshes remain dry for most of the time: they are only inundated during extremely high water.



Figure 2.1: System components of a tidal inlet, where the ebb-tidal delta is displayed in yellow, the channels in blue, the tidal flats in brown and the salt marshes in green.

The different system components in a tidal inlet form a sediment-sharing system in which a continuous exchange of sediment between the elements takes place. Each element, except for the salt marsh, strives to maintain a dynamic equilibrium between the forcing conditions and its own morphology. This means that a small distortion in a tidal inlet affects the entire equilibrium state: the elements will start to exchange sediment until equilibrium is restored. An individual element may reach its equilibrium state in a time scale ranging from years to centuries, whereas an entire system may never find its equilibrium. When morphological equilibrium is reached and the net sediment volume change is small, there will still be a continuous sediment exchange due to sorting effects (Wang et al., 2018).

The forcing mechanisms of water and sediment movement in a tidal inlet are tides, waves, wind and density effects (Van Weerdenburg et al., 2021). The net residual sediment transport in a tidal inlet is governed by flow-driven processes (tide, wind, freshwater input) and short waves. For a large freshwater input, the amount of water flowing into the basin during flood is smaller than the amount of water flowing out during ebb. When a limited freshwater input is present, there is only a relatively small net difference between two large gross flood and ebb transport components. In case of the latter, various barotropic and baroclinic mechanisms cause the net residual transport. A detailed description of these processes is given by Wang et al. (2018).

The morphological development by sedimentation of a tidal inlet can be limited by different causes: accommodation space, sediment supply or transport capacity (Wang et al., 2018). In the first case of an accommodation-limited tidal inlet, there is insufficient space for the sediment to be deposited. The accommodation space of a tidal inlet can increase as a result of SLR or subsidence. Similarly, the deposition of sediment leads to a reduction of accommodation space. Another limitation to morphological development can occur when insufficient sediment is available. If the tidal inlet has a larger demand for sediment than the amount that is supplied, the morphological development will be limited. Lastly, it could happen that the available sediment volume in the tidal inlet is sufficient, but the sediment transport capacity of the tidal inlet is too small. As a consequence, the morphological development of the tidal inlet would not be able to reach its full potential.

2.2 Hydrodynamics

The hydrodynamics in a tidal inlet are crucial for its morphological development. At the same time, the basin morphology has an influence on the hydrodynamics. In essence, it can be said that this is a positive feedback loop: the tidal inlet partly determines its own morphological evolution by adjusting the hydrodynamics.

Tidal inlets are generally tide-dominated, which means that a large difference between high and low tide exists. This difference between high water and low water during a tidal cycle is called the tidal range. Due to a large tidal range, strong currents arise during a tidal cycle. As a result, the influence of waves is small compared to the influence of the tide. Therefore, it can be said that relatively low-energy conditions are characteristic of tidal inlet systems. However, depending on local conditions such as the wind climate, tidal inlets could qualify as mixed-energy wave-dominated. The Dutch Wadden Sea is an example of a tidal inlet system of this kind, even under spring-tide conditions (Wang et al., 2018).

The tidal range is an important hydrodynamic forcing parameter for the morphological development of tidal inlets and salt marshes. The tidal range can vary significantly from day-to-day. This has to do with the forcing components of the tide. The tide consists of an astronomical and a meteorological component, both of which affect the magnitude of the tidal range. The astronomical tide is generated by gravitational forces between the Earth, Moon and Sun. The astronomical tide is locally disturbed by meteorological effects. These meteorological effects concern variations in water levels caused by the wind. The magnitude of the local wind set-up (or set-down) depends on the wind force, direction and duration. The largest wind set-up is found in extreme weather conditions, such as storm surges. The actual tide is a combination of the astronomical tide and meteorological effects (Allen, 2000b).



Figure 2.2: Schematisation of the tidal prism, which is the water volume between Mean Low Water (MLW) and Mean High Water (MHW) that flows in and out of the tidal inlet during each tidal cycle.

The tidal range in combination with the geometry of the tidal basin determines its tidal prism, which is defined as the amount of water that flows in and out of a tidal inlet during one tidal cycle. This volume depends on the tidal range, i.e. the difference between high and low tide, and the tidal inlet area. A schematisation is shown in Figure 2.2. The morphological equilibrium of tidal inlet components is strongly related to the tidal prism (Buijsman, 1997). For a larger tidal prism, flow velocities are generally higher which suggests that channels deepen through erosion. The ebb-tidal delta and tidal flats also decrease in volume. The flow velocities are lower for a smaller tidal prism, which means that sedimentation occurs. Channels become less deep and the tidal flats increase in height.

The morphological equilibrium relation between the ebb-tidal delta volume V_{de} and the tidal prism P was derived by Walton Jr and Adams (1976) and is shown in Equation 2.1. Similarly, the relation for the channels is shown in Equation 2.2 and was derived by Eysink (1990). For the tidal flats, the morphological equilibrium depends on the tidal range h_{fe} in combination with the tidal inlet area A_{fe} , the relation was derived by Renger and Partensky (1974) and Eysink and Biegel (1992). It is shown in Equation 2.3.

$$V_{de} = \alpha_d P^{1.23} \quad (2.1)$$

$$V_{ce} = \alpha_c P^{1.55} \quad (2.2)$$

$$V_{fe} = A_{fe} h_{fe} \quad (2.3)$$

where:

V	equilibrium volume	[m ³]
α	empirical coefficient	[-]
P	tidal prism	[m ³]
A	tidal inlet system area	[m ²]
h	tidal range	[m]

2.3 An Introduction to Salt Marshes

Salt marshes are coastal wetlands in the upper intertidal zone, meaning that they are located between coastal hinterlands and daily flooded coastal areas, the tidal flats. Salt marshes mostly exist in moderate climate zones on mid-latitude coasts (Bartholdy, 2012). Along with the development of tidal inlets, salt marshes started to evolve during the Holocene. Salt marshes consist of vegetated platforms and creeks for drainage, which is clearly visible in Figure 2.3. They are able to develop near the edges of shallow seas that have a considerable tidal range and consist of soft sediment seabeds (Bakker, 2014). The emerged salt marshes can grow rapidly and mature within several hundred years. However, it should be noted that even mature salt marshes are continuously changing: they are in dynamic equilibrium.

Salt marsh development is initiated in the pioneer zone, which is situated just below Mean High Water (MHW). The pioneer zone is flooded for a couple of hours per tidal cycle. The salt marsh itself is typically situated above MHW and contains different zones: the lower, middle and high salt marsh. All of these zones are only flooded during extremely high water, i.e. any water level above MHW is necessary for inundation to occur. This means that the salt marsh is dry most of the time, which enables vegetation to develop relatively easily.

The morphological evolution of a salt marsh depends on a short-term dynamic balance between the inundation frequency, inundation depth, inundation duration, sediment supply, autocompaction and relative sea level rise (rSLR), which includes SLR and deep subsidence, (Friedrichs and Perry, 2001; Van Dobben et al., 2022). The morphological development can be expressed in two terms: vertical changes in height and horizontal extension or regression. Accretion is defined as the sum of sedimentation, erosion and (auto)compaction of the soil (Van Dobben et al., 2022). The evolution of both the vertical and horizontal terms depends on intrinsic and external influences or a combination of both. The halophytic,



Figure 2.3: Salt marsh in the Wadden Sea (Swart, 2014).

i.e. salt-tolerant, vegetation on a marsh (or plant biomass) and (auto)compaction are intrinsic factors. The main external influences that govern the morphological development of salt marshes are sediment supply, rSLR and the combination of tidal & storm regimes (Allen, 2000b).

According to Temmerman et al. (2004), the development of salt marshes is highly dependent on the age of the marsh, the rise of MHW and variations in suspended sediment concentrations (SSCs). In general, the low marsh experiences quick asymptotic growth to an equilibrium level. For the high marsh, a slow accumulation rate comparable to local MHW rise is observed provided that the incoming SSC is sufficient.

Salt marshes exist at locations where the tidal range can vary from a few centimeters to 16 meters (Coleman et al., 2022). The pioneer zone is the only part of a marsh that experiences inundation during a generic tidal cycle. For the lower, middle and high parts of a salt marsh, extreme water levels are important (section 2.3). A considerable spring tidal range ensures the occasional flooding of the salt marsh. The effect on the morphological development of salt marshes is largest for conditions with low atmospheric pressure and strong winds, as this combination leads to positive storm surges. When these conditions coincide with high water spring tide, salt marshes experience severe inundation (Allen, 2000b). The time during which tidal inundation takes place is called the hydroperiod. When the hydroperiod is sufficient, either vertical erosion or deposition takes place (Bakker, 2014).

Besides the hydrodynamic components that affect the tidal inlet components, the groundwater table could have an impact on the salt marsh morphology. The groundwater table has an influence on the salt marsh vegetation, which in turn affects the morphological development. However, the precise effect of the groundwater table on morphological salt marsh development is unknown (Elschot et al., 2017). Therefore, it will not be considered in this research.

2.4 Sediment Dynamics

As discussed in section 2.3, the vertical change in salt marsh height depends on different processes. Accretion includes an increase in height by sedimentation and accumulation due to plant biomass and a decrease in height by autocompaction. This is schematised in Figure 2.4.

The structure of a salt marsh differs depending on the dominant contribution to accretion. Macrotidal salt marshes are mainly dependent on the deposition of mineral sediment (Temmerman et al., 2004). These are also called mineralogenic marshes and consist of allochthonous, i.e. imported into the system, mineral material. Macrotidal salt marshes have extensive networks of drainage creeks and can be found in and around the Mediterranean and northern Europe, for example in the Wadden Sea. The dominance of mineral input generally indicates that the salt marshes are saline to hypersaline (Pont et al., 2002).

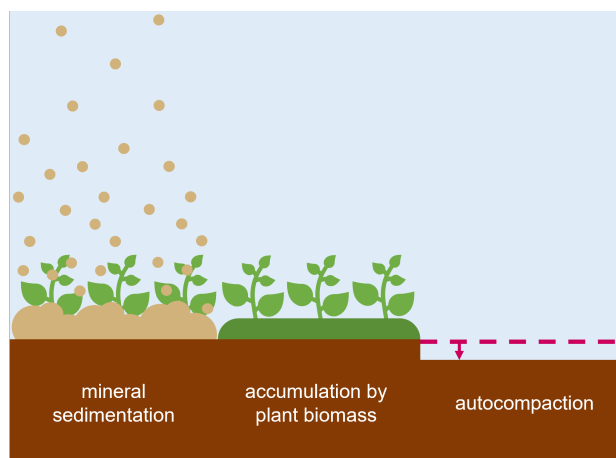


Figure 2.4: Different contributions to salt marsh accretion.

Salt marshes that have a lower soil salinity are usually dominated by accretion due to the in-situ production of organic matter and autocompaction. These are called organogenic marshes and mainly consist of peat (Temmerman et al., 2004). Deposition of organic matter due to root growth and litter deposition is the main contributor to salt marsh development in areas with limited sediment supply and a considerable amount of plant biomass (Mudd et al., 2010). Organogenic salt marshes typically do not have internal channels for drainage. They are mostly located in North America (Van Dobben et al., 2022; Friedrichs and Perry, 2001; De Groot et al., 2011; Reef et al., 2017). The organogenic salt marsh type is not the primary focus of this research and will thus not be further elaborated on.

The first contributor to salt marsh accretion, as shown in Figure 2.4, is the settling of the SSC that is present in the water column. The SSC is defined as the quantity of suspended sediment in a water volume flowing over the marsh platforms and through the creeks. The SSC in the water column along with the sediment texture, settling velocity and hydroperiod determine the magnitude of sedimentation.

The distribution of sediment over a salt marsh is mainly dependent on advection. The largest sediment deposition quantities can be found near the source: the salt marsh edge and/or creeks, since the inundation frequency and hydroperiod are larger at these locations. Accordingly, a concave profile arises between the salt marsh edge and hinterland and/or between two creeks (Bartholdy, 2012). While the marsh surface height increases, a decrease in the inundation frequency and hydroperiod is observed. The inundation frequency stabilizes at a certain marsh height in cases without SLR. This means that the salt marsh has reached its maturation (Van Wijnen & Bakker, 2001). However, for continuous SLR, the inundation frequency will increase facilitating the ongoing occurrence of sedimentation. The SSC tends to vary with the energy level in the tidal inlet (Allen, 2000b). Over the tidal cycle, an increase in SSC and average grain size is generally found for higher velocities.

The sediment supply can be a limiting factor for salt marsh development. The sediment supply onto the salt marsh strongly depends on the horizontal exchange with adjacent tidal inlet components (Allen, 2000b). When the SSC in neighbouring elements is small or these elements have a large sediment demand, no sediment-rich water will flow upon the marsh platforms and thus limited sedimentation will occur. However, for episodic high-energy events such as storm surges, the SSC on the tidal flats increases due to the resuspension of sediment by wave action (Best et al., 2018). This means that marshes are able to trap an increased amount of sediment during storm surges, provided that the hydroperiod is sufficient. The trapping efficiency of a salt marsh also determines whether the SSC deposits or not, more on this will be explained in section 2.5. During high-energy events, the increased waves, wind and currents could lead to surface erosion. In most cases, this is a negligible process for salt marshes due to their vegetation cover, cohesive sediment type and ecological resilience (Kirwan et al., 2010).

Besides the local sedimentation differences on a salt marsh, a global pattern regarding the grain size distribution is present for the entire tidal inlet. A tidal inlet is tide-dominated which means that the tide

plays the most important role in sediment distribution as well. The strength of a tidal current increases for a larger water depth. A strong tidal current will keep the finer particles in suspension, although coarse particles are able to settle. Therefore, coarser sediment fractions can be found in the more energetic and deeper areas of the tidal inlet: sand particles are usually deposited at the ebb-tidal delta, near the tidal inlets and in the tidal channels. Sedimentation of the finest particles, such as silt and clay, occurs on the tidal flats and salt marshes. At these locations, only a small water depth is present during inundation which allows for sedimentation of fine sediments. It can thus be stated that the largest part of the sedimentation on a salt marsh consists of clay and silt.



Figure 2.5: Cliff erosion on a salt marsh (Buzzards Bay Coalition, 2016).

At the exposed edges of the salt marsh, horizontal expansion or erosion takes place. During the expansion phase, the tidal flats experience significant vertical growth, ultimately resulting in their transformation into a salt marsh. Thus, the salt marsh migrates further over the tidal flat in the direction of the channels. When sediment supply is insufficient for both the salt marsh and the adjacent flat to grow at the same rate, the elevation difference between the salt marsh and tidal flat will increase (Elschot et al., 2017). Hence the edge between the salt marsh and tidal flat becomes increasingly steep (Bakker, 2014). Short-term sediment dynamics, such as seasonal variations, play an important role in this process (Bouma et al., 2016). A steep gradient means that the marsh edge is more vulnerable to wave attack. During storms, the increased amount of wave energy may cause the marsh's edge to collapse. This phenomenon is called cliff erosion (Koppel et al., 2005). An example is shown in Figure 2.5.

Following the cliff erosion, renewed room in front of the salt marsh becomes available which generates an opportunity for sedimentation to occur. After a significant amount of sediment deposition, vegetation will be able to establish in the pioneer zone again and acts as a buffer for incoming waves and currents. Moreover, the vegetation inhibits the resuspension of bottom surface sediments. This means that flow velocities are reduced and erosion is weakened. As a result, sediment accumulation is enhanced and the stability of the sediment deposits increases which in turn facilitates more plant growth. Provided that sufficient sediment is available, the salt marsh experiences continuous accretion and will expand seawards again (Zhao et al., 2017). It can thus be said that the sediment dynamics lead to cyclic marsh dynamics by alternating lateral expansion and erosion phases. The lateral expansion phase allowed salt marshes to establish under the continuous SLR until the mid-Holocene, after which the coastline stabilised (Bakker, 2014).

2.5 Vegetation Establishment

As discussed in Chapter 1, salt marshes are known for their large biodiversity, especially when looking at the different types of vegetation on a marsh. The type of vegetation differs per marsh zone: the higher marsh has different vegetation than the lower marsh and pioneer zone. This relates to the inundation frequency and duration: the abiotic conditions vary per marsh zone, which attracts different species (Bakker, 2014). The type of vegetation can also be affected by grazing livestock on a salt marsh (Reef et al., 2017). This effect is mainly seen in a reduction of vegetation height, along with alteration of the species composition and an increase in biodiversity (Elschot, 2015).

The salt marsh vegetation growth knows different phases. At first, only pioneer species are present on the salt marsh. These pioneer plants impede the flow by an increased bed shear stress, which reduces the flow velocities. This has an influence on the different types of salt marsh accretion that were discussed in section 2.4. The increase in bed shear stress facilitates the deposition of the SSC from the water column onto the marsh surface during submerged conditions (Bakker, 2014). Moreover, the vegetation could lead to the direct capture of sediment when particles get stuck behind the leaves or roots. Consequently, the salt marsh elevation increases whereby even more vegetation can establish on the marsh. When a significant amount of vegetation is present, the marsh will produce ample plant biomass for more accretion to occur. The evolution of a salt marsh can thus be described by a positive feedback loop, as shown in Figure 2.6. This positive interaction between biological and physical processes is called biogeomorphic feedback (Bouma et al., 2016).

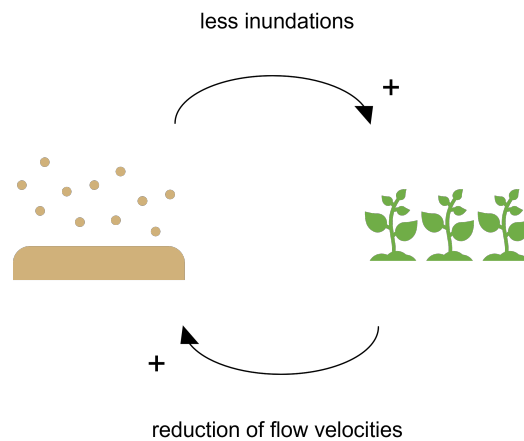


Figure 2.6: Positive feedback mechanism: mineral sedimentation increases the salt marsh height and results in less inundation, which means more vegetation can develop. More vegetation leads to a reduction in flow velocities which allows for sedimentation to occur.

The trapping efficiency of a salt marsh indicates the ability of a marsh to capture sediment and depends on different factors. The main requirement for sediment trapping is prevailing calm hydrodynamics, which allows for sediment to deposit. However, there are some factors that could enhance sediment deposition. For instance, the vegetation structure and plant density play a role. When the marsh vegetation has a rough structure, shear stresses are increased even further. This allows for easier sedimentation and accordingly, it can be said that a larger trapping efficiency is present (Best et al., 2018). Similar reasoning holds for direct capture by vegetation: for example, larger leaves capture more sediment than small leaves. The vegetation structure could have a limited impact on accretion when the sediment deposition is dominated by storms and very high tides. In this case, the inundation depth could be significantly larger than the vegetation height. This would mean that vegetation is not able to affect current velocities and in turn sediment deposition. Additionally, the wave energy during storms could be so large that local vegetation is unable to reduce the shear stresses. The role of vegetation seems to be significant during shallow inundations only (Elschot, 2015).

2.6 Autocompaction and Subsidence

The negative contributor to salt marsh accretion is compaction, which leads to a decrease in marsh surface elevation. Compaction of the marsh surface layer can be classified into shallow and deep compaction. Shallow autocompaction is present in the top layer of the soil and concerns shrinkage, compaction of sediment layers and decomposition of organic material. Deep compaction, or land subsidence, relates to tectonic and isostatic processes (Bakker, 2014). This will be referred to as deep subsidence from now on. Human interventions such as the extraction of natural resources or groundwater could also lead to deep subsidence. Autocompaction and subsidence, in combination with SLR, contribute to more accommodation space in which salt marshes can extend upwards (Allen, 2000b).

According to Elschot (2015), autocompaction immediately follows from increasing age and thickness of a salt marsh. Moreover, this research states that the presence of large grazers, such as cattle, could significantly increase the bulk density, which can have a large influence on autocompaction in the top soil layer. Nolte et al. (2015) and Marin-Diaz et al. (2021) also found that grazing by livestock has a significant effect on shallow autocompaction: the presence of cattle negatively affects the vertical salt marsh accretion. However, a study by Van Dobben et al. (2022) states that livestock does not have a significant effect on autocompaction.

2.7 Effect of Accelerated SLR

Accelerated SLR is expected to affect salt marsh development by altering the hydrodynamic forcing mechanisms. Salt marshes will experience more inundation. As a result, sedimentation is likely to increase meaning that salt marsh growth is enhanced. However, for a significant SLR rate, the marsh may be prone to drowning as the sedimentation may not be able to keep up with the high rate of SLR.

When the only limit of marsh accretion is stated to be sediment supply, a salt marsh would be likely to be able to keep pace with accelerated SLR because more inundation would imply more sedimentation. However, disturbed feedback mechanisms between sedimentation, hydrodynamics and population dynamics of macrophytes (i.e. vegetation) living on the marsh surface could eventually lead to the drowning of the salt marshes under accelerated SLR. As discussed earlier, the trapping efficiency of vegetation is limited when the inundation depth is significantly higher than the vegetation. When the marsh is unable to follow the increase in relative SLR, inundation depths will structurally increase meaning that the trapping efficiency by vegetation reduces. When the marsh elevation becomes lower than the optimum elevation, positive feedback mechanisms would arise as a result of the higher inundation depths and reduction of plant productivity, which means the processes reinforce themselves. This means an unstable situation will arise and eventually, the salt marsh inundation depths could become too large for vegetation to survive (Mudd et al., 2010). However, under these circumstances, it is likely that the sedimentation rates in the salt marsh cannot keep up with the accelerated SLR, and it is improbable that the trapping efficiency alone will determine the survival of the salt marsh.

Due to SLR, higher salt marshes will be drowned more often. However, the water that reaches the high marshes will have a low SSC, because most of the sediment has already settled close to the creeks or marsh edges (Hartig et al., 2002). This means that less sedimentation occurs on the high marsh. Even though the surrounding areas will grow higher, the high marsh itself will stay at its original level. In combination with the fact that the high marshes do not have an extensive drainage system, tidal pools may arise in these locations. Consequently, low oxygen diffusion rates may lead to a local decrease in vegetation since high marsh vegetation is less resilient against anaerobic conditions than for example low marsh vegetation (Crooks et al., 2002; Elschot et al., 2017). This could eventually lead to a transformation of high marshes into low marshes.

2.8 Salt Marsh Extent in Literature

Earlier conducted studies on salt marshes use different definitions for the salt marsh extent. This section will explore and summarize the definitions, that were mainly based on hydrodynamics. The salt marsh extent that shall be applied in this research will be determined based on the summary of literature given in this section and a data analysis that will be carried out in Chapter 5.

Allen (2000a) defines a salt marsh based on a geomorphological classification. It is stated that currently active salt marshes are only present in mesotidal (2 - 4 m) or macrotidal range (> 4 m). The development of a salt marsh is said to be governed by the vertical limits of possible tidal action in combination with atmospheric processes. However, no specific lower and upper hydrodynamic limit for low and/or high salt marshes is given. Therefore, this study is excluded from the summary in Table 2.3.

The definition of a salt marsh according to Bakker (2014) is shown in Figure 2.7. It can be seen that the pioneer zone of the salt marsh is situated below MHW, starting from an inundation duration of a maximum of 3 hours per tidal flooding. The lower marsh is situated above MHW and experiences a minimum of 100 tidal floods per year. At this point, the low marsh transforms into a high marsh. The upper limit of the high marsh is 1 flood per year. Bakker (2014) does not mention the middle salt marsh in the definition.

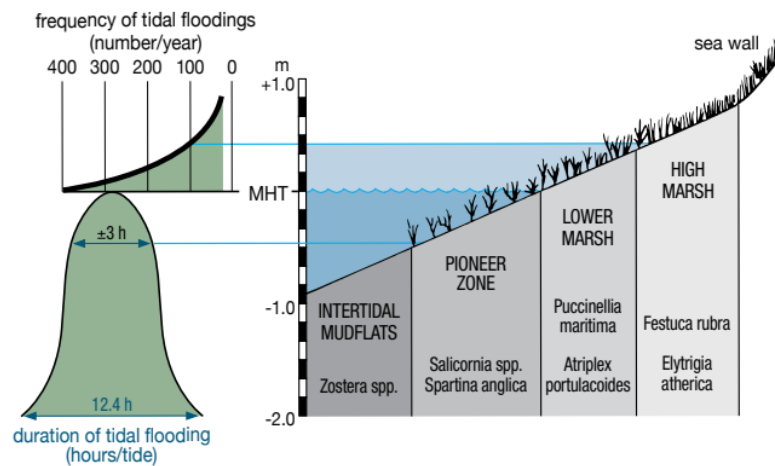


Figure 2.7: Schematic overview of marsh zonation according to Bakker (2014).

Bartholdy (2012) made a marsh zonation as shown in Figure 2.8. The salt marsh pioneer zone is schematised in accordance to Bakker (2014): it is said to experience a maximum of 3 hours of tidal flooding per cycle. Bartholdy distinguished between the lower, middle and upper salt marsh. The lower marsh has a flooding frequency of 200 - 100 times per year. The middle marsh is flooded 100 - 60 times a year. The high marsh occurs for a flooding frequency of 60 - 0 times per year.

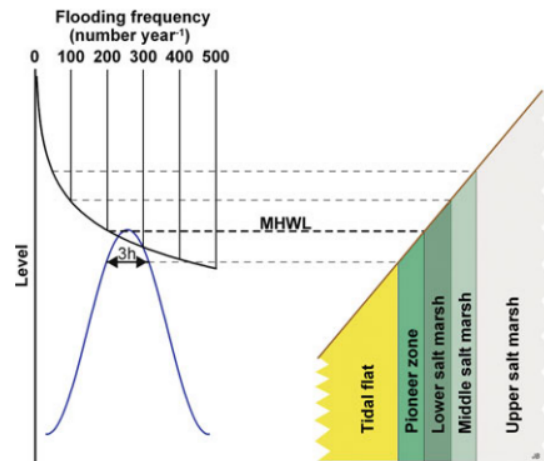


Figure 2.8: Schematic overview of marsh zonation according to Bartholdy (2012).

Bosboom and Stive (2021) define a salt marsh in accordance to Figure 2.9. The lower marsh is situated from Mean Sea Level (MSL) up to approximately Mean High Water Spring (MHWS). The higher marsh reaches from MHWS up to High Astronomical Tide (HAT); the highest tide level which can be predicted to occur under average meteorological conditions and under any combination of astronomical conditions.

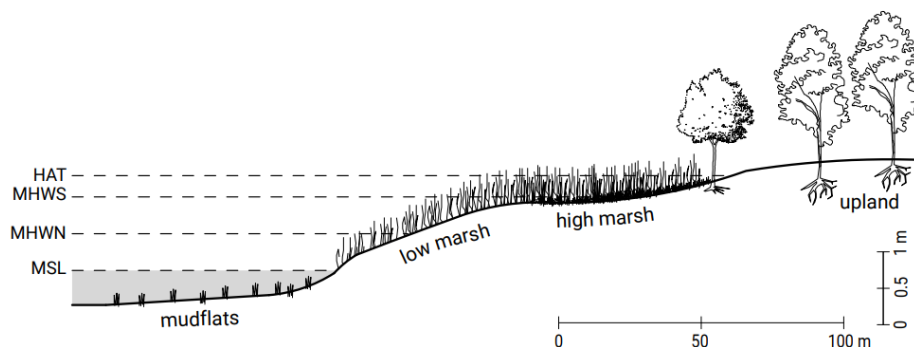


Figure 2.9: Typical cross-section of a salt marsh according to Bosboom and Stive (2021).

Another common method to schematise salt marshes is by classification on the basis of vegetation type. For example, a study by Elschot (2015) uses available vegetation data for marsh classification. The salt marsh is schematised in a low, middle and high part classified based on for instance the presence of specific species and the plant density. This method is less suitable for this study, as the ASMITA model is not able to process such detailed information. Therefore, it is excluded from Table 2.3.

Van Dobben et al. (2022) state that salt marshes occur just above mean sea level. This research studies salt marshes in the Dutch Wadden Sea on the barrier islands Terschelling, Ameland and Schiermonnikoog. The study develops a multiple regression approach to simulate the effect of various SLR rates on marsh accretion. For the model, a hypothetical marsh with initial elevation values relative to NAP is used. These elevation values are based on aerial photographs and vegetation maps of the Dutch Wadden Sea. The marsh edge is situated 75 cm + NAP. The low and high levees have an elevation of respectively 100 and 140 cm + NAP. The marsh platform has an increasing elevation of 70, 100, 140 and 180 cm + NAP. A summary of this research specifically is shown in Table 2.2.

De Groot et al. (2015) describes salt marshes in the Wadden Sea as areas with salt-tolerant vegetation where the accretion of silty material results in an increasing platform height. The study states that salt marshes are situated between MHW and the location where a maximum of 5 floods per year occur.

Location	Initial elevation [cm + NAP]	Initial age [year]	Distance to creek [m]	Creek length [m]
Marsh edge	75	0	1	0
Marsh platform	70	0	250	0
	100	20	250	200
	140	60	250	500
	180	100	250	100

Table 2.2: Initial values for a salt marsh used in the study by Van Dobben et al. (2022).

Figure 2.10 shows the marsh definition by Oost et al. (2020). The pioneer zone is situated below MHW, which means the area is inundated for some time during every tidal cycle. The low marsh is situated between MHW and MHWS. The lower limit of the high marsh is MHWS and the upper limit is storm surge level, which is related to 5 floods per year.

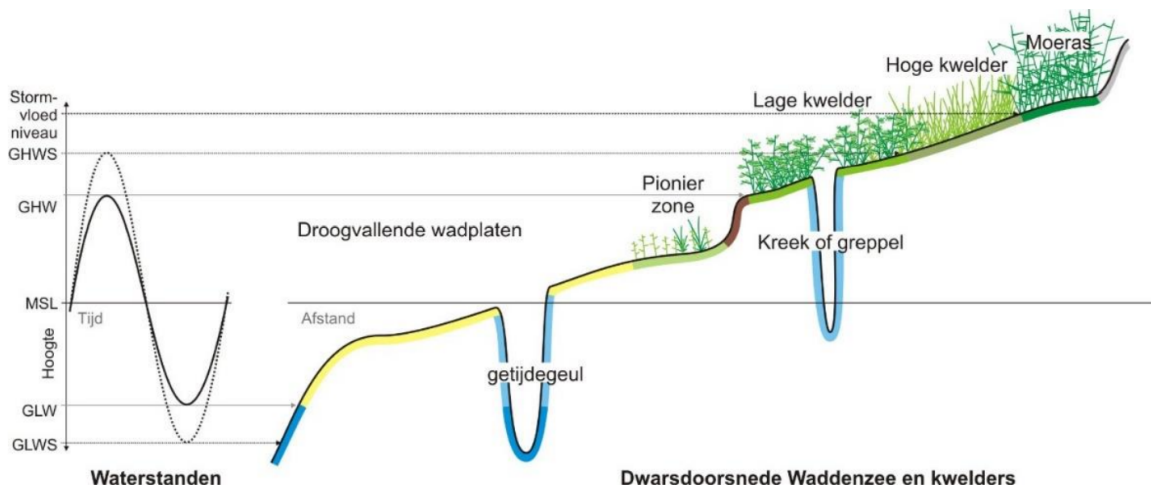


Figure 2.10: Schematic overview of marsh zonation according to Oost et al. (2020).

The overview of all marsh definitions found in the literature above is given in Table 2.3. The main takeaway is that the pioneer zone is situated below MHW in all studies. In some studies, a distinction between three marsh zones is made: the low, middle and high marsh. Whereas other studies only define a low and high marsh. The lower limit of the low marsh is usually MHW and the upper limit is defined as MHWS or a frequency of 100 floods/year. The middle marsh is defined as 100 - 60 floods/year. The high marsh has a lower limit varying from MHWS to 100 - 60 floods/year. The upper limit of the high marsh varies from 5 - 0 floods/year.

Study	Zone	Lower limit	Upper limit
Bakker (2014)	pioneer zone	3 [hrs/cycle]	MHW
	lower marsh	MHW	100 [floods/year]
	middle marsh	-	-
Bartholdy (2012)	higher marsh	100 [floods/year]	0 [floods/year]
	pioneer zone	3 [hrs/cycle]	MHWL: 200 [floods/year]
	lower marsh	MHWL: 200 [floods/year]	100 [floods/year]
Bosboom and Stive (2021)	middle marsh	100 [floods/year]	60 [floods/year]
	higher marsh	60 [floods/year]	0 [floods/year]
	pioneer zone	-	-
Van Dobben et al. (2022)	lower marsh	MSL	MHWS
	middle marsh	-	-
	higher marsh	MHWS	HAT
De Groot et al. (2015)	salt marsh	75 [cm + NAP]	180 [cm + NAP]
Oost et al. (2020)	salt marsh	MHW	5 [floods/year]
	pioneer zone	3 [hrs/cycle]	MHW
	lower marsh	MHW	MHWS
	middle marsh	-	-
	higher marsh	MHWS	storm: 5 [floods/year]

Table 2.3: Overview of different marsh definitions.

2.9 Salt Marsh Accretion Rates

This section provides an overview of characteristic salt marsh accretion rates based on previous research.

According to Temmerman et al. (2004), young salt marshes in the Western Scheldt, an estuary in The Netherlands, have a sedimentation rate of 1.6 - 3.2 cm/year. The MHW rise was equal to 0.3 - 0.6 cm/year, which means that the accumulation rate is very fast. When the young marshes reached an elevation around local MHW, the accumulation rates decreased to 0.4 - 1.8 cm/year. The accumulation rate of the high marsh is typically within the same range of the SLR rise rate, often without exceeding it. A general observation for the Western Scheldt is that young salt marshes quickly accumulate until (quasi-)equilibrium, whereas old marshes experience sedimentation rates close to the rate of SLR. It is noteworthy that the sedimentation rates in the Western Scheldt are relatively high compared to the Dutch Wadden Sea, which will be elaborated upon below. The larger sedimentation rates can be appointed to higher energetic conditions, a significant sediment input from the river, favourable sediment trapping conditions and an abundance of dredging activities (Kirwan et al., 2010).

De Groot et al. (2015) studied salt marshes in the Dutch Wadden Sea. It was seen that the average sedimentation over the entire salt marsh equals 0.5 cm/year. These values could increase to 1 cm/year in the low marsh areas. A similar analysis was carried out by Van Puijenbroek and Sonneveld (2021), which mentioned that these values may not be representative of the entire salt marsh. The measurement locations are situated relatively close to the marsh edges and tidal creeks, where generally the highest sedimentation occurs.

A study on salt marshes in the Dutch Wadden Sea by Van Wijnen and Bakker (2001) reveals that mean accretion rates vary from 0.0 - 1.1 cm/year. The highest rates were found on the low marsh elevations: accretion rates increased linearly with inundation frequency. After the first 100 years of establishment, the marsh elevation increased at a slower pace. For an older marsh, the accretion is more susceptible to shallow autocompaction. As a result, the surface elevation growth is more dependent on the rate of SLR. The difference between salt marsh development in a new marsh versus an old marsh is shown in Figure 2.11, where subsidence relates to shallow subsidence or autocompaction.

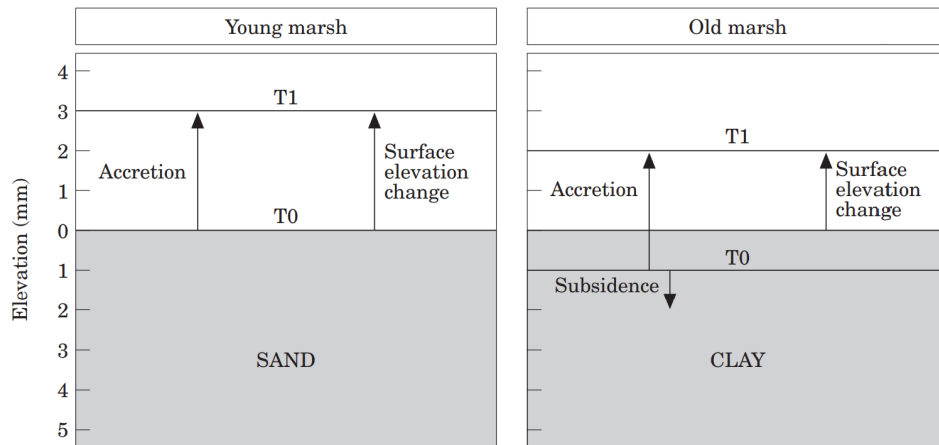


Figure 2.11: Accretion in a young and old salt marsh (Van Wijnen & Bakker, 2001).

Cleveringa (2018) estimated the sedimentation rates for the salt marsh study areas in the Dutch Wadden Sea based on different data types. An overview is given in Table 2.4.

salt marsh	sedimentation [cm/year]	based on	data available since
Neerlandsreid	0.2 - 1.0	height & sedimentation measurements	1986
De Hon	0.2 - 1.0	height data, LiDAR	1986
Het Rif	0.1 - 0.5	sedimentation measurements, PQs	1997
Oosterkwelder	0.1 - 0.5	sedimentation measurements, PQs	1997

Table 2.4: Sedimentation rates according to Cleveringa (2018).

Mudd et al. (2010) states that accumulation by plant biomass contributes to a maximum vertical height increase of 0.3 cm/year. Any accretion rate beyond this value is attributed to inorganic sedimentation.

The rate of autocompaction strongly depends on the age of the marsh and the sediment type. Allen (2000a) gives a range of autocompaction rates between 0.2 - 2.5 cm/year. Often only a small value for autocompaction is present, in the order of mm/year. For an older, grazed marsh, the magnitude of autocompaction could be in the order cm/year.

An overview of the plausible range of mineral sedimentation, accumulation by plant biomass and autocompaction based on the numbers provided in this section is given in Figure 2.12.

Several studies state that measurements of accretion rates may overestimate the response of salt marshes to future SLR scenarios (Saintilan et al., 2022; Van Puijenbroek et al., 2022; Elschot, 2015). Measurements of recent accretion rates showed generally much higher rates than measurements of long-term accretion rates. This suggests that the autocompaction of sediment layers becomes more important with increasing marsh age and could have a negative impact on the marsh surface height.

An overview of the different components that contribute to salt marsh development according to Bakker (2014) and were discussed in the previous sections is given in Figure 2.13.

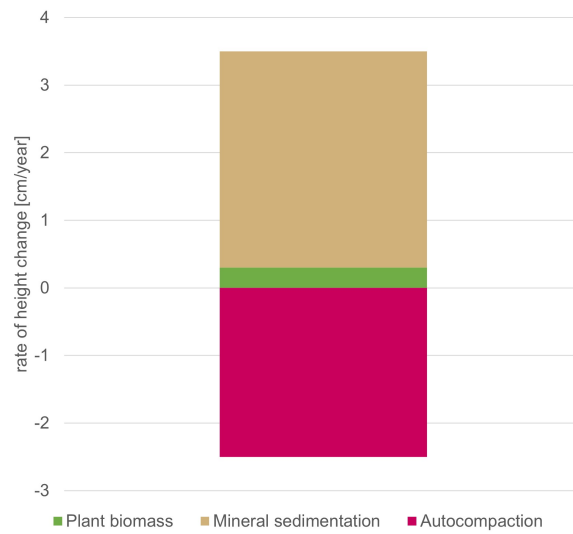


Figure 2.12: Range of contributions to salt marsh accretion, note that autocompaction in the order of cm/year only occurs for older salt marshes with a large biomass component.

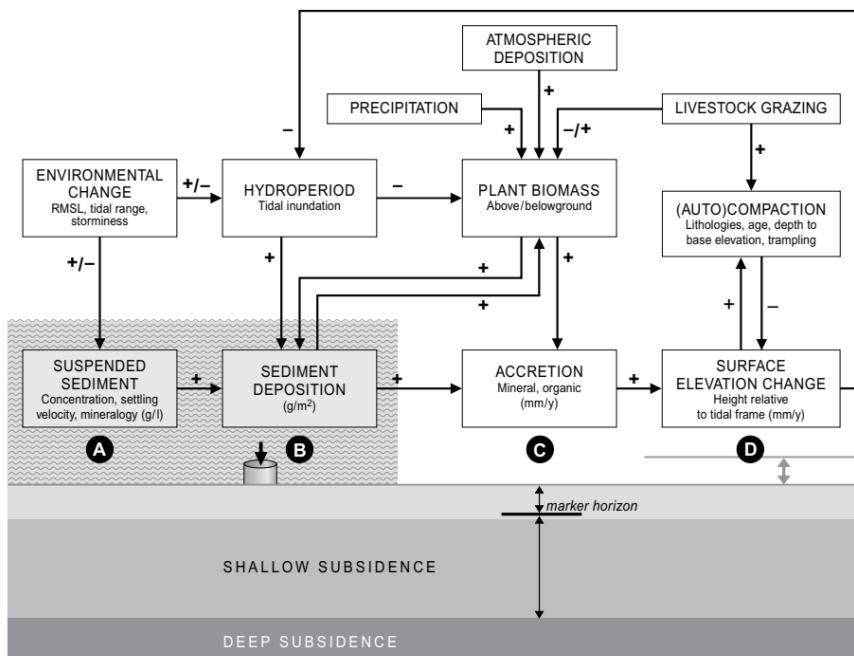


Figure 2.13: Flowchart of marsh accretion by Bakker (2014).

Long-Term Morphological Modelling in ASMITA

This chapter will elaborate on long-term morphological modelling using ASMITA. First, section 3.1 elaborates on the relevance of reduced complexity modelling. The physics behind ASMITA are explained in section 3.2, after which the aggregation is elaborated on in section 3.3. The elements that are currently included in ASMITA are described in section 3.4. The concept of morphological equilibrium and the computational procedure of ASMITA are described in section 3.5, after which section 3.6 elaborates on the parameter setting. Lastly, the multiple element schematisation is given in section 3.7.

3.1 Relevance of Reduced Complexity Modelling

Modelling is a crucial tool for understanding the system behaviour of tidal inlet systems and predicting the future morphological development for different SLR scenarios. Different types of models can be used for simulating morphological development over time:

- Process-based models
- Aggregated models
- Idealised models

Process-based models aim to closely represent reality by numerically solving mathematical equations that describe physical processes at a detailed level. The accuracy of the model outcome depends on the underlying equations and model deployment. Hydrodynamics are simulated by well-known and thoroughly studied equations. However, the model requires sediment transport formulae to simulate the morphological evolution, which typically entail a considerable number of assumptions and unknowns.

Aggregated models represent physical processes on an aggregated spatial and temporal scale. This means that information is combined across larger spatial areas and time intervals, which simplifies complex processes to enhance the computational feasibility. The ASMITA model specifically may be classified as a (semi-)empirical model and is based on the assumption that a morphological system will attain a state of equilibrium after an initial perturbation. Empirical relationships are employed to define this morphological equilibrium (see Chapter 2). The ASMITA model is a long-term morphological model that operates on time scales ranging across decades or even centuries. Accordingly, hindcast data in the order of decades should be available for calibration and validation of the aggregated model.

Idealised models are in fact process-based models that use simplified physical and mathematical formulations for describing the behaviour of a system. The model solely includes the description of fundamental principles, in contrast to incorporating all physical processes (Wang et al., 2018).

Long-term morphological modelling of tidal inlet systems has proven to be a very challenging subject. The relation between hydrodynamics and morphological changes is complex due to strong feedback mechanisms. Where tidal flow is important, both the geometry and bathymetry of a tidal inlet system determine morphological behaviour over time by affecting the tidal prism. The effect of the tidal prism on the morphological development of the tidal inlet system components is described by the empirical equilibrium relations (Chapter 2). This means that in the case of a tidal inlet system, the morphology is a driver for its own development. Due to these feedback mechanisms, the morphological equilibrium cannot be derived from physical mathematical relations. Additional complexity arises from the fact that the residual sediment transport determines morphological changes. In general, it is very difficult to accurately determine the residual sediment transport because it is only a small value compared to the significant flood and ebb transport components (Wang et al., 2008).

Process-based models have proven to be very useful for describing morphological developments on timescales up to 5 years. A study by Luijendijk et al. (2017) proved that it is also possible to use process-based modelling for decadal time-scales of a large initial disturbance, specifically the construction of the Zandmotor. However, with regard to the natural morphological development of tidal inlet systems, small disturbances are present. Several studies tried to use a process-based model for simulating the morphodynamics in tidal inlet systems in the Wadden Sea, but this led to less successful results due to unrealistic inlet channel incision (Wang et al., 2016). An additional constraint is the significant computational time that arises when using process-based models for long-term morphological simulations. Moreover, a morphodynamic spin-up time in the order of decades could be present (Huisman et al., 2022). This is a problem due to comparable time scales between the spin-up time and the morphological response of tidal inlet systems to SLR. Hence, it remains unclear whether specific morphological changes can be attributed to SLR or spin-up time.

For this reason, the aggregated reduced complexity model approach is more suitable for long-term morphological simulations. The aggregation on temporal and spatial scales leads to a reduction in computational time, which means that multiple long-term model simulations can be carried out. Additionally, the aggregated model is not affected by spin-up time because of the morphological equilibrium that is implied.

3.2 Physics

ASMITA is a numerical model that combines empirical relations for morphological equilibrium with the aggregated description of physical processes. The long-term morphological development of tidal inlet systems is simulated based on inlet system-related tidal flows and wave-related hydrodynamics.

The physical processes are included in the model by means of an aggregation of the 3D advection-diffusion equation as shown in Equation 3.1. This can be interpreted as a mass balance of sediment concentrations (Wang & Lodder, 2019). It relates a change in sediment concentration to the net import of sediment by the horizontal fluid velocity and the net upward & downward transport of sediment by the vertical fluid velocity along with turbulent diffusion processes.

$$\frac{\partial c}{\partial t} + \frac{\partial uc}{\partial x} + \frac{\partial vc}{\partial y} + \frac{\partial wc}{\partial z} - \frac{\partial}{\partial x} \left(\epsilon_x \frac{\partial c}{\partial x} \right) - \frac{\partial}{\partial y} \left(\epsilon_y \frac{\partial c}{\partial y} \right) = w_s \frac{\partial c}{\partial z} + \frac{\partial}{\partial z} \left(\epsilon_z \frac{\partial c}{\partial z} \right) \quad (3.1)$$

where:

c	sediment concentration	$[\text{ML}^{-3}]$
t	time	$[\text{T}]$
u, v	horizontal flow velocity components	$[\text{LT}^{-1}]$
x, y	horizontal coordinates	$[\text{L}]$
w	vertical flow velocity	$[\text{LT}^{-1}]$
z	vertical coordinate	$[\text{L}]$
$\epsilon_x, \epsilon_y, \epsilon_z$	turbulent diffusion coefficients in x-, y- and z-direction	$[\text{L}^2\text{T}^{-1}]$
w_s	settling velocity of sediment particles	$[\text{LT}^{-1}]$

No information on the flux of sediment exchange between bottom and water column is given in Equation 3.1. It only describes the kinetics, i.e. the fluid motion and forcing. However, the morphological change of the elements in a tidal inlet system depends on the dynamic part of the suspended sediment transport model. This is defined as the bed boundary condition, which describes the sediment flux between bed and water column and it should be prescribed.

3.3 Aggregation

ASMITA is a reduced complexity model. This means a high level of temporal and spatial aggregation is present. Aggregation can be used within a model to describe real-world problems on an appropriate level of abstraction (Wang et al., 2020). Several small-scale processes are combined in an assumption that describes a larger-scale development or behaviour. Morphodynamic models like Delft3D usually only contain a first degree of aggregation. ASMITA contains both a high temporal and spatial aggregation: elements are schematised from 3D into 2D into 1D into 0D (volumes). This means that ASMITA is not able to compute any spatial differentiation over an element. The model output is a change in overall element volume. The forcing mechanisms are aggregated as well. An example is found in the tidal variation: only the net effect is considered in ASMITA.

The stages of aggregation can be explained from micro- to mesoscale. The aggregation process starts with the 3D advection-diffusion equation that was shown in section 3.2. When this equation is integrated into the vertical, the 2D depth-averaged convection-diffusion equation as shown in Equation 3.2 is obtained. This first aggregation level is present in most process-based models (Wang & Lodder, 2019).

$$\frac{\partial h\bar{c}}{\partial t} + \frac{\partial \alpha_x \bar{u} h \bar{c}}{\partial x} + \frac{\partial \alpha_y \bar{h} h \bar{c}}{\partial y} - \frac{\partial}{\partial x} \left(D_x h \frac{\partial \bar{c}}{\partial x} \right) - \frac{\partial}{\partial y} \left(D_y h \frac{\partial \bar{c}}{\partial y} \right) = f_b \quad (3.2)$$

where:

h	water depth	[L]
α_x, α_y	vertical shape coefficients	[-]
D_x, D_y	dispersion coefficients	[L ² T ⁻¹]
f_b	sediment flux between water column and bed	[LT ⁻¹]

The 2D depth-averaged convection-diffusion equation can be simplified into 1D by integrating over the width. This is the second level of aggregation and results in Equation 3.3. It can also be written as Equation 3.4.

$$\frac{\partial A\bar{c}}{\partial t} + \frac{\partial \alpha \bar{u} A \bar{c}}{\partial x} - \frac{\partial}{\partial x} \left(A D_x \frac{\partial \bar{c}}{\partial x} \right) = F_b \quad (3.3)$$

$$\frac{\partial h\bar{c}}{\partial t} + \frac{\partial s_x}{\partial x} + \frac{\partial s_y}{\partial y} = f_b \quad (3.4)$$

where:

A	cross-sectional area	[L ²]
α	coefficient for flow velocity and sediment concentration distribution within the cross-section	[-]
D_x	dispersion coefficient	[L ² T ⁻¹]
F_b	sediment flux between the water column and bed integrated over the width	[L ² T ⁻¹]
s_x, s_y	suspended sediment transport rate	[L ² T ⁻¹]

The third level of aggregation is obtained when Equation 3.4 is integrated over a morphological element. The result is shown in Equation 3.5. This equation can also be obtained by considering the sediment mass balance in the entire water body.

$$\frac{\partial VC}{\partial t} = \sum_i S_i + F_B \quad (3.5)$$

where:

V	water body volume of the area	$[L^3]$
S_i	sediment transport at open boundary	$[L^3 T^{-1}]$
C	averaged sediment concentration in the element	$[ML^{-3}]$
F_b	sediment flux between the water column and bed integrated over the element	$[L^3 T^{-1}]$

The final equation is obtained by aggregating Equation 3.5 in time. The time over which the integration is done can vary between for example one tidal period or several days. All parameters will scale with the chosen time step. When the time step is chosen to be equal to one tide, the parameters become tidally-averaged values. The resulting equation is shown in Equation 3.6.

$$\sum_i S_i + F_B = 0 \quad (3.6)$$

3.4 Element Definitions

In section 3.1, it was explained that a reduction in temporal and spatial complexity allows for long-term morphological simulations. Hence, ASMITA does not contain a detailed description of a tidal inlet system. Instead, the tidal inlet system is divided into three basic morphological elements that exchange sediment: the ebb-tidal delta, the channels and the tidal flats. These elements communicate with adjacent coastal areas, which is implemented in ASMITA as an outside boundary condition. The bathymetry of each element is represented by one variable, of which the definition is listed below (Wang and Lodder, 2019; Buijsman, 1997):

1. Ebb-tidal delta: total excess sediment volume relative to the undisturbed bed profile [L^3]
2. Channels: total water volume below MLW [L^3]
3. Tidal flats: total sediment volume between MLW and MHW [L^3]

The most common ASMITA schematisation of a tidal inlet system is the 3 element model, which encompasses the aforementioned elements. A visualisation is shown in Figure 3.1. Even though the 3 element model is the most common schematisation for a tidal inlet, it is possible to use any number of interconnected elements. In this way, a distinction between ebb-tidal delta, channel or tidal flat elements with different characteristics can be made.

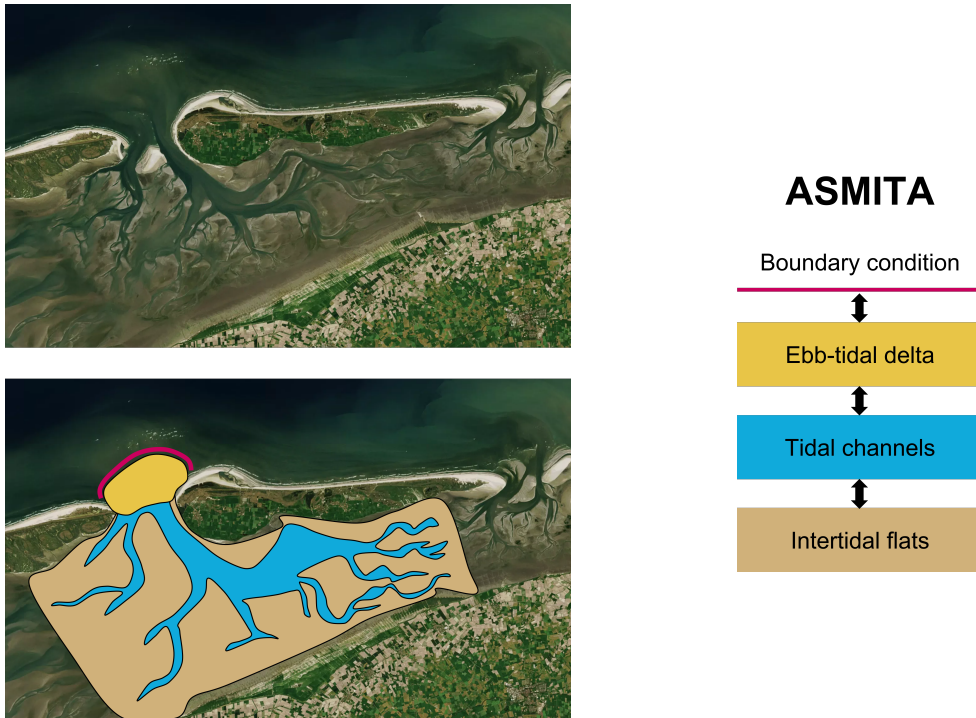


Figure 3.1: 3 element schematisation in ASMITA.

3.5 Morphological Equilibrium & Computational Procedure

ASMITA simulates long-term morphological behaviour by looping through different computational steps. This is done based on the Forward Euler method, meaning that the new time step is a function of the previous time step. A schematisation of the ASMITA computations is given in Figure 3.2.

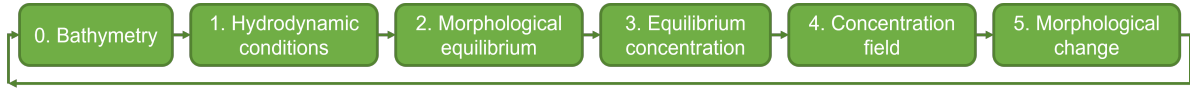


Figure 3.2: Flowchart of the computational procedure carried out by ASMITA.

The ASMITA model takes an initial element volume as input, which is derived from the bathymetry. Specifically, the total volumes of the ebb-tidal delta, channels and tidal flats at time step 0 should be provided. Subsequently, the first model step is to determine the aggregated flow condition by calculating the tidal prism (Huismans et al., 2022). This, along with the tidal range, gives the hydrodynamic conditions that can be used in step 2 to compute the morphological equilibrium per element.

The most important concept used in ASMITA is the hypothesis that each morphological element in the system has an equilibrium state that can be defined based on the hydrodynamic conditions (Wang et al., 2008), which was already explained in Chapter 2. During the ASMITA model runs, changes in hydrodynamic conditions could occur due to morphological changes. This means that the morphological equilibrium condition is subject to change during the simulations and it implies that no sedimentation occurs when all elements are in equilibrium. ASMITA forces all elements towards morphological equilibrium, as the principle of morphological equilibrium is used to determine the concentration field and indirectly the sediment transport between the different elements. This is based on the assumption that all elements in a tidal inlet system will eventually reach equilibrium if enough time passes.

Every element has a certain equilibrium volume that follows from the tidal prism for the ebb-tidal delta & tidal channels and from the tidal range for the intertidal flats. ASMITA determines these equilibrium volumes in the second modelling step based on relations by Eysink (1990), Eysink and Biegel (1992) and Renger and Partenscky (1974). The morphological equilibrium volume formulations for the ebb-tidal delta, channels and tidal flats are depicted in respectively Equation 3.7, 3.8 and 3.9.

$$V_{de} = \alpha_d P^{1.23} \quad (3.7)$$

$$V_{ce} = \alpha_c P^{1.55} \quad (3.8)$$

$$V_{fe} = A_{fe} h_{fe} \quad (3.9)$$

where:

V	equilibrium volume	$[m^3]$
α	empirical coefficient	$[-]$
P	tidal prism	$[m^3]$
A	inlet system area	$[m^2]$
h	tidal range	$[m]$

In the next step, the equilibrium concentration, as can be seen in Equation 3.10, per element is computed. Details on the global equilibrium concentration c_E parameter will be given in section 3.6.

$$c_e = c_E \left(\frac{V_e}{V} \right)^n \quad (3.10)$$

where:

c_e	element equilibrium concentration	[g/m ³]
c_E	global equilibrium concentration	[g/m ³]
V_e	equilibrium volume	[m ³]
V	element volume	[m ³]

The actual morphological development depends on the sediment availability in the water column along with the exchange rates and the difference between the actual element volume and equilibrium volume. Depending on whether an element has a sediment surplus or deficit, it wants to respectively export sediment to or import sediment from another element within the coastal system (Huisman et al., 2022). The horizontal exchange rate δ describes to what extent neighbouring elements are able to exchange sediment. The sediment exchange between the bed and water column is captured by the vertical exchange rate w_s . The actual morphological change is derived from the advection-diffusion equation, which describes the mass balance for suspended sediment (Wang & Lodder, 2019). The concentration field can thus be obtained by solving the aggregated advection-diffusion equation as shown in Equation 3.11 for each element, which corresponds to Equation 3.6. This equation states that the total vertical exchange of sediment between the water column and the bed should be in equilibrium with the total horizontal exchange of sediment between the element and the outside boundary, or neighbouring element.

$$w_s A (c_e - c) = \delta (c - c_E) \quad (3.11)$$

where:

w_s	settling velocity
A	element plan area
c_e	element equilibrium concentration
c	actual concentration
δ	horizontal exchange coefficient
c_E	global equilibrium concentration

Finally, the morphological change per element is determined by solving Equation 3.12, which corresponds to Equation 3.5.

$$\frac{dV}{dt} = w_s A (c_e - c) \quad (3.12)$$

The prescribed bed boundary condition will also be determined via the principle of morphological equilibrium. For steady uniform flow, it is known that the equilibrium sediment concentration is the solution for the sediment concentration vertically far away from the bed boundary. Therefore, the prescribed bed boundary condition must be equal to the equilibrium concentration. Similar reasoning holds for the sediment concentration gradient at the bed (Wang & Lodder, 2019). The equilibrium concentration and concentration gradient balance each other because the downward settling flux and the upward flux due to turbulent mixing are equal in an equilibrium situation. The equilibrium concentration depends on flow conditions and sediment properties for non-cohesive sediment and can be determined with sediment transport formulas such as Van Rijn et al. (1993). The Krone-Partheniades formulations are employed for cohesive sediment, usually by means of a tide-averaged equilibrium concentration (Wang & Lodder, 2019).

3.6 Parameter Setting

An essential aspect of ASMITA is the parameter setting. Two distinct types of parameters exist in ASMITA (Wang & Lodder, 2019). The first type of parameters is for the determination of morphological equilibrium, whereas the second type manages the morphological timescales. The morphological timescale indicates the adaptation capacity of an element to changes in hydrodynamics and geometric forcing (Kragtwijk et al., 2004). The morphological equilibrium coefficients are derived based on field data and previous studies. The parameters on morphological timescales will be determined by including the global equilibrium concentration c_E , the power n in the formulation for the local equilibrium concentration, vertical exchange coefficient w_s and horizontal exchange coefficient δ .

It should be noted that the ASMITA parameters cannot be measured directly, but can be related to field values and physical processes. A guideline for parameter calibration is given by Wang and Lodder (2019), based on Wang et al. (2008):

1. The value of n should be chosen based on an applicable sediment transport formula;
2. The value of w_s should be chosen based on the fall velocity of the sediment particles;
3. The value for δ should be chosen based on Equation 3.13 & 3.14 and previous studies;
4. The value of c_E should be adjusted to give the correct morphological timescale.

Local equilibrium sediment concentration power n

The power n in the local equilibrium sediment concentration must be equivalent to the velocity exponent in the sediment transport formula. In the case of coarse sand particles, the Engelund-Hansen formulations are applicable which corresponds to $n = 5$ (Engelund & Hansen, 1967). For fine sediments, such as mud or silt, the Partheniades-Krone formulations are employed. This conforms to $n = 3$, which implies that on average the speed exceeds τ_{crit} and thus sediment is put into motion.

Vertical exchange coefficient w_s

Parameter w_s describes the vertical exchange of sediment between the water column and bed. It is closely related to the fall velocity of the sediment particles and should be of the same order of magnitude. A greater vertical exchange of sediment occurs for a larger value of coefficient w_s (Buijsman, 1997). In other words, the response of the elements in the tidal inlet system is faster for a large w_s : sedimentation and erosion happens more quickly.

Horizontal exchange coefficient δ

The horizontal exchange coefficient δ represents the diffusive transport of water and sediment in the ASMITA model (Buijsman, 1997). The value depends on the element size, intertidal dispersion coefficient and the distance between two elements, as can be seen in Equation 3.13. Dispersion coefficient D is proportional to the tidal flow velocity, water depth and fall velocity, which is shown in Equation 3.14.

$$\delta = \frac{DA}{L} \quad (3.13)$$

$$\frac{D}{uH} \propto \frac{u}{w_s} \quad (3.14)$$

where:

δ	horizontal exchange coefficient	[m ³ /s]
D	intertidal dispersion coefficient	[-]
A	cross-sectional area linking two elements	[m ²]
L	distance between two elements	[M]
u	tidal flow velocity scale	[m/s]
H	water depth	[m]
w	fall velocity	[m/s]

The equations can be interpreted in the following manner: a sediment particle with a small fall velocity, being smaller in size, is able to remain in suspension for a longer time and travel further into the system, compared to a larger particle with higher fall velocity which results in quickly settling. Thus, a relatively large intertidal dispersion coefficient D corresponds to smaller particles whereas a smaller D corresponds to larger particles.

The horizontal exchange coefficient δ is also influenced by the distance between two elements and the cross-sectional area that connects them. A larger cross-sectional area leads to a greater horizontal exchange. In contrast, a shorter distance between elements results in an increase in δ .

Global equilibrium concentration c_E

The global equilibrium concentration c_E is based on field data and demonstrates the morphological activity in the tidal inlet system. The parameter is put into the ASMITA model as a boundary condition. It represents the morphological equilibrium adjacent to the outer model element. In the case of a three elements model, the global equilibrium concentration c_E represents the morphological activity at a location outside of the tidal inlet, adjacent to the ebb-tidal delta. The parameter is defined as cubic meters of soil per cubic meter of water. The sediment concentration in the water column is defined as mass per volume, for instance kg/m^3 . This amount of sediment in the water column can then be translated to a soil volume change, which is shown in Equation 3.15. An illustration of this is given in Figure 3.3.

$$c_E = \frac{c}{\rho_s} * n \quad (3.15)$$

where:

c_E	global equilibrium concentration	[-]
c	sediment concentration in water column	$[\text{kg}/\text{m}^3]$
ρ_s	sediment density	$[\text{kg}/\text{m}^3]$
n	porosity	[-]

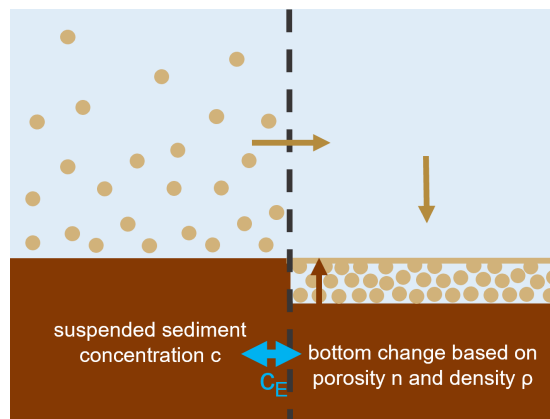


Figure 3.3: Schematisation of how the global equilibrium concentration c_E represents the relation between the suspended sediment concentration and bottom change by employing the porosity and density.

3.7 Multiple Elements Schematisation

As discussed in section 3.4, the most common ASMITA models use the 3 element schematisation. This means that the model consists of an ebb-tidal delta element, a channel element and a tidal flat element. Moreover, it has the potential to be extended to a multiple of the aforementioned elements. In this section, the formulations for the 3 element schematisation will be clarified.

In essence, the 3 element schematisation represents an extension of the formulations outlined in section 3.5. The one-element model is rewritten in a generalised form per element k as documented by Kragtwijk et al. (2004). The local equilibrium concentration is calculated according to Equation 3.16 and 3.17.

$$c_{k,e} = c_E \gamma_k \quad (3.16)$$

$$\gamma_k = \left(\frac{V_{k,e}}{V_k} \right)^{n\mu_k} \quad (3.17)$$

$c_{k,e}$	local equilibrium concentration	[kg/m ³]
c_E	global equilibrium concentration	[kg/m ³]
γ_k	ratio of local equilibrium concentration over global equilibrium concentration	[-]
$V_{k,e}$	equilibrium volume	[m ³]
V_k	actual volume	[m ³]
n	transport coefficient	[-]
μ_k	morphological element state: wet = -1 ; dry = 1	[-]

The sediment balance for element k is shown in Equation 3.18.

$$\sum_m \delta_{k,m} (c_k - c_m) = w_{s,k} A_k (c_{k,e} - c_k) + c_E \delta_{k,E} \quad (3.18)$$

$\delta_{k,m}$	horizontal exchange coefficient	[m ³ /s]
c_k	actual concentration of element k	[kg/m ³]
c_m	actual concentration of neighbouring element m	[kg/m ³]
$w_{s,k}$	vertical exchange coefficient	[m/s]
A_k	element plan area	[m ²]
$c_{k,e}$	equilibrium concentration	[kg/m ³]

The rate of volume change can be derived from the sediment balance and can be observed in

$$\frac{dV}{dt} = \mu_k A_k w_{s,k} (c_{k,e} - c_k) \quad (3.19)$$

The above equations describe the morphological development of one single tidal inlet element k . In the case of the 3 element schematisation, this process applies to three sets $k = 1, 2, 3$. For that reason, the equations are written in matrix form which is seen in Equation 3.20, 3.21 and 3.22 (Kragtwijk et al., 2004).

$$\frac{dV}{dt} = \mathbf{MW} (\vec{c}_e - \vec{c}) \quad (3.20)$$

$$\mathbf{D}\vec{c} = \mathbf{W} (\vec{c}_e - \vec{c}) + c_E \vec{\delta}_E \quad (3.21)$$

$$\vec{c}_e = c_E \vec{\gamma} \quad (3.22)$$

where:

$$\mathbf{M} = \begin{pmatrix} 1 & 0 & 0 \\ 0 & -1 & 0 \\ 0 & 0 & 1 \end{pmatrix} \quad (3.23)$$

$$\mathbf{W} = \begin{pmatrix} w_s A_1 & 0 & 0 \\ 0 & w_s A_2 & 0 \\ 0 & 0 & w_s A_3 \end{pmatrix} \quad (3.24)$$

$$\mathbf{D} = \begin{pmatrix} \delta_{12} & -\delta_{12} & 0 \\ -\delta_{21} & \delta_{21} + \delta_{23} & -\delta_{23} \\ 0 & -\delta_{32} & \delta_{32} + \delta_E \end{pmatrix} \quad (3.25)$$

When an ASMITA model with any different number of elements is desired, the setup can be adjusted by extending the matrices for the preferred number of elements. Additionally, it is possible to use more than one sediment fraction by introducing a subset of the above equations for each fraction. Accordingly, the parameter setting must be performed separately per sediment fraction.

Study Areas

This section will elaborate on the chosen study areas for the data analysis on historical salt marsh development. Section 4.1 lays out the requirements for a study area to qualify. The characteristics of the Dutch Wadden Sea are introduced in section 4.2. The salt marshes on Ameland and Schiermonnikoog, which will be used as study areas, are described in respectively section 4.3 and 4.4.

4.1 Requirements

There are three requirements that have to be met for a study area to qualify:

1. The salt marsh has had a natural development in the past,
2. A hindcast dataset on the hydrodynamics and salt marsh development with a minimum duration of ten years is available,
3. The hypsometric curve of the salt marsh is obtainable.

The first requirement is that the salt marsh has had a natural development in the past, i.e. no large human interventions such as land reclamations have been carried out. Interventions may undermine the natural processes by which the salt marsh development will be simulated in ASMITA. Areas that were influenced by past interventions are therefore unsuitable.

Secondly, a hindcast dataset on the hydrodynamics and salt marsh development of the study area with a minimum duration of ten years must be available. The hydrodynamic data can be used for deriving model parameters. Since ASMITA is a long-term morphological model, data on salt marsh development in the order of years should be present for model calibration and validation.

Lastly, the hypsometric curve of the salt marsh should be obtainable. This information is required for the derivation of the ASMITA model parameters. Moreover, it can be used to improve the interpretation of the model results.

Combining the above considerations, salt marshes on two barrier islands in the Dutch Wadden Sea have been qualified as study areas: Ameland and Schiermonnikoog.

4.2 The Dutch Wadden Sea

The Wadden Sea is a unique ecosystem situated along coasts in The Netherlands, Germany and Denmark. It is separated from the North Sea by barrier islands. The total area spans almost 500 km making it one of the largest intertidal wetlands in the world.

The Dutch part of the Wadden Sea is situated in the northern part of the country and consists of six tidal inlet systems. An overview of the different barrier islands and tidal inlets is shown in Figure 4.1. The tidal inlet systems are separated by the tidal watersheds, or tidal divides, indicated by the dashed lines. A tidal watershed is a location where two tidal waves traveling through adjacent inlets meet. Intertidal flats accrete at these locations, because the flow velocities are close to zero and thus sediment can settle. In this study, the locations of tidal watersheds are considered to be morphological boundaries between two tidal inlets. However, it should be noted that in reality a certain amount of flow is present over the tidal watersheds (Lodder et al., 2019).

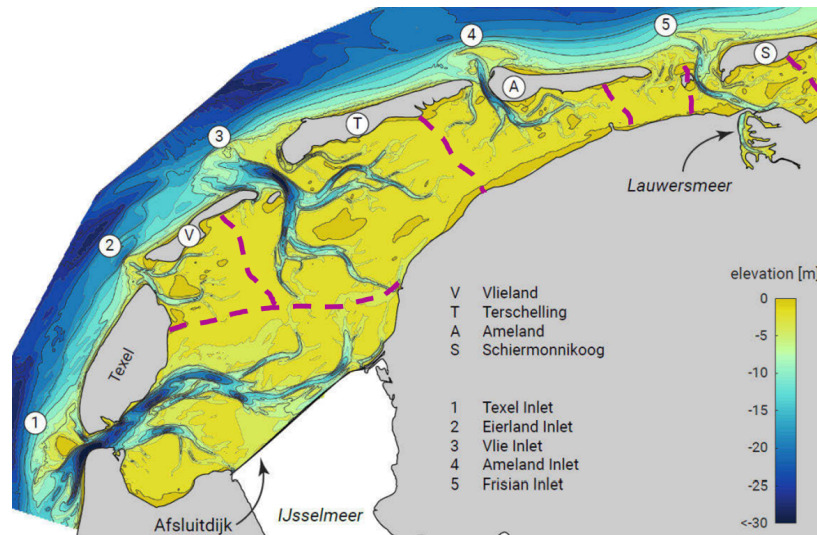


Figure 4.1: Tidal inlets in the Dutch Wadden Sea (Bosboom & Stive, 2021).

The morphological development of the Dutch Wadden Sea is governed by a driving force, which is the accommodation space, and a supply: the sediment import into the tidal inlet system. For the latter, three dominant processes are recognized in the Dutch Wadden Sea: residual flow, tidal asymmetry and dispersion. The residual flow is the relatively small and subtle difference between the two gross flood and ebb transports. Tidal asymmetry includes the difference between ebb and flood in terms of peak flow velocities and slack duration, which affects the quantity and grain size of the imported sediment. Dispersion causes sediment transport when a sediment concentration gradient is present in the tidal inlet system (Elias, 2006).

The eastern part of the Dutch Wadden Sea currently experiences a high rate of rSLR due to salt and gas mining, which causes land subsidence and increases the accommodation space. However, the Ameland inlet and Frisian inlet are characterised as accommodation space limited systems. This means that only a small amount of net sediment import occurs due to the fact that these systems are already close to their morphological equilibrium (Wang et al., 2018).

4.3 Salt Marshes on Ameland

Ameland is one of the barrier islands in the Wadden Sea, located in the northern part of the Netherlands. There are two salt marshes present on the island: Neerlandsreid and De Hon, as shown in Figure 4.2. Both salt marshes have different ages, histories and characteristics, which will be discussed per marsh in this section. A commonality is the fact that both salt marshes experience continuous deep subsidence caused by natural gas extraction that has occurred on the island since 1986 (Piening et al., 2017).

4.3.1 Neerlandsreid

Neerlandsreid is indicated by the pink area in Figure 4.2. It is situated near the tidal watershed of two tidal inlets: the Ameland inlet (Borndiep) and Frisian inlet (Pinkegat) (Oost and Cleveringa, 2017; Oost et al., 2020). Neerlandsreid started to develop as a salt marsh at the end of the 19th century, after the construction of a sand-drift dike (Slim et al., 2011). It was originally a washover area, which means that a dune was overtopped during high water and as a result, the deposition of sandy sediment behind the dune occurred (Oost & Cleveringa, 2017). Because the salt marsh originates from a washover, the soil composition is relatively sandy. A sediment layer of ~ 50 cm thickness was deposited 125 years after the construction of the sand-drift dike. The accretion was smaller for areas on the marsh with a less sandy subsoil (Oost et al., 2020).

Neerlandsreid has always been grazed by cattle. This may have affected marsh accretion significantly, especially due to the enhanced autocompaction by trampling (see section 2.6). The trampling activity of large grazers can negatively impact accretion rates due to increased autocompaction, whereas small grazers do not seem to exhibit such an effect. The consideration of the former is recommended by

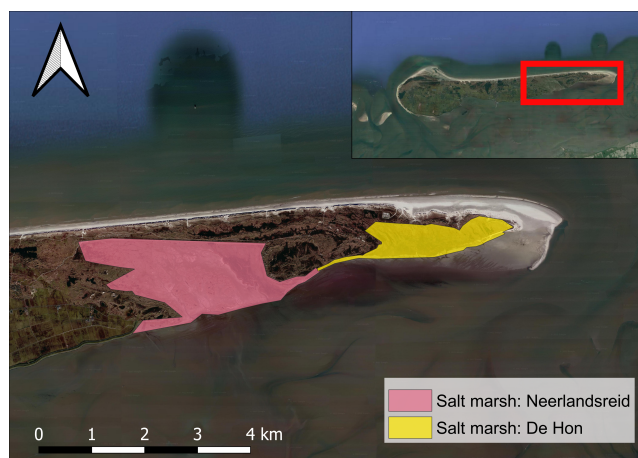


Figure 4.2: Locations of the Ameland salt marshes Neerlandsreid & De Hon.

Elschot (2015) in predictions of salt marsh survival under accelerating SLR. Moreover, the succession of plants on the salt marsh is affected. According to (Elschot, 2015), large grazers delay succession as they bring back young-successional plant species. This means that biodiversity is boosted. Small grazers are known to slow down succession. Both small and large grazers reduce vegetation height, but their impact on sediment deposition is negligible. The vegetation height on Neerlandsreid is around 5 cm due to grazing.

Research by Van Puijenbroek et al. (2022) reveals that Neerlandsreid experiences vegetation regression. This is especially common at locations with limited drainage further away from a sediment source. Additionally, locations with a significant amount of deep subsidence are prone to this phenomenon. The sedimentation is insufficient at these locations, and not able to keep up with SLR. As a result, more inundations occur which leads to wetter and saltier conditions. The changed conditions initiate vegetation regression and result in a transition from high marsh to low marsh vegetation. When drainage is insufficient, tidal pools are expected to arise at these locations (Hartig et al., 2002). At some locations on Neerlandsreid, bare patches occurred due to high stress.

According to Kuiters and Wegman (2020), 2.5 - 3.0 % of the total area of Neerlandsreid consists of creeks. An increase in this drainage system was observed during the last 20 years, especially in the northeastern part. This implies that more inundations of the higher northeastern marsh occurred. The water that inundated the marsh had to be drained and thus an increase in creeks was observed.

Neerlandsreid experienced a significant amount of cliff erosion during the period between 1949 and 1998, which led to a 2.8 % decrease in the marsh area. To avoid further erosion, a shore protection consisting of dump stone has been installed on the southern part of the marsh (Oost & Cleveringa, 2017). The shore protection is shown in Figure 4.3.



Figure 4.3: Shore protection on the Neerlandsreid salt marsh, Ameland (Wang, 2022).

As stated before, the effect of subsidence due to gas extraction is found on both the Ameland salt marshes. Neerlandsreid is located further away from the extraction point which means it also experiences less subsidence than De Hon (Piening et al., 2017; Elschot et al., 2017). The subsidence on Neerlandsreid since 1986, the year in which the extraction started, is 6 - 27 cm with an average rate of 7 mm/year (Kuiters & Wegman, 2020).

Van der Lugt et al. (2020) states that the Neerlands Reid salt marsh is situated between approximately 100 - 180 cm + NAP. Moreover, the local difference in high water levels between Neerlands Reid and De Hon is found to be small: in the order of 5 - 10 [cm]. However, it should be noted that this difference could increase due to storm set-up.

4.3.2 De Hon

De Hon is the younger salt marsh on Ameland and is entirely situated in the Frisian inlet (Pinkegat) (Oost et al., 2020). The salt marsh started to emerge around 1960 behind a natural dune row (Slim et al., 2011). De Hon has had an entirely natural development since no grazing by cattle took place on this salt marsh. Consequently, the salt marsh vegetation could go up to 30 cm in height.

Cliff erosion is observed in the southwestern part of De Hon. An expansion of the salt marsh area is seen in the southeastern part (Elschot et al., 2017; Oost et al., 2020). The area directly on the eastern side of the higher dunes shows an increase in surface height of 1 m during 12 years, despite the deep subsidence due to gas mining. A significant spatial variation is observed in this large elevation gain, given the presence of washovers and embryo dunes in close proximity to the salt marsh (Oost et al., 2020). The clay layer that was deposited on De Hon is significantly smaller than the clay layer on Neerlandsreid (Elschot et al., 2017).

The subsidence on De Hon since the beginning of the gas extraction in 1986 is 26 - 38 cm. This relates to an average subsidence rate of 10 mm/year, which is 3 mm/year larger than on Neerlandsreid (Kuiters & Wegman, 2020). Due to the large amount of subsidence, some locations on De Hon experience a decrease in surface height. Similar to Neerlandsreid, these locations are generally situated further from a sediment source. There are no bare patches on salt marsh De Hon since less stressful conditions prevail as a consequence of the absence of cattle.

4.4 Salt Marshes on Schiermonnikoog

Schiermonnikoog is situated next to Ameland in the barrier island chain in the Netherlands. A large part of the barrier island can be characterized as a salt marsh. Het Rif is the young salt marsh on the southwestern part of the island. Oosterkwelder is the larger salt marsh on the eastern part of the island.

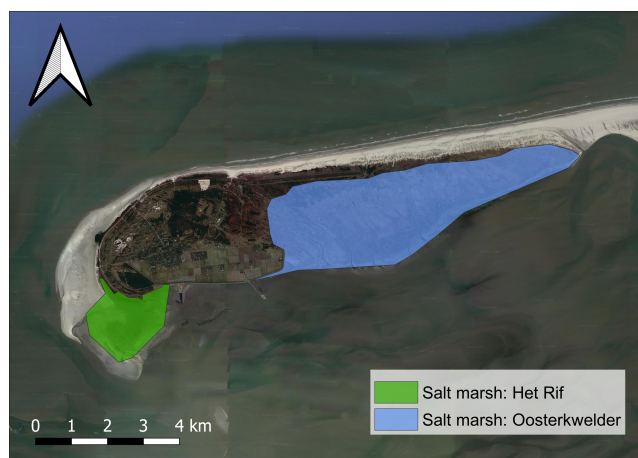


Figure 4.4: Locations of the Schiermonnikoog salt marshes Het Rif & Oosterkwelder.

4.4.1 Het Rif

Het Rif is a young salt marsh that mainly consists of a pioneer zone and low marsh. The area is located in the southwestern part of Schiermonnikoog, see Figure 4.4. Het Rif used to be a relatively high tidal flat. Due to the Lauwerszee closure, a large amount of sand became available. This allowed Het Rif to gain height over the course of approximately 30 years, after which vegetation could start to develop (Oost et al., 2020). The first observations of salt marsh vegetation occurred in the period around 2000. The marsh is not grazed and does not experience deep subsidence caused by the gas extractions on Ameland.

4.4.2 Oosterkwelder

The formation of the Oosterkwelder on Schiermonnikoog started when relatively large dunes developed on the northern part of the island. The area behind the dunes did not experience daily inundations by water from the North Sea anymore, only by water coming from the South. Current velocities and wave action in the Wadden Sea are much more limited than in the North Sea, which means that pioneer vegetation was able to establish on the sandy subsoil. As a result of the calmer hydrodynamic conditions and the newly established vegetation, fine-grained sediment was captured on Schiermonnikoog and the salt marsh was created (Olf et al., 1997; Elschot, 2015).

The marsh on Schiermonnikoog is characterized by a natural chronosequence, which refers to salt marsh areas that have developed at different points in time (Olf et al., 1997). Similar characteristics are recognized along the island but the age of the marsh and specifications such as plant succession stages and sediment deposition differ depending on the location. The oldest part of the marsh is situated on the western side and it becomes gradually younger while moving towards the east. The salt marsh in the southeastern part of the island is young and consists of a low marsh and pioneer zone only. In general, the younger marsh is said to have a thinner layer of silt on top of the sandy subsoil than the older marsh. The thickness of the fine-grained sediment layer ranges from 20 to 7 cm from west to east (Elschot, 2015).

The oldest marsh in the southwestern part of the Oosterkwelder is grazed. The remaining parts of the Oosterkwelder are relatively undisturbed by humans. In opposition to the salt marshes on Ameland, there is no significant amount of subsidence related to gas extraction.

Data Analysis

This chapter will present the data analysis that was conducted to achieve two main objectives: understanding & quantifying salt marsh development and generating datasets that can be used for the ASMITA model calibration, validation and derivation of parameters. Section 5.1 describes a hydrodynamic data analysis. Moreover, salt marsh vegetation was assessed in section 5.2. The salt marsh extent used in this research is explained in section 5.3. Data on subsidence rates on the salt marshes is discussed in section 5.4 Hereafter, vertical marsh height changes are assessed by examining different data types in section 5.5.

5.1 Hydrodynamic Data Analysis

The hydrodynamic data analysis is conducted to quantify the flooding frequency of salt marshes, which is defined as the average number of yearly inundations per marsh height. The number of inundations could subsequently be employed as an indicator for the salt marsh extent, which was previously elaborated upon in section 2.8. Moreover, the hydrodynamic data analysis will be used as a physical basis for the derivation of ASMITA salt marsh model parameters that were highlighted in Chapter 3.

The hydrodynamic data is obtained via Rijkswaterstaat (2022a). There are several water level measurement stations in the Wadden Sea from which hydrodynamic data can be extracted. As discussed in Chapter 4, the salt marshes on Ameland and Schiermonnikoog are primarily situated in the Frisian inlet. Neerlandsreid on Ameland is located next to the tidal watershed and experiences influence from two tidal basins. The same holds for the Oosterkwelder on Schiermonnikoog. Nonetheless, for simplicity, it is assumed that the salt marshes are mostly affected by the Frisian inlet. Consequently, hydrodynamic data was only extracted for the Schiermonnikoog station, as this is the only available data collection point in the Frisian inlet, see Figure 5.1.

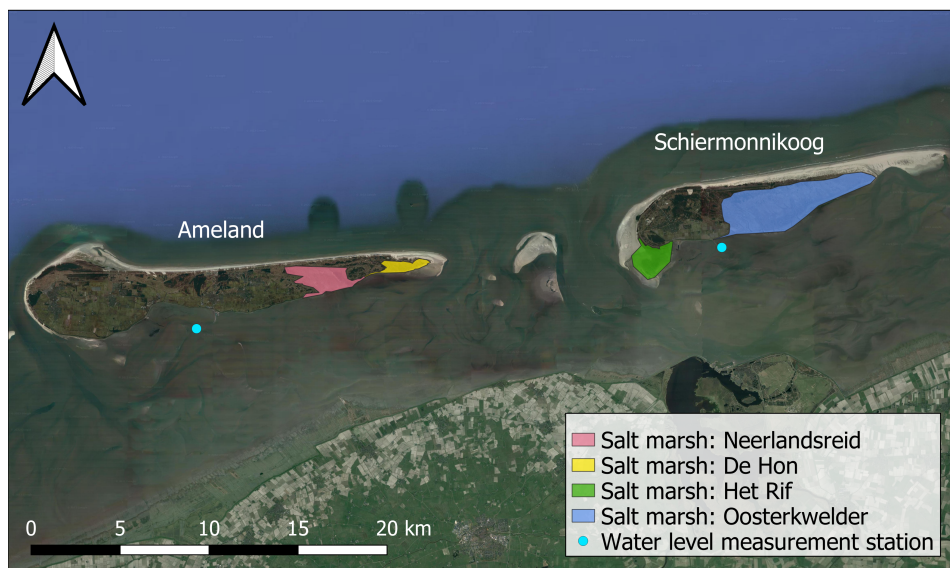


Figure 5.1: An overview of the salt marsh locations on Ameland and Schiermonnikoog along with the water level measurement stations.

The hydrodynamic data analysis consists of a peak water level analysis for the past ten years, from which the average number of yearly inundations per marsh height is obtained. The result is used to determine the salt marsh extent, which in most literature is defined based on the inundation frequency (see Chapter 2). The main goal of the hydrodynamic data analysis was to acquire insight into the average number of yearly salt marsh inundations. The hydrodynamic dataset includes the rate of SLR that was present over the past decade, which leads to an increase in yearly marsh inundations. It is thus beneficial that the SLR rate of the past decade is included in the hydrodynamic dataset since it directly affects the average number of yearly marsh inundations.

Figure 5.2 demonstrates the average number of yearly inundations on the y-axis for the corresponding marsh height on the x-axis. The analysis was based on water level measurements from 2012 up to and including 2022. The exact values for yearly inundations are given in Table 5.1. It can be observed that MHW, which is defined as the average of all high tides, is situated between a height of 100 and 110 cm + NAP as this corresponds to ~ 365 yearly inundations. This matches the MHW analysis that was carried out by Stolte et al. (2022), in which MHW is said to be around 106 cm + NAP in 2022.

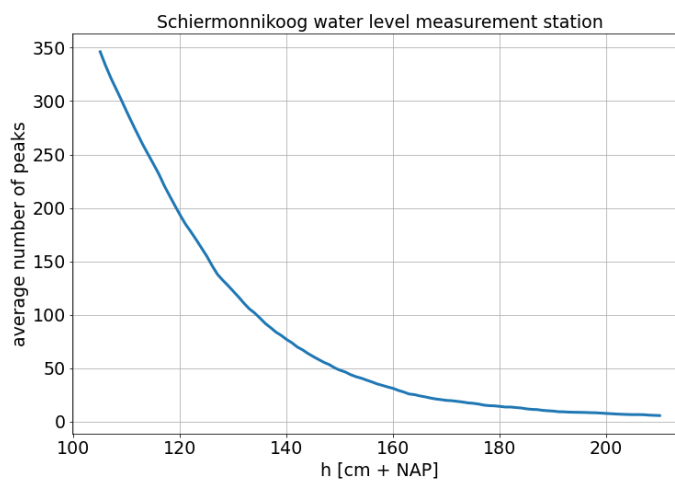


Figure 5.2: Average yearly inundations per water level from 2012 - 2022.

h [cm + NAP]	average yearly inundations
100.0	404.5
110.0	289.8
120.0	193.3
130.0	121.8
140.0	76.7
150.0	48.0
160.0	30.9
170.0	19.7
180.0	14.1
190.0	9.7
200.0	7.5
210.0	5.5
220.0	4.2
230.0	3.3
240.0	2.2

Table 5.1: Average yearly inundations per marsh height above NAP out of a 10-year dataset for the Schiermonnikoog station.

5.2 Vegetation Zonation

The different types of vegetation on the Ameland & Schiermonnikoog salt marshes will be analysed. Section 2.5 already elaborated on the process of vegetation establishment on a salt marsh and declared that the type of vegetation provides insight into the marsh elevation and inundation frequency.

Rijkswaterstaat monitors salt marshes in the Netherlands and maps the areas according to different criteria for vegetation. No strict requirements in terms of mapping frequency and coverage are present, but every six years a statement must be made regarding the vegetation changes in Dutch salt marshes over a time span of twelve years. The vegetation mapping is carried out by an analysis of aerial photos in combination with fieldwork (Rijkswaterstaat, 2022b).

For Ameland and Schiermonnikoog, the most recent vegetation maps stem from respectively 2020 and 2016. They are shown in Figure 5.3a and 5.3b. A distinction is made between different zones: the prepioneer zone, pioneer zone, low marsh, middle marsh and high marsh. The zones are composed based on vegetation types, the occurrence of species, abiotic factors and other characteristics of a certain structure. Details on this for respectively Ameland and Schiermonnikoog are given by Rijkswaterstaat Publicatie Platform (2016) and Rijkswaterstaat Publicatie Platform (2012).

According to this classification, Neerlandsreid consists of a low, middle and high marsh. The largest part of the other salt marsh on Ameland, De Hon, is a low marsh. In the southeastern part of De Hon, a pioneer zone is present. Small zones of middle or high marsh can also be observed. Het Rif on Schiermonnikoog is a young salt marsh, which is also revealed by the vegetation zonation map: it includes a pioneer zone and a low marsh only. The Oosterkwelder marsh is older and mainly composed of middle and high marsh zones. A low marsh and pioneer zone is present near the southern part of the Oosterkwelder, which is located closer to the Wadden Sea.



(a) Ameland: Rijkswaterstaat (2020).



(b) Schiermonnikoog (Rijkswaterstaat, 2016).

Figure 5.3: Salt marsh vegetation zones.

5.3 Salt Marsh Extent

Different definitions are used to determine the salt marsh boundaries (see section 2.8). Some use a number of inundations per year for the classifications (refs), others base it on vegetation type (ref). Here we compare the data analyses of the flooding frequencies per marsh height from section 5.1 and the vegetation zonation of Rijkswaterstaat from section 5.2 to come to a marsh extent definition for Asmita. The two datasets have been compared by superimposing the water level and vegetation maps.

A comparative analysis was established between the flooding frequencies per marsh height based on the hydrodynamic data analysis that was carried out in section 5.1 and the vegetation zonation of Rijkswaterstaat (section 5.2). The two datasets have been compared by superimposing the water level and vegetation maps. The hydrodynamic data analysis was leading to determining the final marsh extent.

The salt marsh extent for this research is set at a range from 105 - 210 cm + NAP. This corresponds to frequencies of approximately 350 - 5 floodings per year. The specifications are shown in Figure 5.4. The lower marsh is situated between approximately 105 - 145 cm + NAP. This was found by comparing the vegetation zonation maps from section 5.2 with height maps of the salt marsh. It also complements the inundation frequencies found in section 5.1 compared to previous studies, in which the upper limit for the low marsh was within the inundation frequency range of 60 to 100 (section 2.8). The high marsh is situated between 145 - 210 cm + NAP. The upper limit of the salt marsh extent used for this research corresponds to roughly 5 inundations per year, which also corresponds to the salt marsh extent in literature.

Salt marsh extent in this research = 105 - 210 cm + NAP.

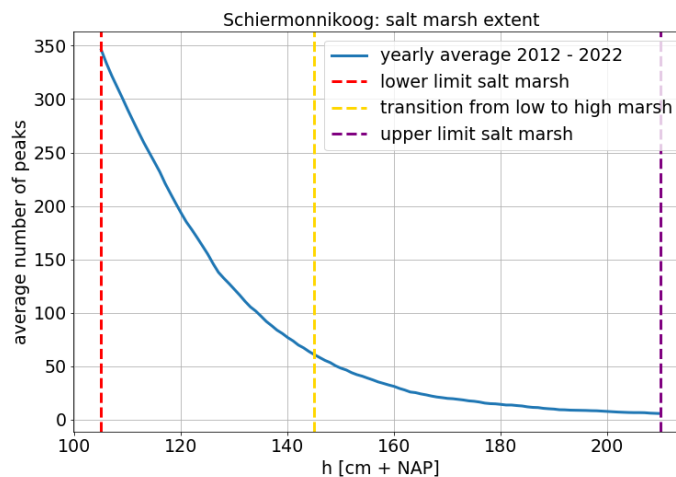


Figure 5.4: Salt marsh extent to be used in this research.

5.4 Subsidence

As discussed in Chapter 4, a significant deep subsidence rate is recorded on Ameland due to gas extraction. This strongly affects the salt marshes, as can be seen in Figure 5.5. The largest subsidence is experienced on salt marsh De Hon since this marsh is situated closer to the gas extraction source. The magnitude of subsidence on De Hon decreases when moving from west to east and is equal to -150 up to -330 mm since 1986. For Neerlandsreid, less subsidence is experienced and the magnitude decreases when moving from east to west. Since 1986, the subsidence in the eastern part of Neerlandsreid can be equal to -270 mm which decreases to -50 mm at the western boundary of the salt marsh. Piening et al. (2017) states that an average subsidence of 7 mm/year is experienced on Neerlandsreid and this value is equal to 10 mm/year on De Hon.

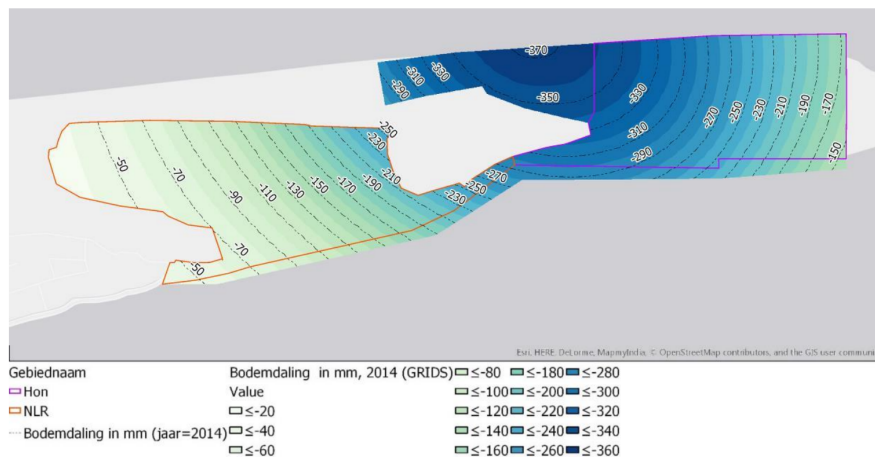


Figure 5.5: Deep subsidence due to gas extraction on Ameland: Neerlandsreid is roughly indicated by the orange line and De Hon is roughly indicated by the pink line (Elschot et al., 2017).

For Schiermonnikoog, no deep subsidence is present. The shallow autocompaction due to aging and trampling by cattle is of a different order of magnitude than the deep subsidence on Ameland. Moreover, the salt marshes on Ameland experience shallow autocompaction as well. An estimation of the shallow autocompaction is given in Figure 5.6. It corresponds to ~ -0.9 mm/year for Schiermonnikoog. The shallow autocompaction is most likely in the same order of magnitude on Ameland but could be somewhat larger on Neerlandsreid due to grazing activities.

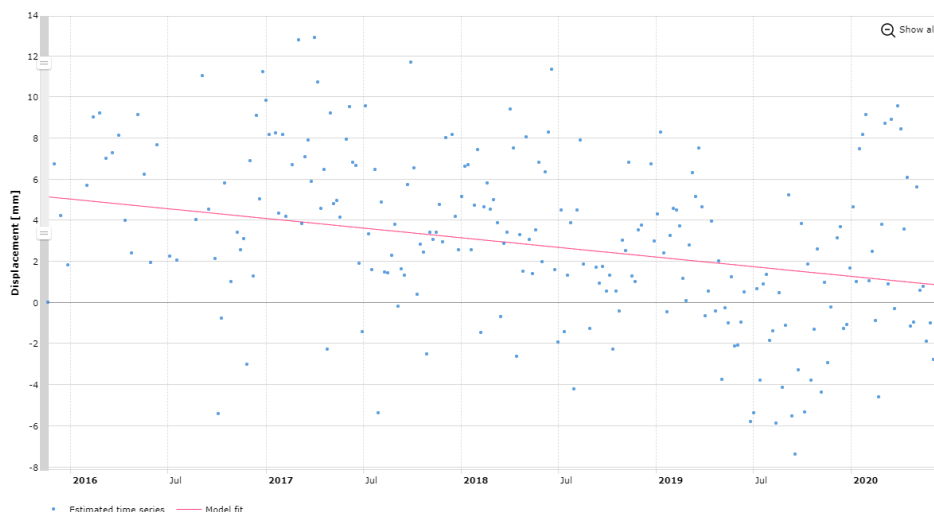


Figure 5.6: The estimated shallow autocompaction on the Oosterkwelder salt marsh on Schiermonnikoog is equal to -0.9 mm/year (Nederlands Centrum voor Geodesie en Geo-informatica (NCG), 2022).

5.5 Historical Salt Marsh Development

The historical development of the salt marshes on Ameland and Schiermonnikoog must be assessed in order to validate the ASMITA model extension. The salt marsh development will be studied by analysing Digital Terrain Models of the study areas in subsection 5.5.1. Moreover, local measurements that were obtained by sedimentation erosion bars (SEBs) will be investigated in subsection 5.5.2. A comparison between the two data types will be conducted in subsection 5.5.3.

5.5.1 Digital Terrain Models

A Digital Terrain Model (DTM) is a height map that captures the bare Earth's surface. The data is obtained by laser altimetry using airplanes, which is why it is called Laser imaging Detection And Ranging (LiDAR) data. The raw point clouds that are obtained from LiDAR data contain ground and non-ground points. The point cloud can be transformed into a Digital Surface Model (DSM) by interpolation (Chen et al., 2017). This results in a height map that fully covers the area evaluated by the airplanes.

The blue line in Figure 5.7a shows the heights that are captured in a DSM. The raw point cloud data is classified into ground and non-ground points, which enables the construction of a DTM by removing all natural and man-made features. This yields a height map of the bare earth surface, as indicated by the blue line in Figure 5.7b.

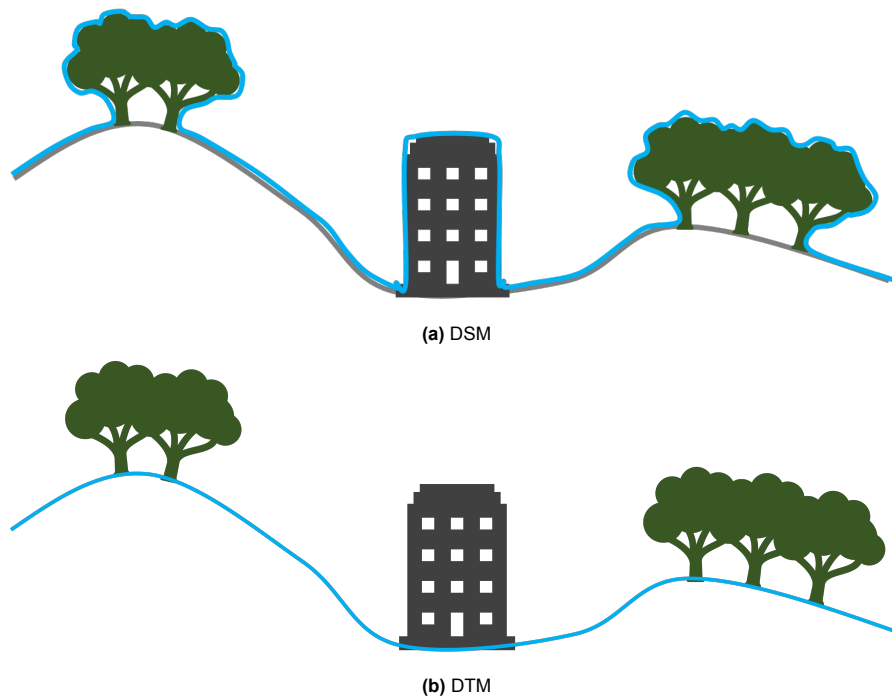


Figure 5.7: The difference between a Digital Surface Model (DSM) and a Digital Terrain Model (DTM).

The bathymetry of the salt marshes on Ameland and Schiermonnikoog can be obtained by an analysis of DTMs provided by Van Natijne (2021). The DTMs used in this study are part of the Actueel Hoogtebestand Nederland (AHN) and have a resolution of 5x5 m. The Dutch government set up the AHN in 1997 and ever since four LiDAR datasets of the altitude in The Netherlands have been obtained. These datasets do not stem from one year, but each dataset is collected over a couple of years. The full timespan of the AHN data is approximately 25 years. It should be noted that the exact date of data collection at the salt marsh locations is unknown. Table 5.2 shows an overview of the years in which the different data was collected for The Netherlands and Ameland & Schiermonnikoog specifically. The different AHN datasets will be compared in order to say something about the change in elevation for the salt marshes on Ameland and Schiermonnikoog.

dataset	range of collection years	collection for Ameland & Schiermonnikoog
AHN 1	1997 - 2004	1998 - 1999
AHN 2	2007 - 2012	2008
AHN 3	2014 - 2019	2014
AHN 4	2020 - 2022	2020

Table 5.2: Collection years of the AHN datasets according to Actueel Hoogtebestand Nederland (2022).

The hypsometric curves, which are extracted from the AHN data, will be studied in this section. A hypsometric curve depicts the wetted surface area as a function of the water level. In the context of this research, the hypsometric curve shows the cumulative marsh surface area as a function of the salt marsh heights. A steep hypsometric curve indicates little intertidal storage area: for every water level, the wetted surface area of the basin continuously increases. A hypsometric curve with a flatter course indicates that there is a considerable intertidal storage area: the wetted surface area suddenly increases significantly for a minor increase in the water level. The latter is expected for the salt marshes.

Vertical development of hypsometric curves corrected for rSLR

It is worth emphasizing that the DTMs from which the hypsometric curves were extracted include rSLR, which includes deep subsidence and SLR. To get a better idea of the salt marsh development in terms of accretion, a correction for rSLR was carried out. For this analysis, it is assumed that the SLR rate during AHN data collection was equal to 2 mm/year. As discussed in section 5.4, significant deep subsidence occurs on Ameland. For Neerlandsreid and De Hon, the subsidence rate is equal to respectively 7 and 10 mm/year. Schiermonnikoog is not influenced by deep subsidence. Table 5.3 summarizes the values that are used for the rSLR correction per salt marsh and AHN dataset.

AHN	year of data collection	Neerlandsreid [cm]	De Hon [cm]	Het Rif [cm]	Oosterkwelder [cm]
1	1998 - 1999	18.9	25.2	4.2	4.2
2	2008	10.8	14.4	2.4	2.4
3	2014	5.4	7.2	1.2	1.2
4	2020	0	0	0	0

Table 5.3: AHN hypsometry correction values for rSLR.

The hypsometric curves of the Ameland salt marshes with a correction for rSLR are shown in Figure 5.8. It can be observed that the order of the hypsometric curves now corresponds to a higher hypsometry for more recent data. This shows that sedimentation occurred on the Ameland salt marshes, which could not yet be derived from the hypsometric curves in the previous section due to the significant deep subsidence in combination with SLR. For both Neerlandsreid and De Hon, the hypsometry data for AHN 1 - 3 roughly coincide. This implies that the sedimentation rate was adequate to match rSLR but insignificant to generate an increase in marsh height. The hypsometric curve for AHN 4 is situated relatively far above the other AHN curves. Appendix A shows the result for the hypsometric curves without correction for rSLR, in which AHN 4 is also observed to be an outlier: the AHN 4 curve is larger than AHN 3 for the Ameland salt marshes whereas it was expected to be smaller. Hypotheses for this anomaly will be discussed in Chapter 8.

Figure 5.9 shows the corrected hypsometric curves for the Schiermonnikoog salt marshes. A gradual increase in salt marsh hypsometry is observed for Het Rif. For the Oosterkwelder, AHN 1 is situated relatively far below the other three datasets. AHN 2 and AHN 3 are consecutively higher. However, AHN 4 demonstrates atypical results again, given its placement below AHN 3.

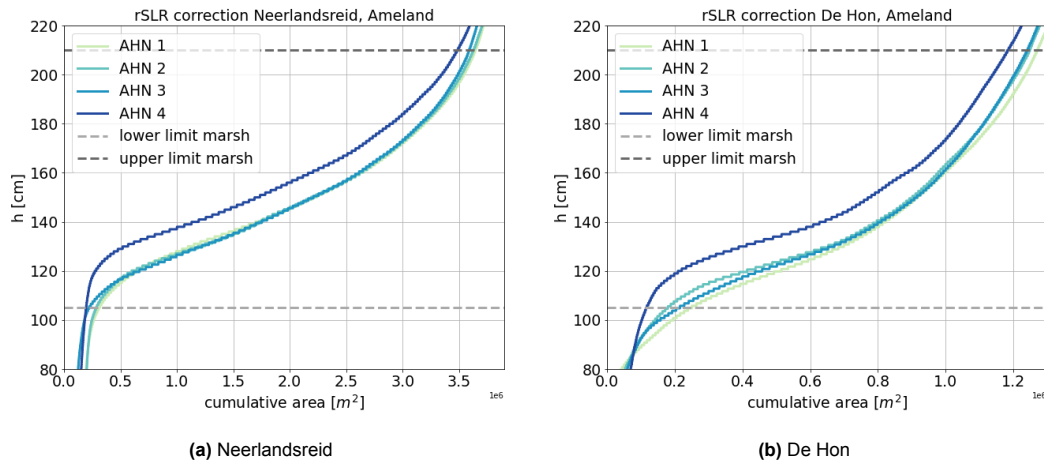


Figure 5.8: Ameland: hypsometric curves corrected for rSLR, where the y-axis represents the height relative to MHW (indicated by the lower limit marsh).

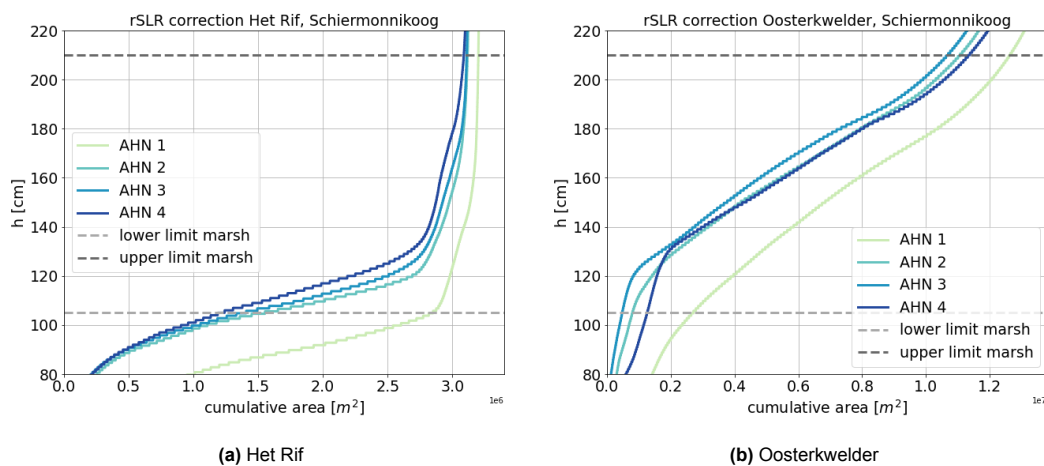


Figure 5.9: Schiermonnikoog: hypsometric curves corrected for rSLR, where the y-axis represents the height relative to MHW (indicated by the lower limit marsh).

Spatial differences in salt marsh development

The hypsometric curves give a qualitative idea about the general patterns in salt marsh development. However, the spatial distribution of sediment over the salt marsh strongly varies depending on the location. As previously mentioned, sedimentation is highly influenced by the distance to the nearest sediment source: a creek or marsh edge. Generally speaking, the closer the marsh location is to the sediment source, the more sedimentation occurs. Areas that are situated further away receive a reduced amount of sediment. The spatial patterns in salt marsh development over time will be discussed here. In opposition to the previous analysis, no correction for rSLR was carried out for the spatial analysis: the raw AHN datasets are used, which were also studied in Appendix A.

The spatial analysis is carried out for the oldest and youngest datasets: AHN 1 and AHN 4. Table 5.2 shows that the time lag between AHN 1 and AHN 4 is 21 - 22 years. The spatial differences over time can be observed in respectively Figure 5.10 and 5.11 for the salt marshes of Ameland and Schiermonnikoog.

Both Neerlandsreid and De Hon experienced a significant height decrease over the 21-22 years between AHN 1 and AHN 4, which is indicated by the blue colour. The areas close to a sediment source, like a creek or marsh edge, remained at the same level or even experienced a minor height increase, as indicated by the white and red coloured areas. The impact of the proximity to the nearest sediment

source is primarily visible for Neerlandsreid in Figure 5.10a. The areas surrounding the marsh edge and the large creek on the eastern part of the salt marsh remain lightly red coloured. Whereas the locations further away from a sediment source experienced a substantial decline in marsh height. The spatial patterns for De Hon are somewhat less apparent. The entire western part of De Hon experienced a decrease in height, which may be appointed to the significant effect of gas extraction at this location. An increase in salt marsh height is observed around the creeks and on the southeastern part of the marsh, which is most likely due to the close proximity to the sediment source.

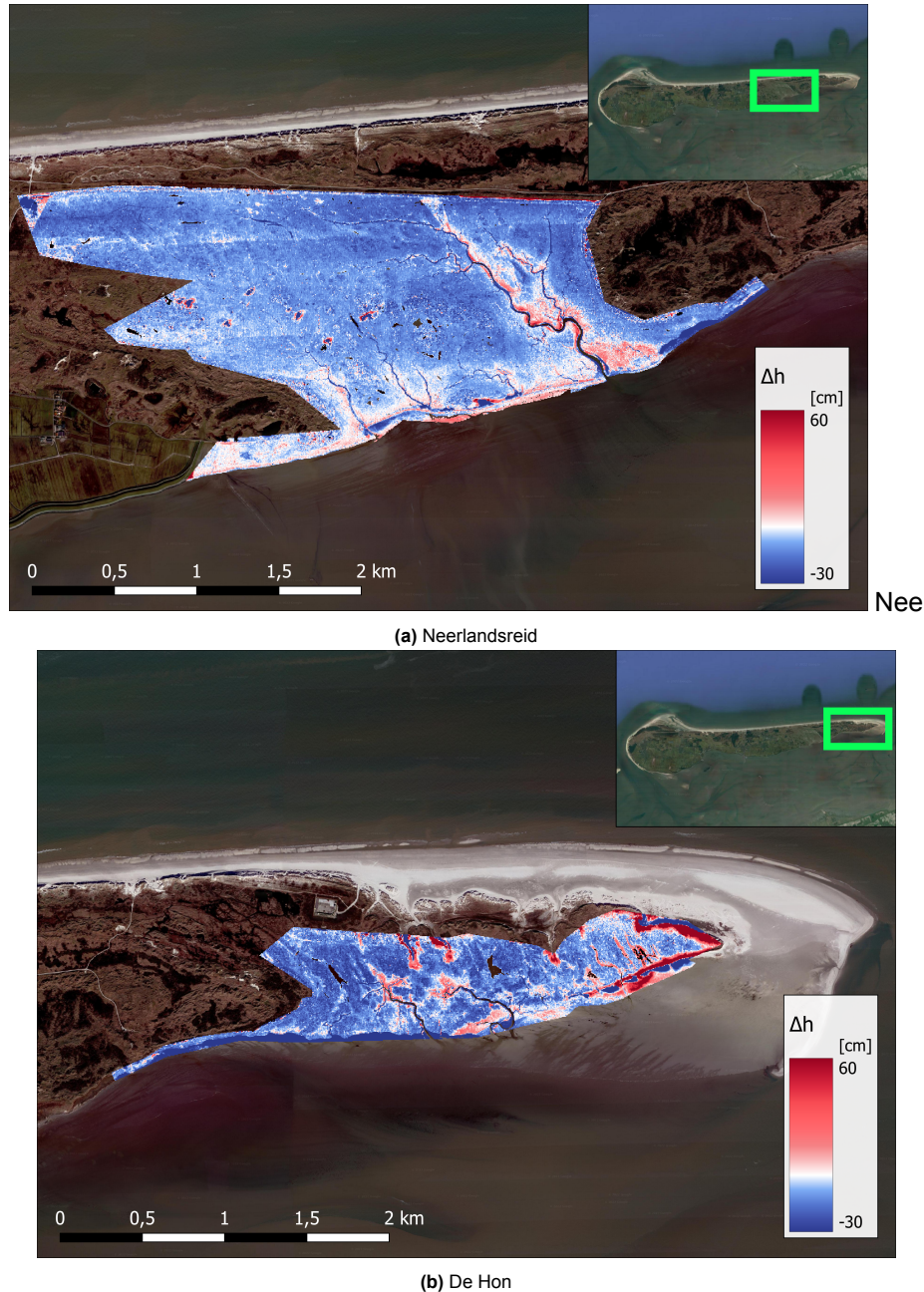
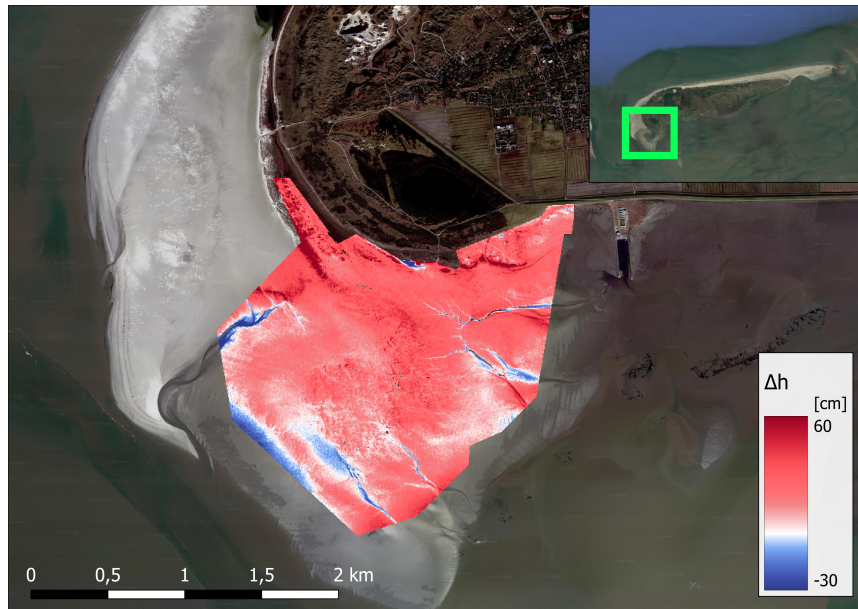
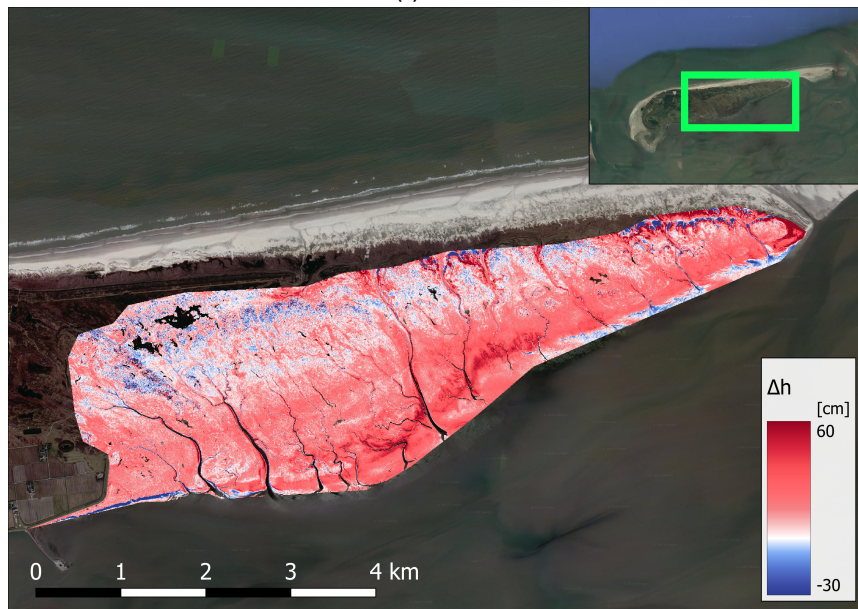


Figure 5.10: Spatial differences between AHN 4 (2020) and AHN 1 (1998 - 1999) for the Ameland salt marshes without correction for rSLR.

The spatial patterns over time for the salt marshes on Schiermonnikoog are very different compared to Ameland. Figure 5.11 depicts a predominantly positive trend in terms of height change during the timespan between AHN 1 and AHN 4, since the largest part of the salt marshes is coloured red and white. This is in line with the expectations: no major subsidence is present and thus sediment accumulation is the dominant process for marsh development. The largest height increase is not necessarily located closest to the marsh edges for both Het Rif and Oosterkwelder. Instead, the darkest red areas are situated slightly further inland. The outer edges of the salt marshes are generally light-red, white, or even blue. This could possibly point to cliff erosion. For Oosterkwelder, the northwestern part of the salt marsh experiences a decrease in height. This may indicate the formation of tidal pools.



(a) Het Rif



(b) Oosterkwelder

Figure 5.11: Spatial differences between AHN 4 (2020) and AHN 1 (1998 - 1999) for the Schiermonnikoog salt marshes without correction for rSLR.

5.5.2 Local Measurements: SEBs

Local measurements on the salt marshes were carried out by sedimentation-erosion bars, which will be referred to as SEBs from now on. Measuring sticks are installed at different locations on the salt marsh, as illustrated in Figure 5.12. A SEB involves two or three poles separated by a minimum distance of 2 m horizontally. They are installed at a minimum depth of 1 m. The SEBs measure the change in surface layer thickness. This includes sedimentation, deposition of plant biomass and autocompaction of the soil layer. It should be noted that deep subsidence, for example due to gas mining, is not measured by the SEBs since the measurement set-up experiences subsidence as well (Elschot et al., 2017). Local government benchmarks were used to relate the elevation of the SEBs elevation to NAP. This was done by means of geodetic methods. Additionally, a geostatistical model was employed for the temporal and spatial interpolation between precision leveling of benchmarks (De Groot, 2009).

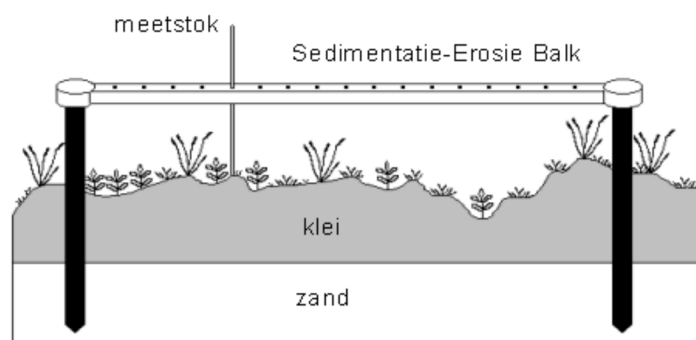


Figure 5.12: SEBs measurement method (Elschot et al., 2017).

The SEBs on Ameland consist of two poles with 17 pin measurement points. For Schiermonnikoog, a triangle set-up with three poles was used which corresponds to 51 pin measurement points. The SEB measurements on Ameland and Schiermonnikoog are carried out twice a year: during early spring and late summer. The latter provides the best indication for net accretion since the largest amount of sedimentation occurs in winter and the maximum autocompaction is reached in summer (Elschot et al., 2017). The salt marsh accretion for a specific SEB is calculated by the difference in surface height between two subsequent measurements. As previously mentioned, sedimentation, erosion, autocompaction and swelling or shrinkage are included in this accretion measurement (Van Dobben et al., 2022). For both study areas, the late summer measurement was selected for further analyses. The years over which measurements are available differs per area.

SEBs on Ameland

The SEB locations on the Ameland salt marshes Neerlandsreid and De Hon are shown in respectively Figure 5.13 and 5.16. The SEBs are clustered based on their locations. Specifications per SEB are given in Table 5.4 and 5.5.

The surface height change for salt marsh Neerlandsreid can be observed in Figure 5.14a. The surface height relative to NAP is shown in green. The x-axis contains the PQ number, for which the distance to the marsh edge increases from left to right. The right-hand side is situated further away from the marsh edge than the left-hand side. The PQs are distributed across a 1 km stretch. The exact distances to the marsh edge for each PQ are shown in Table 5.4, along with the distance to the nearest creek. The dark green colour corresponds to the oldest year from which data was available: 1995. The most recent data is indicated by the light green colour. The data shows that the lower part of the salt marsh generally maintains a steady surface height relative to NAP. The high marsh experiences a decrease in surface height over the time span 1995 - 2021.

As previously mentioned, a significant rate of deep subsidence is present on Ameland. Therefore, the change in surface height does not directly translate to the accretion. The cumulative accretion from 1993 - 2018 on Neerlandsreid is illustrated in Figure 5.14b. The darkest colour corresponds to the largest cumulative accretion and the most recent data. Lighter shades signify lower cumulative accretion and greater age of the corresponding data. It becomes evident that a relatively large accretion rate is present on the lower marsh. The high marsh only receives a limited volume of sediment. A peak

in de cumulative accretion is seen for locations near a creek, for example PQ 305 and 308.

Finally, the average accretion rate per PQ is shown in Figure 5.15. Relatively high accretion rates prevail on the lower part of Neerlandsreid. The highest PQs even display a negative accretion rate, which indicates erosion. An average value of 4.25 mm/year is recorded for salt marsh Neerlandsreid on Ameland for a time span of 25 years.

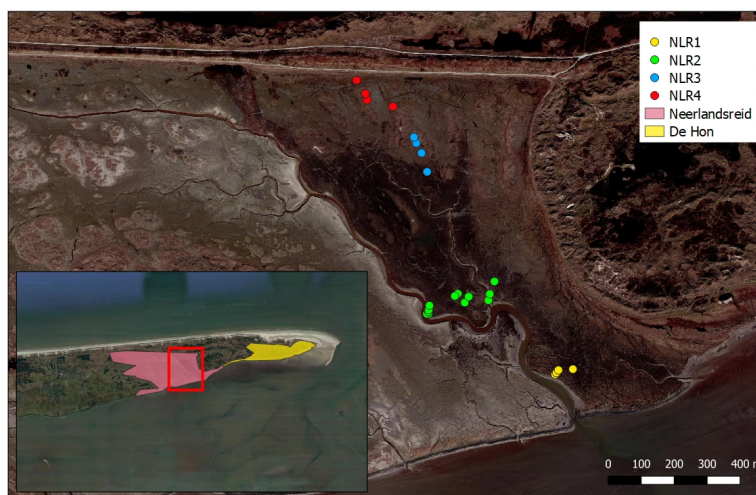
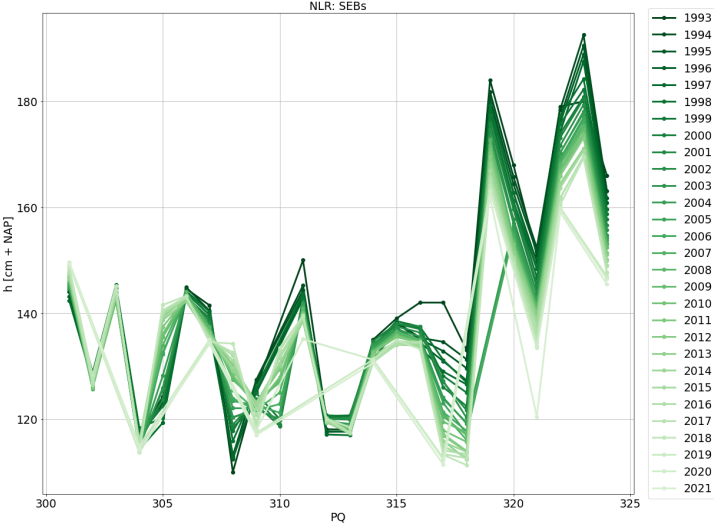


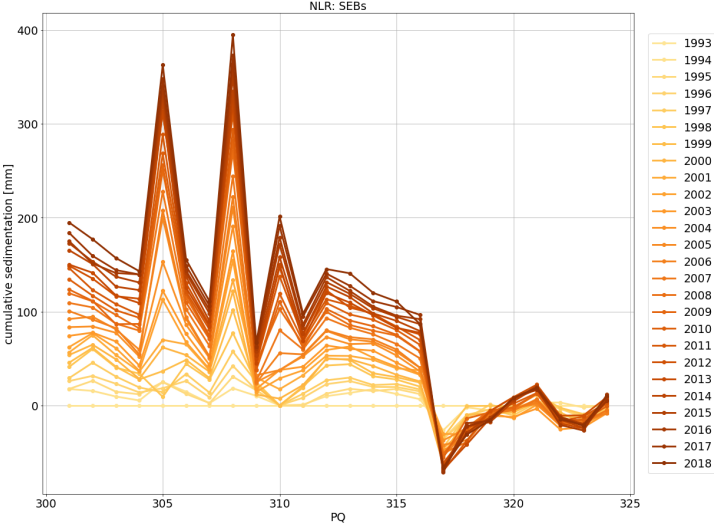
Figure 5.13: Neerlandsreid

cluster	PQ	distance to nearest creek [m]	distance to marsh edge [m]
NLR1	301	20	162
	302	26	164
	303	36	168
	304	29	150
NLR2	305	3	428
	306	6	447
	307	5	480
	308	0	433
	309	21	449
	310	0	463
	311	7	458
	312	8	420
	313	7	422
	314	15	427
	315	16	432
316	15	444	
NLR3	317	122	935
	318	124	940
	319	126	942
	320	128	953
NLR4	321	174	1058
	322	188	1095
	323	208	1115
	324	250	1161

Table 5.4: SEB clusters for salt marsh Neerlandsreid, Ameland.



(a) Surface height relative to NAP.



(b) Cumulative accretion.

Figure 5.14: SEBs on Neerlandsreid, Ameland.

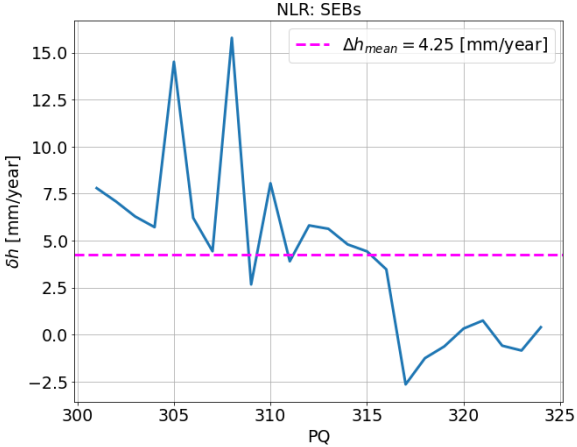


Figure 5.15: Neerlandsreid, Ameland: average accretion rate.

Salt marsh De Hon is situated in the eastern part of Ameland. The SEBs are grouped closer together compared to Neerlandsreid. They are located within a 400 m range. The surface height change is presented in Figure 5.17a. Again, the darker colours represent the oldest data and the lighter colours represent more recent data. A slight decrease in surface height is observed for the lower part of salt marsh De Hon. A larger magnitude of decrease in surface over time is seen as we move further inland, i.e. from left to right in the plot. The high marsh sinks more rapidly than the low marsh.

The cumulative accretion from 1995 - 2018 on De Hon is illustrated in Figure 5.17b. From dark to light, a high to low cumulative accretion is shown for younger to older data. Similar to the observations for salt marsh Neerlandsreid, it is apparent that a large accretion rate occurs on the lower marsh. The high marsh is characterized by lower cumulative accretion.

Figure 5.18 shows the mean accretion rate for salt marsh De Hon. A comparable trend as for Neerlandsreid is observed. However, the magnitude of the accretion rates is somewhat smaller. The mean accretion rate is equal to 2.72 mm/year.

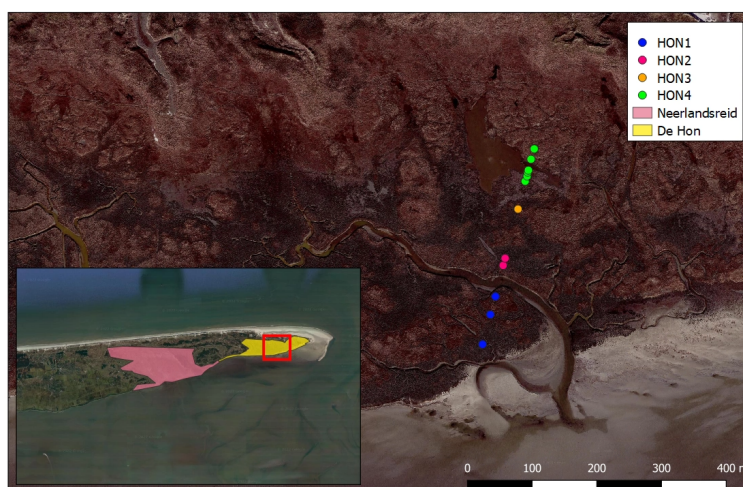
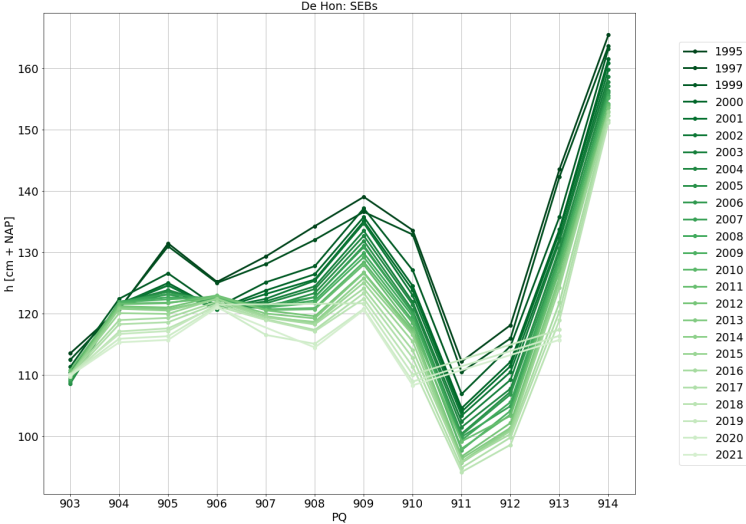


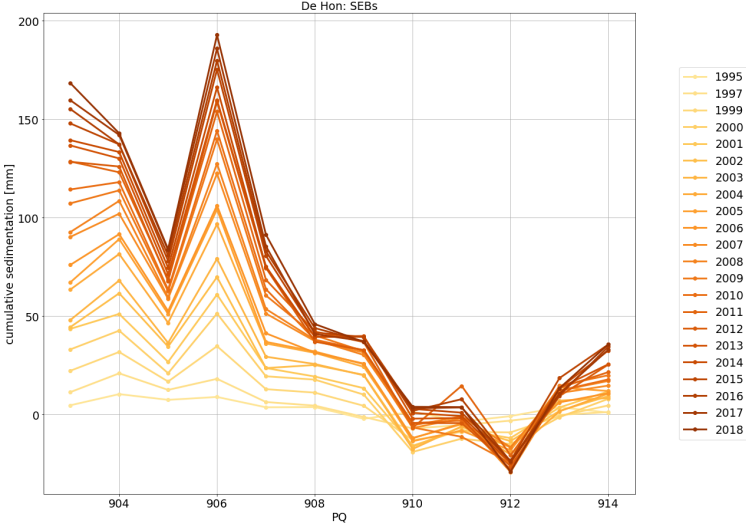
Figure 5.16: De Hon

cluster	PQ	distance to nearest creek [m]	distance to marsh edge [m]
HON1	903	7	122
	904	17	162
	905	8	183
HON2	906	10	223
	907	21	233
HON3	908	97	301
HON4	909	89	339
	910	87	345
	911	86	350
	912	86	350
	913	87	368
	914	91	381

Table 5.5: SEB clusters for salt marsh De Hon, Ameland.



(a) Surface height relative to NAP.



(b) Cumulative accretion.

Figure 5.17: SEBs on De Hon, Ameland.



Figure 5.18: De Hon, Ameland: average sedimentation rate.

SEBs on Schiermonnikoog

The SEBs on Schiermonnikoog are only situated in the Oosterkwelder. They are clustered in different locations, which are indicated by the names T0, T1, T2, T3, T5 and OBK. The locations of the SEBs on the Oosterkwelder are shown in Figure 5.19. For every location, less spatial differentiation is present than on the Ameland SEBs. Typically, the distance between the SEBs within one cluster is in the order of 10 m.

There are two types of SEB measurement set-ups for the Oosterkwelder: SCH1 and SCH2. The SCH1 measurement set-ups are situated at the interface between depressions and elevated parts of the marsh platform. This measurement set-up is present at all cluster locations: SCH1-T0, SCH1-T1, SCH1-T2, SCH1-T3, SCH1-T5 and SCH1-OBK. The SCH2 set-ups are more uniform in height. SCH2 is only available for the locations that are portrayed as SCH-T0, SCH-T1, SCH-T2 and SCH-T3 in Figure 5.19. Location specifications per SEB are given in Table 5.6 and 5.7 for the SCH1 and SCH2 data. The clusters T0, T1 and OBK are found closest to the marsh edge. The largest distance to the marsh edge is observed for T3 and T5. All clusters are situated within 300 m of the nearest creek.



Figure 5.19: Locations of SEBs on Schiermonnikoog.

In opposition to Ameland, no significant deep subsidence is present for Schiermonnikoog. Therefore, the change in surface height can be directly related to accretion as measured by the SEBs. Consequently, no separate plot for the cumulative accretion is given for Schiermonnikoog. The surface height change for the different SEB clusters of SCH1 and SCH2 are shown in Figure 5.20 and 5.21.

Figure 5.20 shows that a positive change in surface height is detected for all SEBs. As mentioned before, the spacing between the different SEBs is relatively small: in the order of 10 m. This means that there is no relation between the location on the x-axis and the distance to the marsh edge, as was the case for the Ameland SEBs. However, when comparing Table 5.6 with the Figure 5.20, it is seen that the clusters located closer to the marsh edge, e.g. T0 and T1, generally experience more accretion than clusters located further away, such as T5. The OBK cluster demonstrates a relatively small change in surface height. This may be attributed to the presence of lower vegetation due to grazing. The OBK cluster is the only part of the Oosterkwelder where grazing takes place.

The SCH2 measurements predominantly show the same trend as SCH1. It can be observed in Figure 5.21 that the oldest data points relate to a lower surface height than the newer data. This means that accretion leads to an increase in marsh surface height over time. An exception is seen for the most recent years: 2010 and 2011. These are situated lower than the oldest data points that correspond to 1996 and 1997. The largest sedimentation rates are seen for the SEB closest to the marsh edge: cluster T1. This cluster is also in the closest proximity of a creek. Cluster T3 has the smallest range of surface heights, which may be due to the fact that it is located furthest away from the marsh edge.

The accretion rates for the SCH1 clusters are shown in Figure 5.22. The mean accretion rate ranges from 2.34 - 5.37 mm/year. The mean accretion rate for SCH2 is not illustrated because the last few

dataset	cluster	PQ	distance to nearest creek [m]	distance to marsh edge [m]
SCH1	T0	1_1	290	160
		1_3	290	160
		2_1	274	180
		2_3	274	180
		3_1	279	168
		3_3	279	168
	T1	1_1	168	148
		1_3	168	148
		2_1	211	113
		2_3	211	113
		3_1	196	124
		3_3	196	124
	T2	1_1	113	288
		1_3	113	288
		2_1	105	287
		2_3	105	287
		3_1	110	270
		3_3	110	270
	T3	1_1	140	551
		1_3	140	551
		2_1	140	575
		2_3	140	575
		3_1	135	552
		3_3	135	552
	T5	1_1	112	619
		1_3	112	619
		2_1	102	633
		2_3	102	633
		3_1	84	658
		3_3	84	658
OBK	1_1	90	177	
	1_3	90	177	
	2_1	94	183	
	2_3	94	183	
	3_1	76	157	
	3_3	76	157	

Table 5.6: SEB clusters SCH1 for salt marsh Oosterkwelder, Schiermonnikoog.

data points seem to be outliers and may give a wrong indication of the typical salt marsh development.

dataset	cluster	PQ	distance to nearest creek [m]	distance to marsh edge [m]
SCH2	T0	1	214	226
		2	246	151
		3	205	229
	T1	1	45	197
		2	50	196
	T2	1	102	391
		2	91	387
	T3	1	102	610
		2	99	609

Table 5.7: SEB clusters SCH2 for salt marsh Oosterkwelder, Schiermonnikoog.

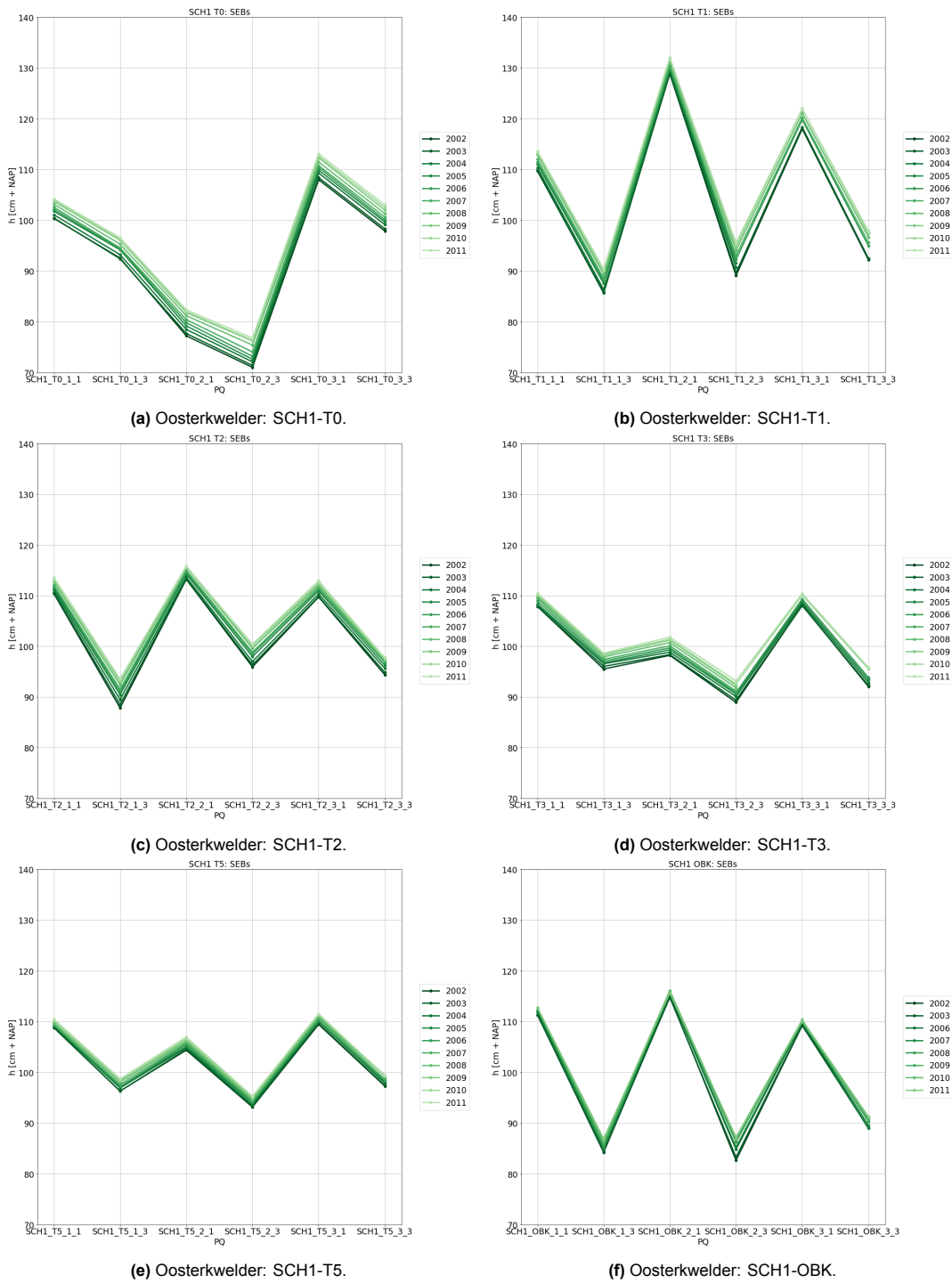


Figure 5.20: Surface height relative to NAP for SCH1 on Oosterkwelder, Schiermonnikoog.

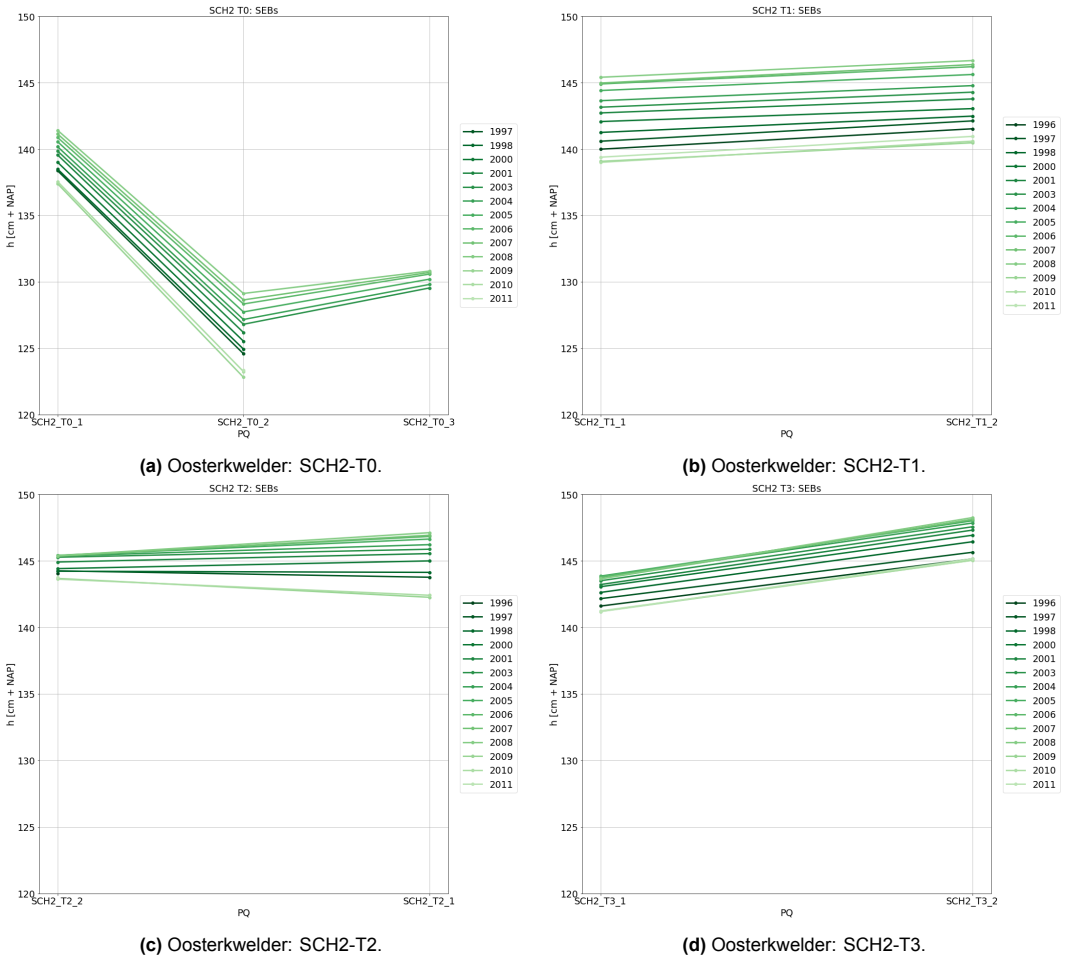
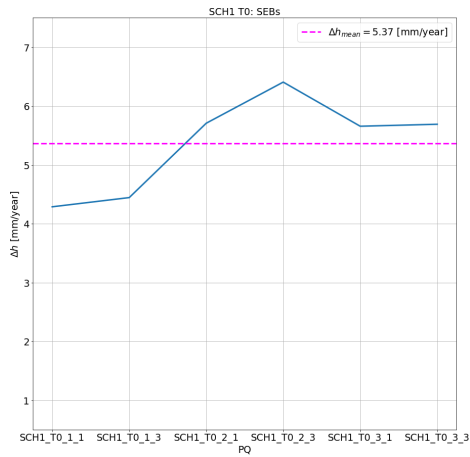
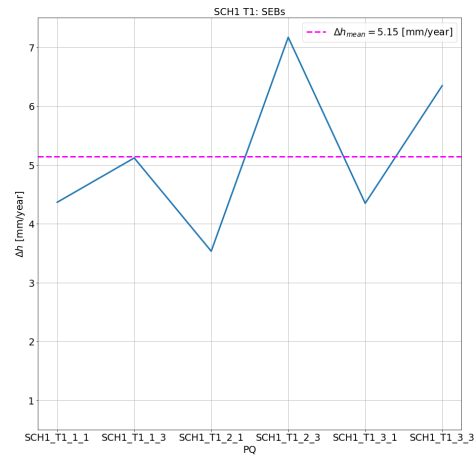


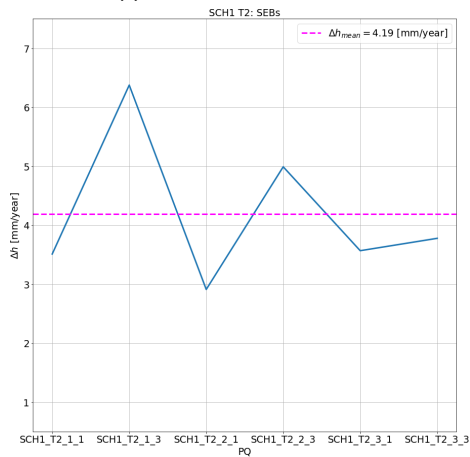
Figure 5.21: Surface height relative to NAP for SCH2 on Oosterkwelder, Schiermonnikoog.



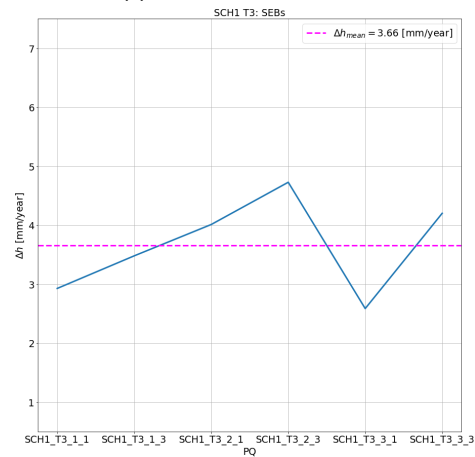
(a) Oosterkwelder: SCH1-T0.



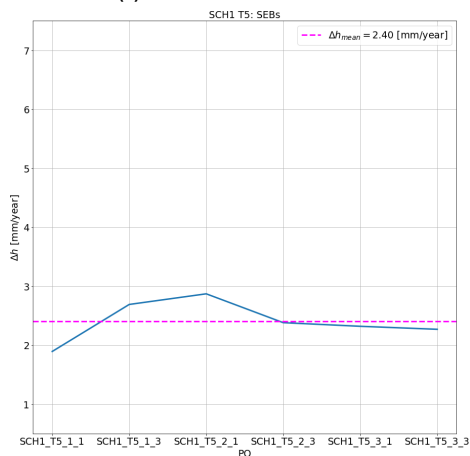
(b) Oosterkwelder: SCH1-T1.



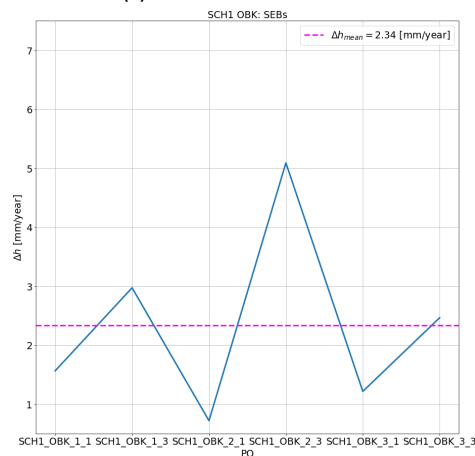
(c) Oosterkwelder: SCH1-T2.



(d) Oosterkwelder: SCH1-T3.



(e) Oosterkwelder: SCH1-T5.



(f) Oosterkwelder: SCH1-OBK.

Figure 5.22: Accretion rates for SCH1 on Oosterkwelder, Schiermonnikoog.

5.5.3 Comparison between Digital Terrain Models and Local Measurements

The two data types, the AHN DTMs and the local SEBs, that were discussed in the two previous subsections will be compared here. First, the AHN data is sampled at the SEB locations to allow for a local comparison of the two datasets. The results can be observed in Appendix B. As previously mentioned, SEBs on Schiermonnikoog are only present for the Oosterkwelder. Therefore, salt marsh Het Rif is excluded from this analysis. The AHN data plots will be compared to the SEB data for the following years: 1998/1999, 2008, 2014 and 2020.

The comparison for salt marsh Neerlandsreid can be observed in Figure 5.23, where the blue line corresponds to the AHN data and the green line indicates the SEB measurements. The y-axis shows the marsh surface height relative to NAP and the PQ number is given on the x-axis, which moves from the Wadden Sea land inwards from left to right. It can be observed in Figure 5.23a and 5.23b that the AHN and SEB data roughly coincide for 1998 and 2008. The AHN data contains measurements that are approximately 10 cm larger than the SEBs for the highest PQs. In 2014, the SEB measurements record a higher surface height than the AHN data, as illustrated by Figure 5.23c. The opposite is visible for 2020 in Figure 5.23d, where the SEB measurements indicate lower values than the AHN data. For 2020, the maximum difference in surface height is ~ 20 cm.

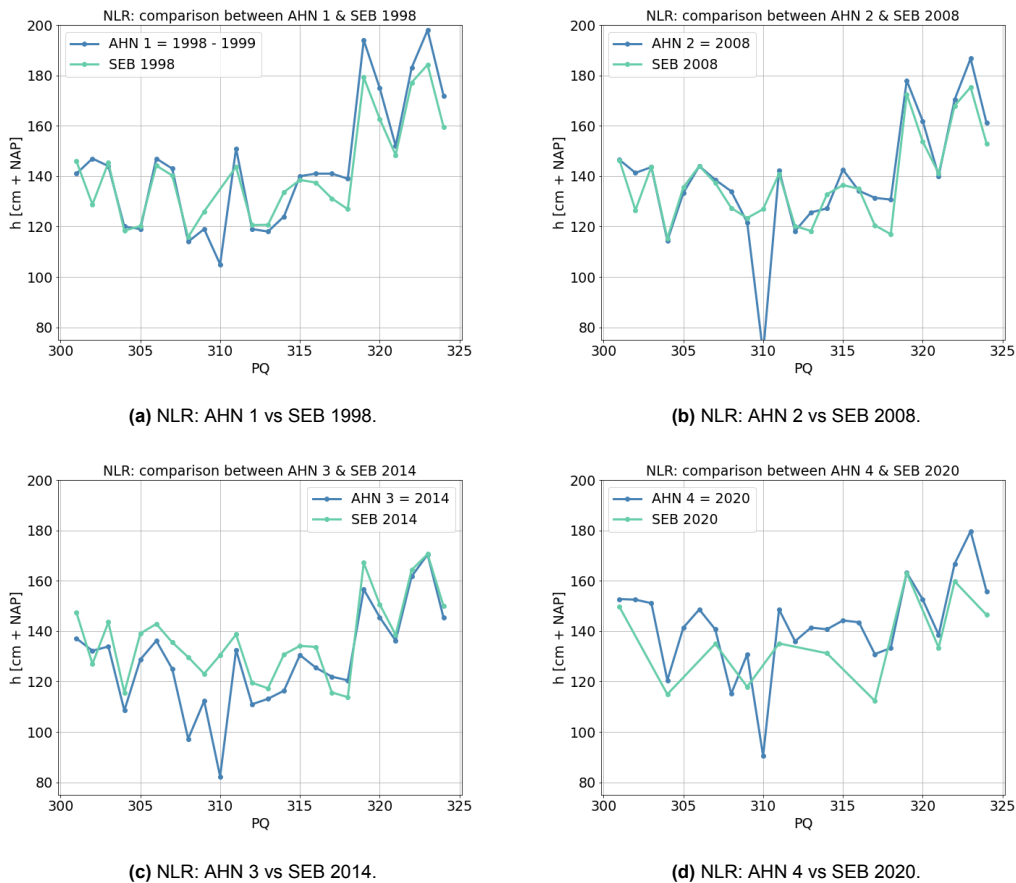


Figure 5.23: Local comparison between AHN and SEB data for Neerlandsreid, Ameland.

The comparison between the AHN and SEB data for De Hon is illustrated in Figure 5.24. Surface heights from the AHN data generally exceed those obtained from the SEBs. This is clearly visible for 1999, 2008 and 2020 as shown by respectively Figure 5.24a, 5.24b and 5.24d. The variation falls within the range of approximately 5 - 20 cm. The results in 2014 show minimum differences between the two data types, as demonstrated by Figure 5.24c. For some PQs, the AHN 3 data gives a surface height approximately 5 cm higher than the one provided by SEB measurements. However, for PQ 904 and 912, the SEB measurements are approximately 5 cm higher than the AHN 3 data.

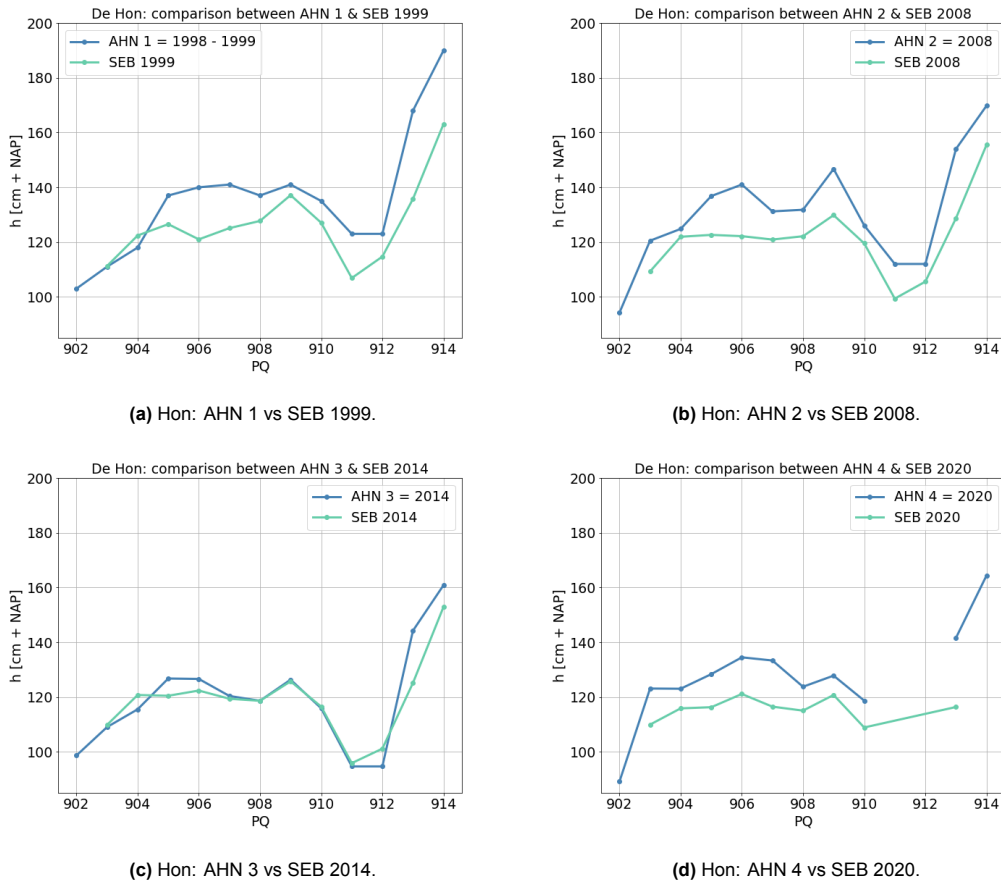
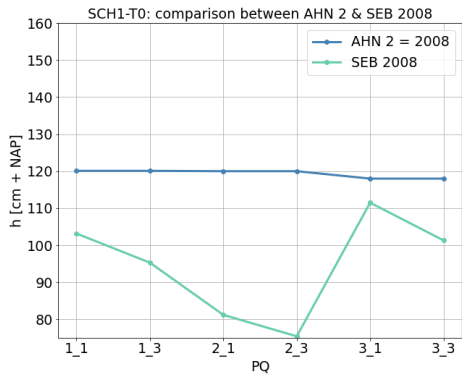


Figure 5.24: Local comparison between AHN and SEB data for De Hon, Ameland.

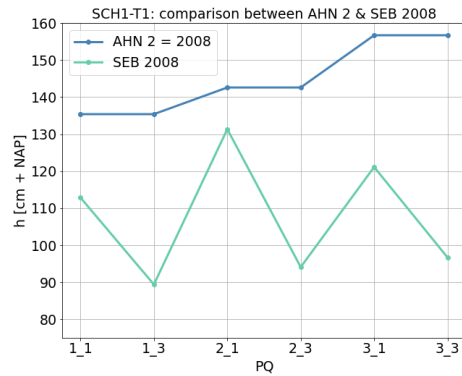
A comparative analysis between AHN data and SEBs for Schiermonnikoog is conducted per cluster. For the SCH1 locations, it is possible to make a comparison between the AHN data and SEBs for the year 2008 only, since the SEB data is not available for each year in which the AHN data was obtained. The result for the SCH1 locations is shown in Figure 5.25. The SEBs on locations SCH2 have data available for the years 1998 - 1999 and 2008, which corresponds to AHN 1 and 2. Figure 5.26 illustrates the comparison. It is worth acknowledging that only one coordinate per PQ was available for the Schiermonnikoog SEBs. The SEBs differentiate between for example SCH1_T0_1_1 and SCH1_T0_1_3, where 1 corresponds to a locally elevated part and 3 to a local depression. However, the coordinates for these SEBs are only available for SCH1_T0_1 in the example case. This means that the AHN data extraction does not distinguish between SCH1_T0_1_1 and SCH1_T0_1_3, the AHN measurement is extracted for SCH1_T0_1 only.

The comparative analysis between the AHN and the SCH1 SEBs in Figure 5.25 reveals a similar trend. It becomes evident that the AHN data structurally depicts a significantly higher marsh surface elevation than the SEB measurements. The observed range of height difference is $\sim 10 - 55$ cm.

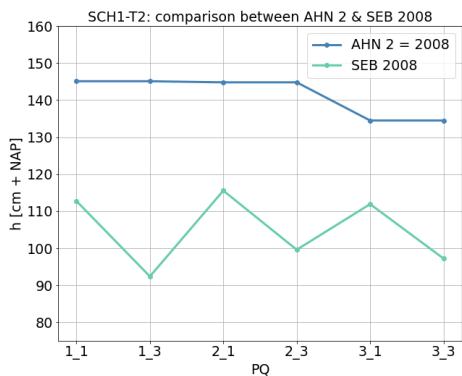
Upon examining the AHN vs SEB measurements for the SCH2 dataset, a clear difference is seen between the years 1998 and 2008. The left plots in Figure 5.26 indicate that the SEBs measured higher surface heights than the AHN dataset. The contrary is observable in the right plots in Figure 5.26: a greater surface height is measured in the AHN data compared to the SEBs. The range of height difference for SCH2 is smaller than in the case of the SCH1 locations and comes down to ~ 2 - 15 cm.



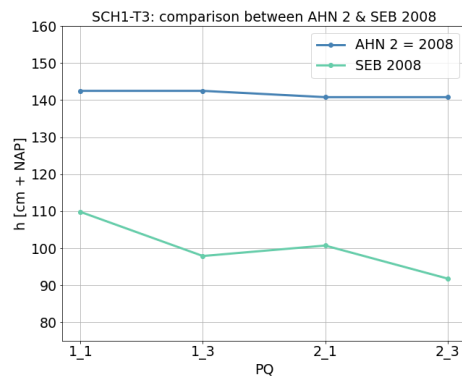
(a) SCH1-T0: AHN 2 vs SEB 2008.



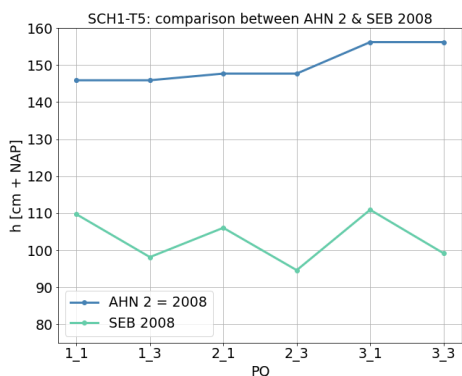
(b) SCH1-T1: AHN 2 vs SEB 2008.



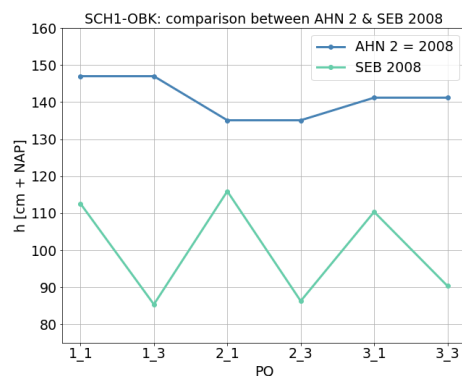
(c) SCH1-T2: AHN 2 vs SEB 2008.



(d) SCH1-T3: AHN 2 vs SEB 2008.



(e) SCH1-T5: AHN 2 vs SEB 2008.



(f) SCH1-OBK: AHN 2 vs SEB 2008.

Figure 5.25: Local comparison between AHN 2 and SEB data for Oosterkwelder, Schiermonnikoog.

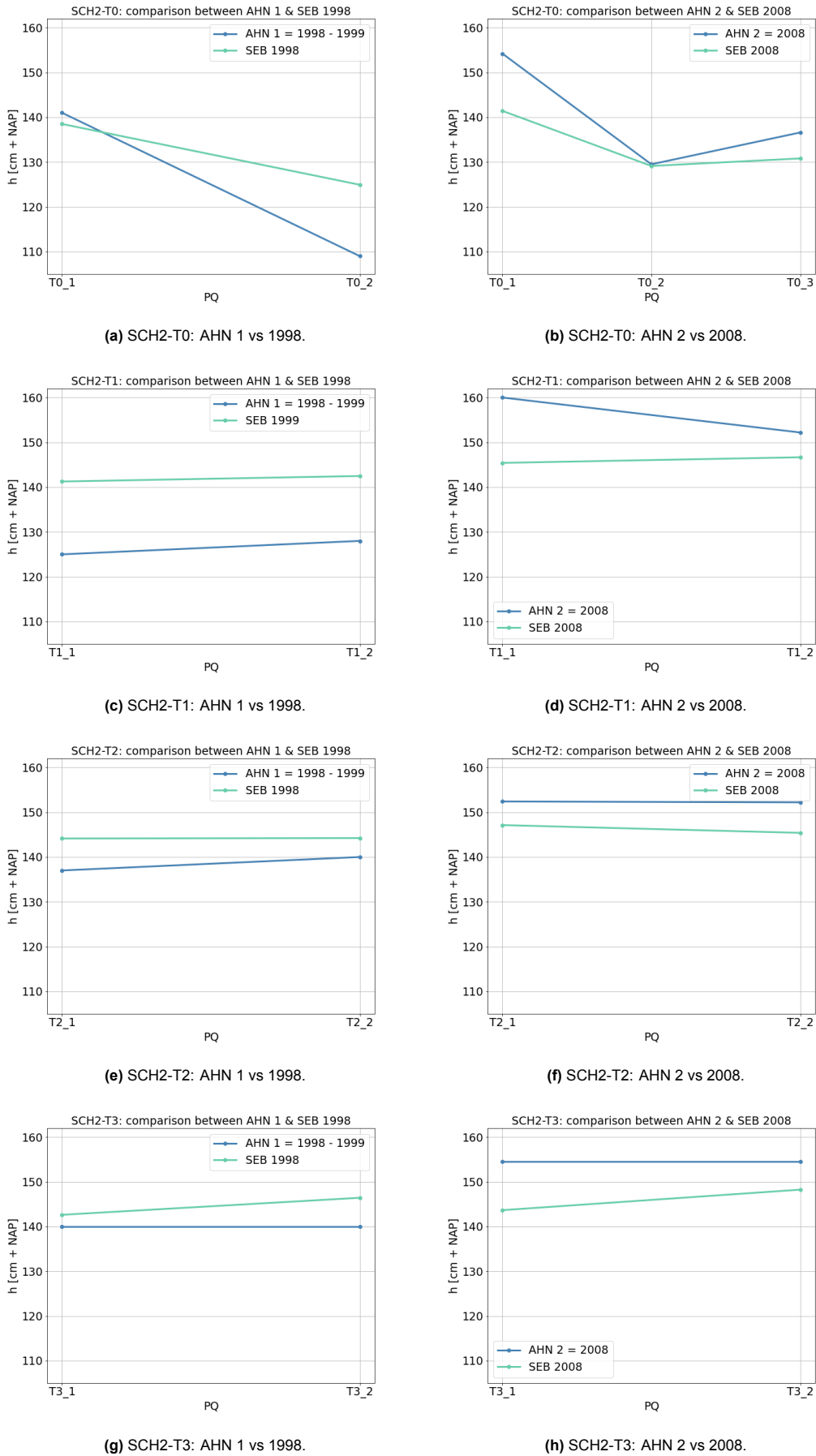


Figure 5.26: Local comparison between AHN 1 + 2 and SEB data for Oosterkwelder, Schiermonnikoog.

5.5.4 Salt Marsh Hypsometry Correction

The hypsometric curves of the salt marsh study areas have to be obtained for the ASMITA salt marsh model extension. The hypsometric curves of the salt marshes on Ameland and Schiermonnikoog will be extracted from the most recent Digital Terrain Model: AHN 4. However, subsection 5.5.3 found that there is a significant difference between the marsh heights in the AHN data compared to the SEBs. Except for Neerlandsreid, the AHN dataset shows consistently higher salt marsh elevations, which may be attributed to factors such as vegetation coverage in the AHN data or errors introduced during the transformation from point cloud to raster layer. As a consequence, the hypsometric curves derived from the AHN data are expected to overestimate the true salt marsh surface elevation.

Since no other data on the salt marsh bathymetry is available, it was decided to use the AHN hypsometric curves for the ASMITA model extension after applying a height correction that represents the difference in surface heights between the two data types. The height correction differs per salt marsh and is based on a comparison between the AHN data and the height data from the SEB plots.

An overview of the height correction for the hypsometric curve of each salt marsh is shown in Table 5.8. Neerlandsreid showed a clear spatial pattern in the height differences over the spatial marsh. A larger height difference was observed on the low marsh compared to the high marsh. Therefore, a non-uniform height correction is applied. For the other marshes, the difference between the AHN data and SEB plots was approximately equal for all locations and the height correction is thus applied uniformly. No SEB plots are present for salt marsh Het Rif on Schiermonnikoog. Accordingly, the height correction for Het Rif is assumed to be equal to the correction for De Hon on Ameland. Both marshes are relatively young and may thus contain similar vegetation.

salt marsh	height correction [cm]
	low marsh: -15
Neerlandsreid	middle marsh: transition
	high marsh: -5
De Hon	- 10
Het Rif	- 10
Oosterkwelder	- 20

Table 5.8: Height correction for the hypsometric curves of the studied salt marshes.

Extending ASMITA

This chapter explains the salt marsh extension in the ASMITA model. The governing processes for the salt marsh implementation in ASMITA are summarized in section 6.1. The computational procedure is described in section 6.2. Hereafter, the formulations for the one-element salt marsh model are elaborated on in section 6.3. The derivation of horizontal and vertical exchange parameters is discussed in respectively section 6.4 and 6.5. The derivation of the sediment concentration boundary condition is elaborated on in section 6.6. The multiple element model is discussed in section 6.7. Finally, the initial parameter setting is shown in section 6.8.

6.1 Governing Processes for Salt Marsh Implementation

Details on salt marsh development were already elaborated on in Chapter 2. The governing process for salt marsh development is accretion, which includes sedimentation, accumulation due to plant biomass and autocompaction. An overview of the different contributions and their magnitudes was shown in Figure 2.12. Forcing mechanisms for salt marsh development are the sediment availability, accommodation space and sediment transport capacity.

For the ASMITA salt marsh implementation, the only component of accretion that will be modelled is the mineral sedimentation. The sedimentation on a salt marsh depends on the horizontal and vertical exchange of sediment between the marsh element and the outer elements (section 2.4). Since the study areas in this research have a dominant mineral sediment input (Chapter 4) and the contribution of plant biomass to accretion is negligible, the organic component of accretion will not be considered in the model extension. Autocompaction is also excluded from the salt marsh extension, as it is often only a small contributor to accretion and in the order of mm/year. For an older, grazed marsh, the magnitude of autocompaction could be in the same order of magnitude as sedimentation (section 2.6). However, a formulation would depend on relatively many variables that are difficult to quantify. Therefore, it was decided not to implement autocompaction in the ASMITA salt marsh model extension.

The forcing mechanisms of sediment availability and sediment transport capacity will be included in the model parameters. The change in accommodation space is governed by relative sea level rise (rSLR), which includes SLR and deep subsidence.

Another governing process for salt marsh development is the regression and transgression of marsh cliffs. Despite the potential significance of cliff formation and erosion on lateral salt marsh development, it will not be incorporated in the ASMITA extension for salt marshes. This is due to the fact that the aggregated ASMITA schematisation adds complexity to the inclusion of a varying marsh surface area. Therefore, this research will prioritize vertical salt marsh development instead of horizontal salt marsh development.

Sedimentation is fully dependent on the amount of water that flows onto the marsh during a certain time period and the Suspended Sediment Concentration (SSC), which deposits on the salt marsh and causes a vertical height increase (Chapter 2). The physical process of sedimentation should be captured in the ASMITA parameters in order to model salt marsh development on an aggregated spatial and temporal scale. The sediment dynamics are caught in the horizontal exchange coefficient δ , vertical exchange coefficient w_s and sediment concentration c . More details on the model formulations and parameter setting will be explained in the following sections.

6.2 Computational Procedure Salt Marsh Element

The salt marsh extension for the ASMITA model is configured in a different manner compared to the existing ASMITA formulations (Chapter 3). Figure 6.1 shows the updated computational procedure. As opposed to the existing ASMITA model elements, the salt marsh element lacks a morphological equilibrium condition that is based on the tidal prism or tidal range. This is due to the fact that the salt marsh does not experience inundation during every tidal cycle. Hence, model steps 1 and 2 are bypassed.

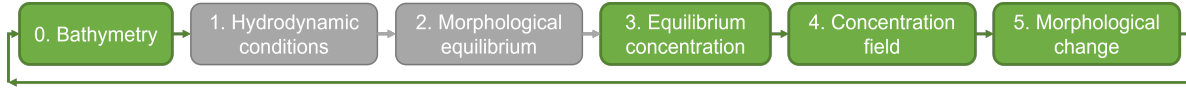


Figure 6.1: Flowchart of the computational procedure carried out by ASMITA for the salt marsh extension.

For the implementation of a salt marsh in ASMITA, the model starts with an initial bathymetry and directly moves towards the equilibrium concentration. It is stated that the local equilibrium concentration $c_e = 0$ for the salt marsh element, which means that all sediment that flows onto the marsh is captured. Consequently, the local equilibrium concentration on the marsh is equal to zero, since the water column no longer contains any sediment. Since salt marshes are typically located in sheltered locations with relatively calm hydrodynamic conditions and small water depths, the sediment is able to deposit quickly. Moreover, fast settling is enhanced due to the large amount of small-grained sediment on a salt marsh. Poirier et al. (2017) state that 76 - 83% of the deposits on a salt marsh in Canada consist of flocs. Sedimentation in a highly flocculated environment occurs relatively fast meaning that barely any sediment remains in suspension. The parameter setting of $c_e = 0$ includes enhanced settling effects by vegetation and turbulence.

Model steps 4 and 5 are similar to the existing ASMITA formulations: the concentration field is computed which then determines the morphological change of the salt marsh element. The adjusted formulations will be explained more extensively in the subsequent section for the simplified one-element salt marsh model.

6.3 One-Element Salt Marsh Model

The first implementation of a salt marsh in ASMITA will be a one-element model. This means that one salt marsh element will communicate with an outside boundary. No other elements than the salt marsh are present. A schematisation of this model set-up can be observed in Figure 6.2. The simplified approach is chosen as an initial step to assess the capability of ASMITA in reproducing salt marsh development. Since the marsh can only exchange sediment with an outside boundary in the one-element model, it is less complex to calibrate the model and the parameters.

The equations used in the one-element model are based on the aggregated advection-diffusion equation, see Equation 6.1. The aggregation process of the advection-diffusion equation was elaborated on in section 3.3.

$$w_s A (c_e - c) = \delta (c - c_E) \quad (6.1)$$

where:

w_s	vertical exchange rate	[m/s]
A	total marsh plan area	[m ²]
c_e	local equilibrium concentration	[m ³ /s]
c	actual concentration	[m ³ /s]
δ	aggregated horizontal exchange rate	[m ³ /s]
c_E	global equilibrium concentration	[-]

For the implementation of a salt marsh in ASMITA, it is stated that the local equilibrium concentration $c_e = 0$. When this is implemented in the aggregated advection-diffusion equation, a formulation for the actual sediment concentration is found, as shown in Equation 6.2.

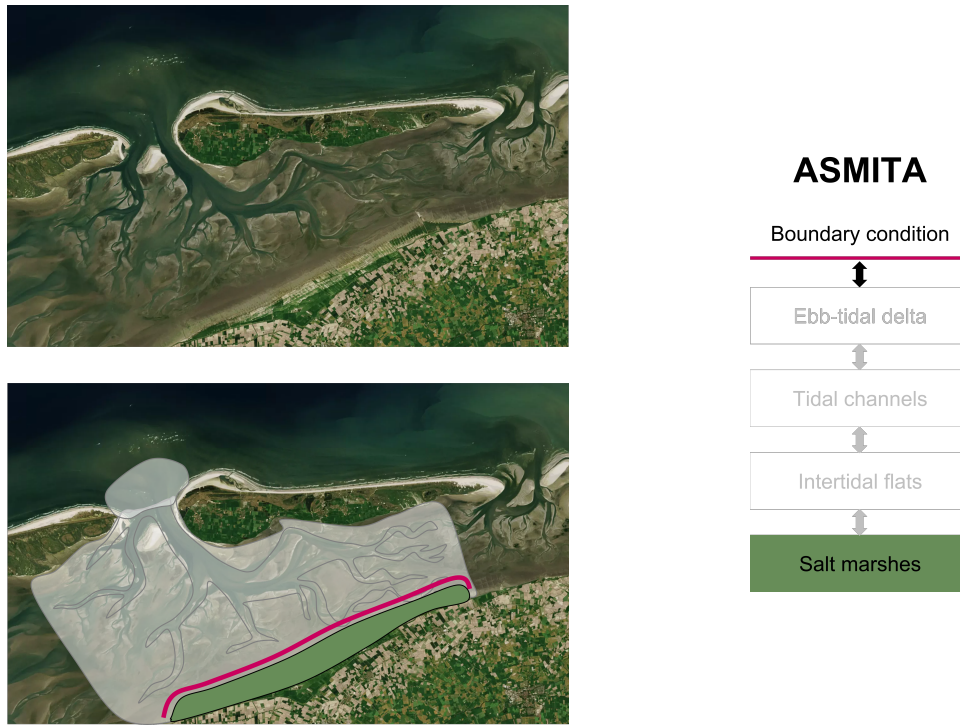


Figure 6.2: One-element salt marsh schematisation in ASMITA.

$$c = \frac{\delta}{\delta + w_s A} c_E \quad (6.2)$$

The volume change of the salt marsh depends on the vertical marsh growth due to mineral sedimentation (Equation 6.3) and the loss of volume due to SLR (Equation 6.4). The latter is only valid under the assumption that the salt marsh has a fixed surface area. The final formulation for the marsh volume change is given in Equation 6.5.

$$\Delta V_{sed} = w_s A c \Delta t = \frac{w_s A \delta}{\delta + w_s A} * c_E * \Delta t \quad (6.3)$$

$$\Delta V_{SLR} \sim h_{SLR} * A_{marsh} * \Delta t \quad (6.4)$$

$$\Delta V_{marsh} = \Delta V_{sed} - \Delta V_{SLR} \quad (6.5)$$

where:

ΔV_{sed}	marsh volume change due to sedimentation	[m ³]
ΔV_{SLR}	marsh volume change due to SLR	[m ³]
h_{SLR}	sea level rise	[m/s]
A_{marsh}	marsh plan area	[m ²]

An overview of the model loop for the one-element salt marsh model in ASMITA is shown in Figure 6.3. The model will walk through all steps for the number of time steps that are chosen for any given simulation.

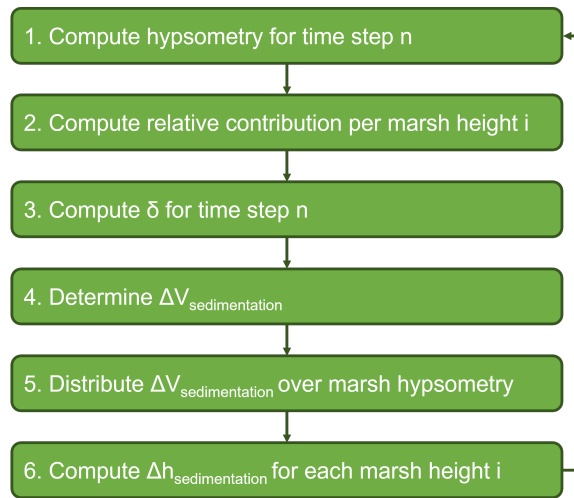


Figure 6.3: Computational loop of the ASMITA salt marsh element.

1. Compute hypsometry for time step n

The starting point of every simulation is the hypsometry of the current time step n. All calculations are based on the salt marsh hypsometry. The hypsometry shows how much surface area each marsh height has at and below this level. For time step n, it is based on the hypsometric curve from the previous time step and the height increase by sedimentation and height decrease by SLR. This is shown in Equation 6.6

$$hypso_n = hypso_{n-1} + \Delta h_{sedimentation} - h_{SLR} \quad (6.6)$$

$hypso_n$	hypsometric curve at current time step n
$hypso_{n-1}$	hypsometric curve at previous time step n - 1
$\Delta h_{sedimentation}$	sedimentation per marsh height
h_{SLR}	uniform height decrease due to SLR

2. Compute relative contribution per marsh height i

The relative contribution determines how the sediment will be distributed over the salt marsh. Essentially, the marsh heights that are inundated more often are supposed to experience a relatively large amount of sedimentation compared to marsh heights that are rarely inundated. In other words, marsh heights with a large relative contribution to the aggregated exchange volume should receive more sedimentation than marsh heights with a smaller relative contribution to the exchange volume. The relative contribution per marsh height is thus computed as shown in Equation 6.7 and 6.8.

$$V_{exchange,i} = \sum (h_w[h_w > M_i] - M_i) * A_i \quad (6.7)$$

$$rc_i = \frac{V_{exchange,i}}{\sum V_{exchange,i}} \quad (6.8)$$

$V_{exchange,i}$	exchange volume for marsh height i	[m ³]
h_w	water levels	[m]
M_i	marsh height i	[m]
A_i	surface area for marsh height i	[m ²]
rc_i	relative contribution of marsh height i	[-]

3. Compute δ for time step n

The horizontal exchange coefficient δ represents the temporally and spatially averaged horizontal diffusion. For the salt marshes, this is the volume of water that flows on the marshes each tide. As discussed in section 6.4, this volume can be derived from long-year water level data and the initial salt marsh bathymetry.

When the ASMITA model is employed, the salt marsh element will either experience sedimentation or erosion. This means that the hypsometric curve changes. When sedimentation occurs, the hypsometric curve experiences an increase in height. As a result, the horizontal exchange of sediment between the marsh and the adjacent boundary will change. A higher marsh will receive less water and the horizontal exchange rate δ will thus be lower. This means that the salt marsh development slows down. The opposite happens for erosion. This phenomenon should be represented in the one-element model in order to be able to properly simulate the salt marsh growth.

Consequently, the hypsometric curve is adjusted in each time step as described in the first step of the model loop. In this step, a new horizontal exchange coefficient is computed based on this new hypsometric curve. The formula for the horizontal exchange coefficient δ can be found in section 6.4.

4. Determine $\Delta V_{sedimentation}$

The sedimentation volume at time step n is computed with Equation 6.3.

5. Distribute $\Delta V_{sedimentation}$ over marsh

The total sedimentation volume can be distributed over the salt marsh hypsometry according to the relative distribution that was computed in step 2, see Equation 6.9.

$$\Delta V_{sedimentation,i} = rc_i * \Delta V_{sedimentation} \quad (6.9)$$

6. Compute $\Delta h_{sedimentation}$ for each marsh height i

Finally, sedimentation height for each marsh height can be computed by dividing the sedimentation volume by the corresponding area of marsh height i. This is also shown in Equation 6.10.

$$\Delta h_{sedimentation,i} = \frac{\Delta V_{sedimentation,i}}{A_i} \quad (6.10)$$

$\Delta h_{sedimentation,i}$	sedimentation height for marsh height i
$\Delta V_{sedimentation,i}$	sedimentation volume for marsh height i
A_i	surface area for marsh height i

6.4 Derivation of Horizontal Exchange Coefficient δ

The temporally and spatially averaged horizontal diffusion between the salt marsh element and the adjacent element or outer boundary is captured by the parameter δ . For the salt marsh element, the exchanged sediment quantity depends on the exchange of water volumes that flow onto the salt marsh in combination with the suspended sediment concentration (SSC). The horizontal exchange coefficient δ captures the exchanged water volume during a certain time period in m^3/s . The ASMITA model is spatially and temporally aggregated, which means that δ is not computed per tidal cycle. Instead, it is a representative aggregated water volume per time unit.

The exchange volume is computed as shown in Equation 6.11. Water level data is compared to the marsh hypsometry. For every marsh height, the exchange volume is computed by multiplying the water depth on the marsh with the total area of that marsh height. By taking the sum of the exchange volume per marsh height, the exchange volume for the entire marsh is obtained.

$$V_w = \sum (h_w [h_w > M_i] - M_i) * A_i \quad (6.11)$$

where:

V_w	aggregated exchange volume	$[\text{m}^3]$
h_w	water level	$[\text{m}]$
A_i	marsh area corresponding to water height M_i	$[\text{m}^2]$
M_i	marsh height	$[\text{m}]$

The exchange volume per marsh height is different for every salt marsh because the bathymetry and water levels differ from marsh to marsh. Therefore, it is necessary to compute a unique set of exchange volumes per salt marsh height for every salt marsh that will be studied in ASMITA.

A hydrodynamic dataset was used to derive the exchange volume per marsh height. In this case, ten years of water level data was used. Extreme situations such as storm events are thus included. For every marsh height, the amount of water levels higher than the marsh height is extracted and multiplied by the area corresponding to the marsh height. This gives the exchange volume for all marsh heights. The total aggregated exchange volume is obtained by taking the sum of all exchange volumes per marsh height. The final value for δ is determined by applying Equation 6.12. The total exchange volume is divided by the total time of the hydrodynamic dataset. A representative horizontal exchange rate in m^3/s is found.

$$\delta = \frac{1}{T} * V_w \quad (6.12)$$

where:

T	time span of water level dataset	$[\text{s}]$
V_w	exchange volume	$[\text{m}^3]$

This methodology was applied to all study areas. A summary of all horizontal exchange rates along with the plan area of the different salt marshes is given in Table 6.8. As expected, the largest horizontal exchange coefficient is present for the salt marsh with the biggest plan area: the Oosterkwelder on Schiermonnikoog. This can be derived from Equation 6.11. The horizontal exchange coefficient decreases with decreasing marsh plan area. However, the shape of the hypsometric curve also influences the magnitude of the horizontal exchange coefficient. For example, δ for Neerlandsreid and Het Rif are relatively close together, even though the surface area of Neerlandsreid is almost twice the size of Het Rif. The horizontal exchange coefficient is in the same order of magnitude because the hypsometric curve of Het Rif is situated lower in the profile compared to Neerlandsreid, which is clearly visible in Figure 6.4.

salt marsh	A [m ²]	δ [m ³ /s]
Neerlandsreid	3.28e6	2.46
De Hon	1.07e6	1.09
Het Rif	1.90e6	2.24
Schiermonnikoog	1.08e7	7.60

Table 6.8: Marsh surface area and δ .

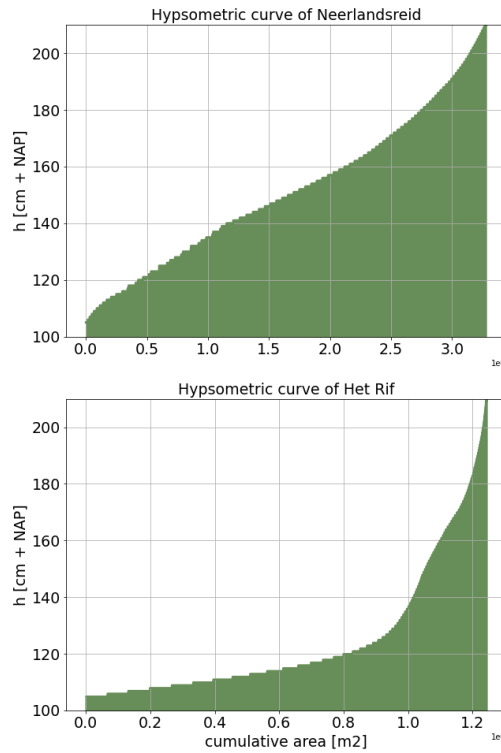


Figure 6.4: Hypsometric curve of Neerlandsreid compared to Het Rif.

6.5 Derivation of Vertical Exchange Coefficient w_s

Besides the horizontal exchange rate δ , it is important to consider the vertical exchange between the water column and bed. This is done in ASMITA by the vertical exchange rate w_s . The vertical exchange coefficient is closely related to the settling velocity, but it is not exactly the same. This was already elaborated on in Chapter 3. However, the order of magnitude should be similar to the settling velocity.

For salt marshes, it is known that the deposited sediment mainly consists of fine materials such as mud and silt. These particles may experience flocculation, which affects the settling velocities. According to Van Maren and Winterwerp (2013), the settling velocity of silt and flocculated mud is typically in the range of 0.1 - 2 [mm/s]. This range will be used for the implementation of salt marshes in ASMITA.

$$1e^{-4} \leq w_s \leq 2e^{-3} [m/s] \quad (6.13)$$

6.6 Derivation of Global Equilibrium Concentration c_E

The global equilibrium concentration c_E indicates the morphological activity in an area. The derivation of this parameter was explained in section 3.6. For the salt marsh element, the value for c_E should capture the average suspended sediment concentration (SSC) during marsh inundation. Salt marshes are mostly inundated during extreme weather events, in which the SSC in the water column is generally rather large due to prevailing high-energy conditions (Chapter 2). As there are no SSC measurements available for the study areas in this research, a range of values is derived from previous studies on salt marsh sediment concentrations:

- Oenema and DeLaune (1988) state that salt marsh accretion significantly increases during storm conditions and spring tides, which can be appointed to the increased flooding periods and SSC.
- Colosimo et al. (2020) conducted SSC measurements on a high mudflat in the Wadden Sea, which is the adjacent element to a salt marsh. The measurement location was at ~ 1 km from the land boundary and had a submergence time of nearly 100%. The range of the SSC varies between 0.1 - 8 g/L. The highest SSC value is observed during high wind events.
- Poirier et al. (2017) collected measurements of the SSCs on a salt marsh in a tidal inlet system in Canada. According to this research, the higher sediment deposition on salt marshes that is observed in autumn and winter is due to a higher SSC in these periods. The range of SSCs observed in this study is between 0.1 - 2 g/L and shown in Figure 6.5.
- Moskalski and Sommerfield (2012) measured SSCs in a range of 0.01 - 0.30 g/L on a salt marsh in Delaware, USA. The studied salt marsh is located in a river, 6 km upstream from the river mouth.
- A range of 0.05 - 0.12 g/L was measured on a salt marsh in Delmarva, USA by Christiansen et al. (2000). This salt marsh mainly consists of mineral sediment. However, it is situated in a bay that is expected to have a relatively small sediment input compared to a tidal inlet system such as the Dutch Wadden Sea.
- Measurements on a tidal flat in the Ems estuary gave SSC values ranging from 0.10 - 0.55 g/L (Schrijvershof, personal communication, March 14, 2023).

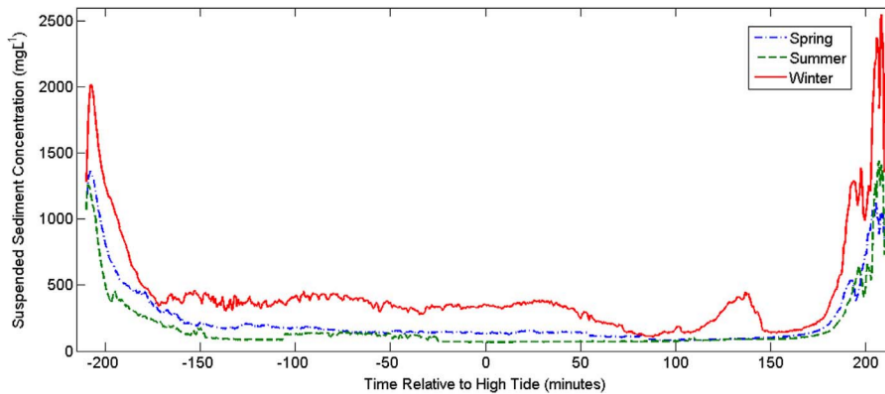


Figure 6.5: The Suspended Sediment Concentration (SSC) on a salt marsh in different seasons (Poirier et al., 2017).

The value for the suspended sediment concentration c in the ASMITA model extension will be in the range of the observed values in the literature. The study areas are located in the Dutch Wadden Sea, where mineral sedimentation is dominant. As a result, the SSC values are relatively large. Thus, the range of c for the Dutch Wadden Sea excludes the very low values such as $c = 0.01$ g/L. The sediment concentration should represent the average salt marsh inundation, which means that the highest values found in the literature are excluded as well. The final range that will be applied in the model extension contains the intermediate values and can be observed in Equation 6.14. The global equilibrium concentration c_E can then be obtained by applying Equation 3.15.

$$0.1 \leq c \leq 3.0[g/L] \quad (6.14)$$

6.7 Four Elements Model: Implementation of Salt Marshes

This section will elaborate on the extension of the existing ASMITA 3 elements model. The extended model will contain four elements: the ebb-tidal delta, channels, tidal flats and salt marshes. A schematisation of the 4 elements ASMITA model can be observed in Figure 6.6.

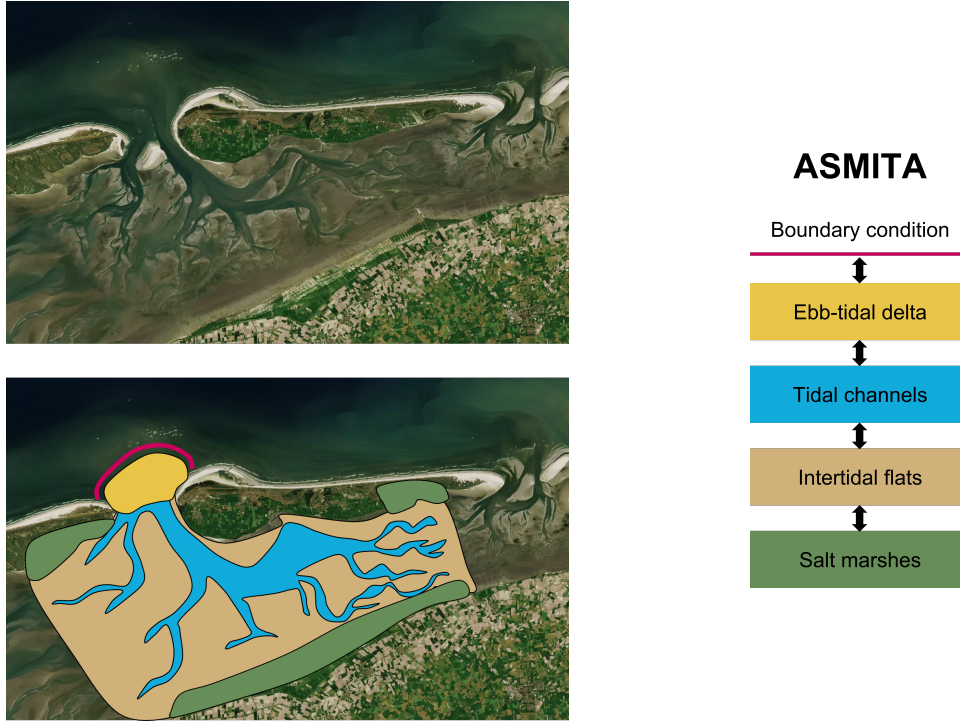


Figure 6.6: 4-element schematisation in ASMITA.

The formulations for the ebb-tidal delta, channels and tidal flats in the 4 elements model are equal to the formulations in the 3 element model, which was elaborated on in section 3.7. The (3x3)-matrices and (3x1)-vectors from the existing ASMITA model will be modified into (4x4)-matrices and (4x1)-vectors due to the additional salt marsh element. The formulations for the salt marsh element are identical to the ones illustrated in section 6.3. For further reference, each element in the multiple elements model corresponds to a numerical value, as demonstrated below:

1. Salt marsh
2. Tidal flat
3. Channel
4. Ebb-tidal delta

The horizontal exchange matrix D is shown in Equation 6.15 and describes the incoming and outgoing horizontal exchange for all elements. The consecutive elements only exchange sediment with each other.

$$D = \begin{pmatrix} \delta_{12} & -\delta_{12} & 0 & 0 \\ -\delta_{21} & \delta_{21} + \delta_{23} & -\delta_{23} & 0 \\ 0 & -\delta_{32} & \delta_{32} + \delta_{34} & -\delta_{34} \\ 0 & 0 & \delta_{43} & \delta_{43} + \delta_E \end{pmatrix} \quad (6.15)$$

The vertical exchange is described by w_s , similar to the one-element model. The global equilibrium concentration c_E boundary condition is situated outside of the tidal inlet, adjacent to the ebb-tidal delta element.

6.8 Initial Parameter Setting

The multiple elements simulations will be carried out for the tidal inlet system Zoutkamperlaag, which is located in the Dutch Wadden Sea. Zoutkamperlaag is part of the Frisian inlet, further details on the system were provided in Chapter 4. The four elements model includes two sediment fractions: sand and mud. Due to high-energy conditions that prevail at the ebb-tidal delta, it is assumed that no mud sedimentation can occur there. This is included in the model by a vertical exchange rate w_s of zero. Moreover, for simplicity, it is assumed that no sedimentation of sand occurs on the salt marsh. The sedimentation on the salt marsh is composed of mud only.

The parameter setting for the initial model simulations is given in Table 6.9. These parameters are based on field measurements, tidal inlet bathymetry and equilibrium relations. The subscript c refers to the coarse sediment fraction (sand), whereas the subscript f indicates the fine fraction (mud). Some calibration, within a limited range of values, was conducted for the values of c_E , δ and w_s .

<i>element</i>	A [m ²]	V_0 [m ³]	δ_c [m ³ /s]	δ_f [m ³ /s]	$c_{E,c}$ [-]	$c_{E,f}$ [-]	$w_{s,c}$ [m/s]	$w_{s,f}$ [m/s]	α [-]	β [-]
1	1.1e7	1.7e7	1e-5	8	4e-4	4e-5	0	0.001	0.7e8	0
2	1.1e8	1.0e8	2147	12882	4e-4	4e-5	0.006	0.001	1.14e8	0
3	4.6e7	2.2e8	302	3023	4e-4	4e-5	0.01	0.001	1.8e-5	1.55
4	7.8e7	1.5e8	896	8960	4e-4	4e-5	0.01	0	5.54e-3	1.23

Table 6.9: Parameter setting for the 4 elements model runs based on tidal inlet system Zoutkamperlaag in the Dutch Wadden Sea.

This chapter shows the model results that were obtained by employing the extended ASMITA model. First, section 7.1 describes the results for one-element model simulations with zero SLR. Hereafter, the one-element model simulations including SLR are shown in section 7.2. A sensitivity analysis is carried out in section 7.3. The 4 elements model excluding SLR is elaborated on in section 7.4. Next, section 7.5 discusses the result from employing the 3 + 1 elements model. Hereafter, different SLR scenarios for both the one-element model and the 3 + 1 elements model are analyzed in section 7.6. Finally, the sand-mud distribution in the 3 + 1 elements model is elaborated upon in section 7.7.

7.1 One-Element Model: Zero SLR

The results of the one-element salt marsh model for zero SLR applied to the Oosterkwelder salt marsh on Schiermonnikoog are given in this section. Table 7.1 shows the initial parameter setting.

parameter	value	unit
Δt	3	days
w_s	1e-3	m/s
ρ_s	2650	kg/m ³
n	0.80	-
A_{marsh}	1.01e7	m ²
δ_0	7.60	m ³ /s

Table 7.1: Initial values for the different parameters in the one-element salt marsh model based on Oosterkwelder, Schiermonnikoog.

The first one-element model simulations are conducted for zero SLR. The results are strongly related to the chosen suspended sediment concentration (SSC). The SSC that is put into the model corresponds to the physical sediment concentration on the tidal flats during extreme conditions for which marsh inundation occurs. It is represented in the ASMITA model by the global equilibrium concentration c_E , as explained in section 3.6. A possible range for this parameter was given in section 6.6. The parameter should be calibrated against field data. However, the field data was obtained during the past decade, which means that some amount of SLR is integrated. Therefore, the calibration is unattainable for this case without SLR. Therefore, the primary assumption for a sediment concentration on the tidal flat of $c = 0.3$ g/L is applied. This corresponds to $c_E = 9e-5$. The modelled yearly salt marsh sedimentation rates after a simulation of $T = 20$ years are shown in Figure 7.1.

The results for a longer simulation of $T = 200$ years are shown in Figure 7.2. It can be observed that the yearly sedimentation rates per marsh height significantly decreased. This can be explained by looking at the course of the horizontal exchange coefficient δ and the marsh volume V_{marsh} over time, which is illustrated in respectively Figure 7.3a and 7.3b. For the model simulations without SLR, the horizontal exchange coefficient δ decreases over time as the salt marsh grows higher. With an increase in marsh volume, less water flows onto the marsh which also leads to a decrease in sedimentation over time. The marsh growth curve flattens over time. As a result, the average sedimentation rate decreases for longer simulation times. However, morphological equilibrium was not reached during this simulation of 200 years. The horizontal exchange coefficient does not approach zero and the marsh volume growth curve still shows an upward trend.

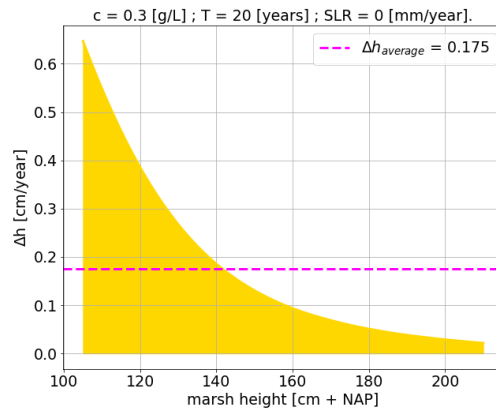


Figure 7.1: Modelled salt marsh height change Δh for a simulation time of 20 years.

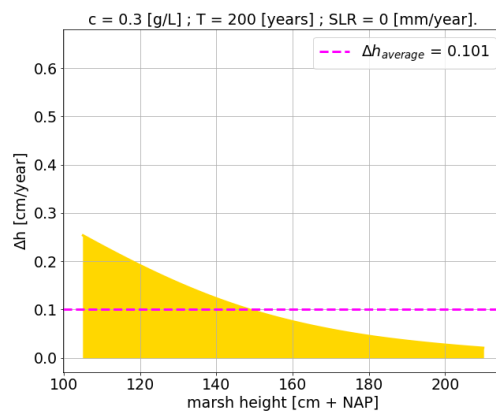


Figure 7.2: Modelled yearly salt marsh height change Δh for a simulation time of 200 years.

The results for a simulation time of 500 years are shown in Figure 7.4 and 7.5. A further decrease in the average yearly sedimentation height indicates that morphological equilibrium has almost been reached. It can be observed that the horizontal exchange coefficient δ approaches zero after 500 years of model simulations.

The hypsometric curves of the salt marsh change over time due to the sedimentation that takes place. The hypsometry after different simulation times can be observed in Figure 7.6. The initial profile at $T = 0$ years is displayed in brown and is relatively steep. The sedimentation for different simulation times is shown in yellow. As time progresses, the salt marsh hypsometry becomes less steep and more uniform. This can be explained by the fact that the lower parts of the marsh experience more inundation. The higher part of the salt marsh is only inundated during events of extremely high water, which does not occur frequently. As a result, the lower marsh areas receive more sediment and grow at a higher pace than the higher marsh. This leads to a more uniform hypsometric curve for larger simulation times.

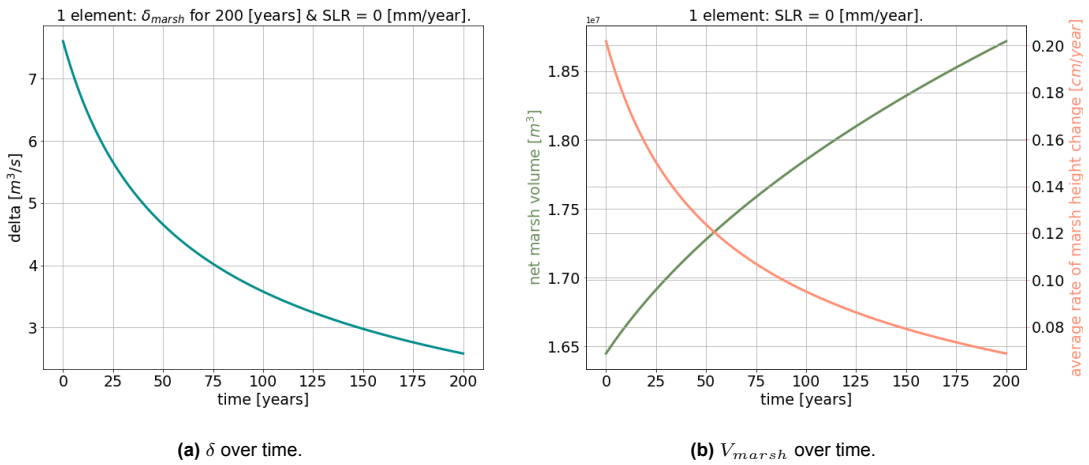


Figure 7.3: Model simulation for T = 200 years & SLR = 0 mm/year.

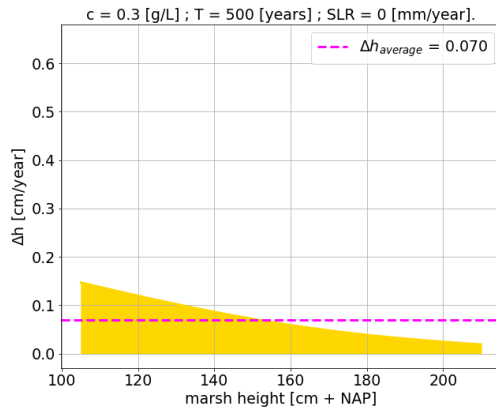


Figure 7.4: Modelled yearly salt marsh height change Δh for a simulation time of 500 years.

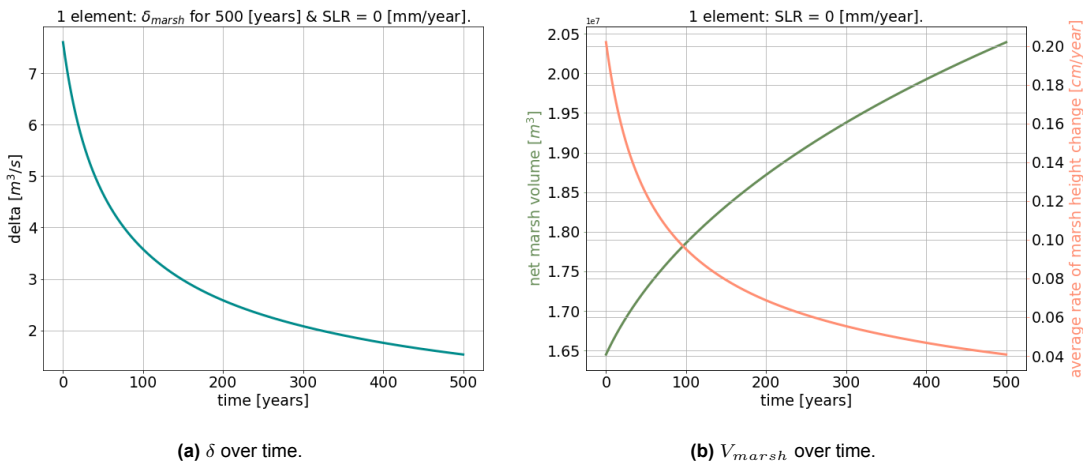


Figure 7.5: Model simulation for T = 500 years & SLR = 0 mm/year.

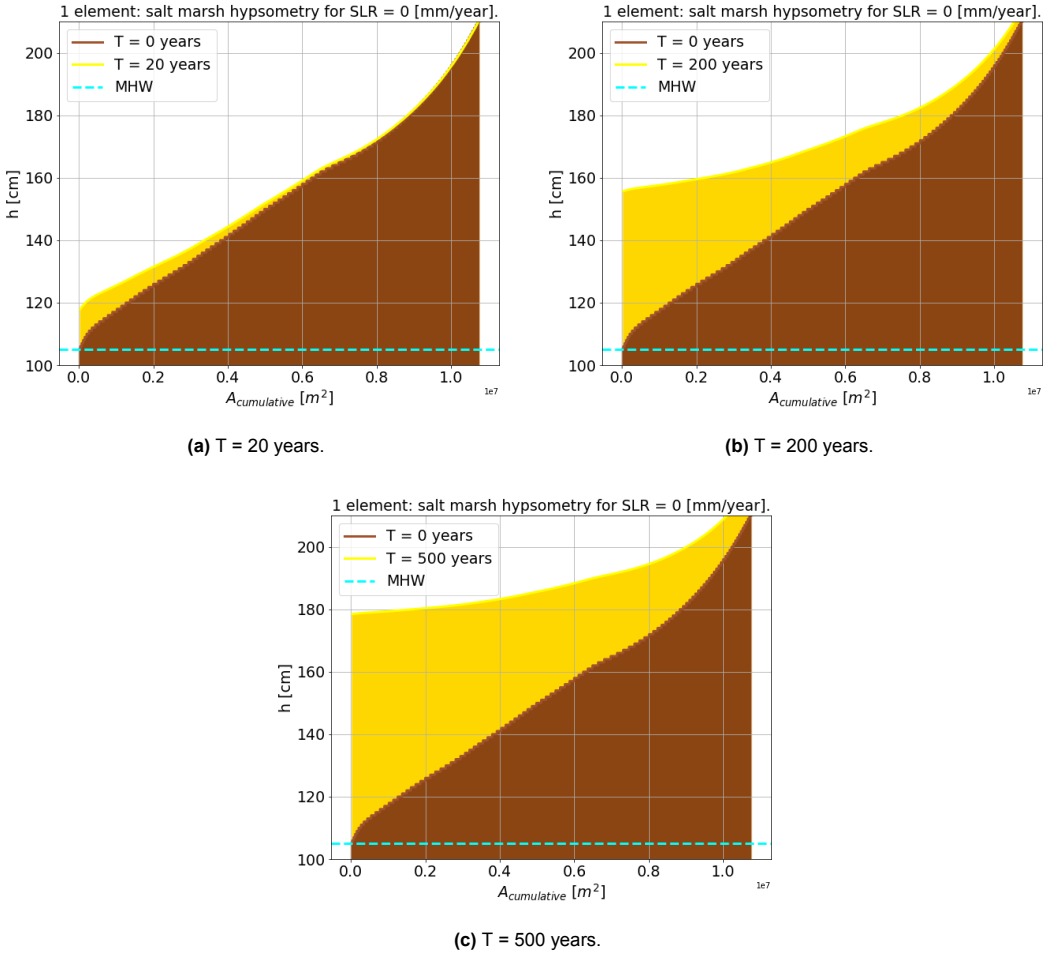


Figure 7.6: Hypsometric curves for different simulation times & SLR = 0 mm/year.

7.2 One-Element Model: SLR

The results of implementing SLR into the one-element model for long-term salt marsh development of the Oosterkwelder salt marsh on Schiermonnikoog are presented in this section. The one-element model results for the remaining study areas are shown in Appendix C.

The outside boundary condition c_E , which corresponds to the sediment concentration on the tidal flats, will be calibrated to SEB field values. Figure 7.7 shows the modelled height change per marsh height for a situation with SLR of 2 mm/year and different values for the sediment concentration c accompanied by the SEB field values that are depicted as the blue dots.

It is recognized that the net height change becomes negative for the higher marsh. This means that the sedimentation at the high marsh cannot keep up with SLR. This was also observed in the spatial patterns between the different AHN datasets in subsection 5.5.1. A sediment concentration of $c = 0.5$ g/L will be used in further model scenarios that include SLR. This corresponds to $c_E = 1.5e-4$. For a lower sediment concentration, the yearly sedimentation rates become negative too quickly, at elevations that correspond to the lower extents of the salt marsh (see Figure 7.7a). It is known from Chapter 2 and 5 that a negative marsh height change occurs for locations at the high marsh only. When the sediment concentration exceeds $c = 0.5$ g/L, the yearly sedimentation rates on the lowermost section of the salt marsh attain disproportionately large levels (Figure 7.7c).

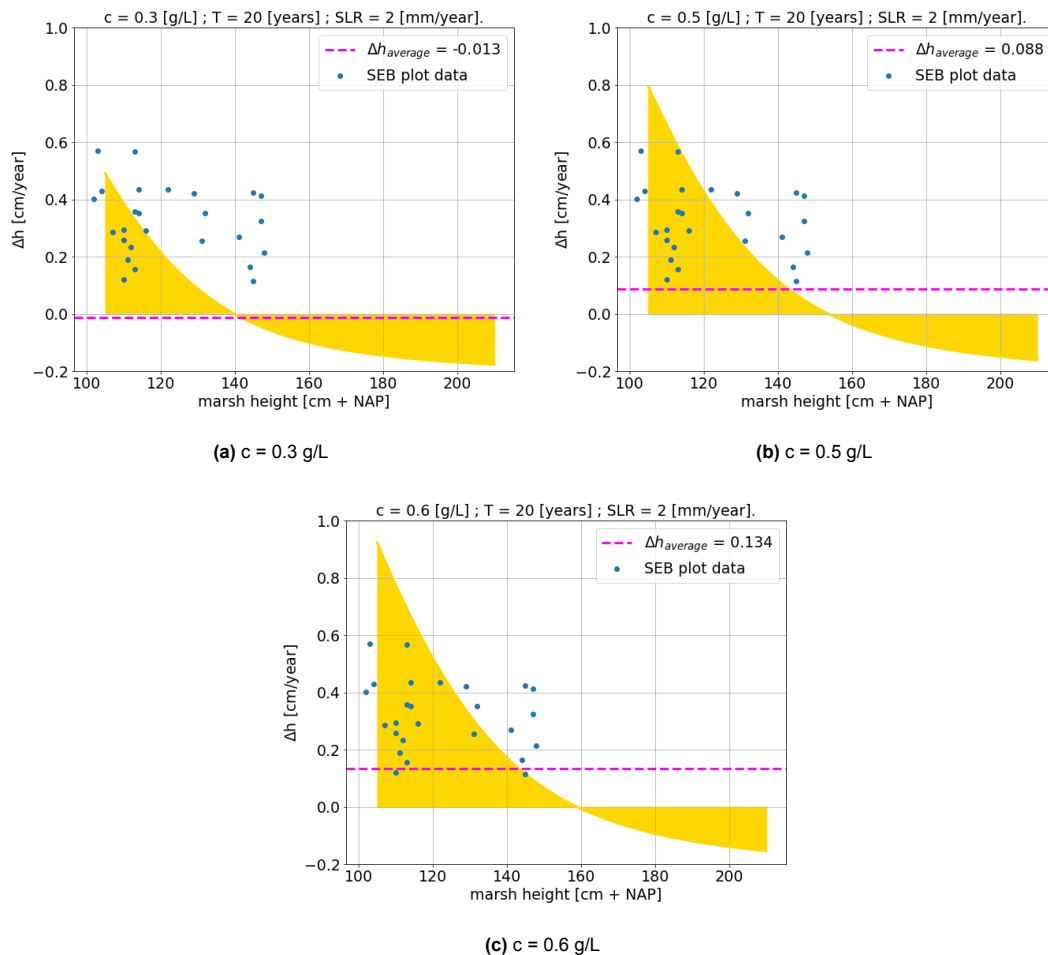


Figure 7.7: Modelled yearly salt marsh height change Δh for a simulation time of 20 years.

The model results for marsh sedimentation in a simulation of $T = 200$ years are shown in Figure 7.8. The sedimentation is positive for all marsh heights. However, Mean High Water (MHW) increases due to SLR and for marsh growth to occur, the sedimentation rate must be larger than SLR. The blue line shows

that the latter is the case for marsh heights up to $\tilde{145}$ cm + NAP. For larger marsh elevations, the rate of SLR is larger than the sedimentation rate. Therefore, the high marsh experiences a relative decrease in height and is situated lower (relative to MHW) after the simulation than before the simulation.

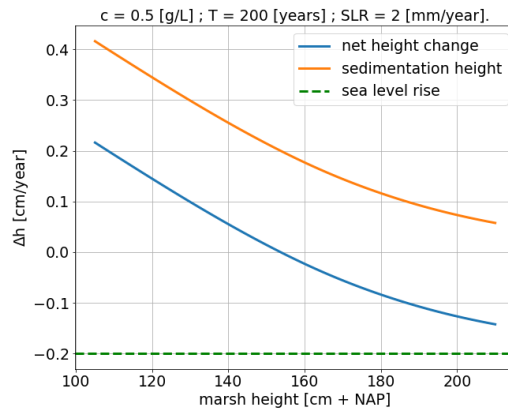
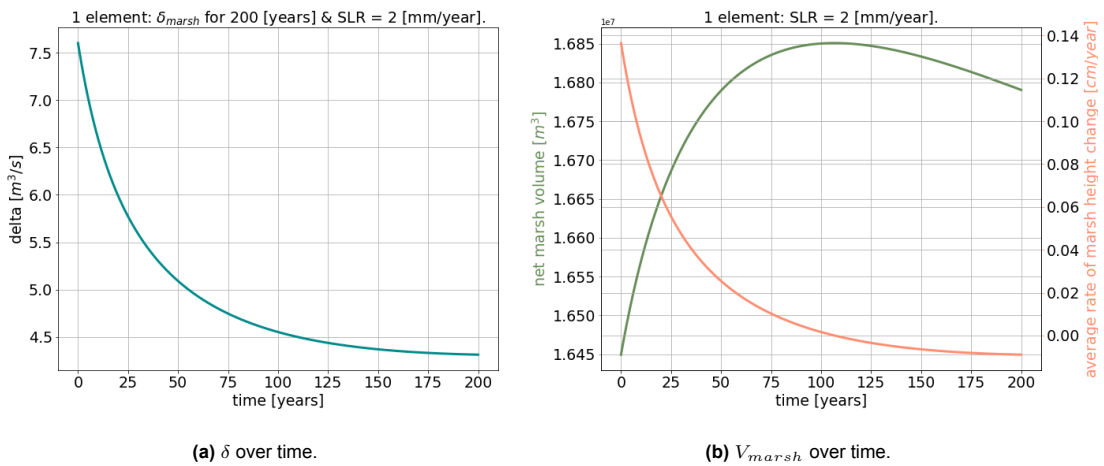


Figure 7.8: Modelled salt marsh net height change Δh , sedimentation height change and height change due to SLR for a simulation time of 200 years.

The course of δ over the simulation time $T = 200$ years is shown in Figure 7.9a. Throughout the simulation, the horizontal exchange coefficient δ continuously decreases. δ levels off at a somewhat higher value than for the case without SLR. The horizontal exchange will not approach zero because new accommodation space is constantly introduced due to SLR. The marsh growth can thus continue.

Figure 7.9b depicts the net marsh volume and the average rate of marsh height change. During the first 100 years of simulation, the net marsh volume increases which implies that the marsh volume increase due to sedimentation is larger than the volume loss due to SLR. After 100 years, the net marsh volume starts to decrease. From this point onwards, the volume loss due to a rise in MHW is larger than the sedimentation volume, which can be explained by studying the hypsometric curves.



(a) δ over time.

(b) V_{marsh} over time.

Figure 7.9: Model simulation for $T = 200$ years & $SLR = 2$ mm/year.

The net hypsometric curves for a simulation time of $T = 20$ years, $T = 200$ years and $T = 500$ years are illustrated in Figure 7.10. It should be noted that MHW increases over time due to SLR. These plots show that the hypsometric curve becomes less steep and more uniform in height over time. Throughout all simulations, the salt marsh remains substantially situated above MHW. For a simulation of $T = 200$ years, the low marsh experienced a significant amount of sedimentation but the overall net salt marsh volume will not be much larger after the simulation than before the simulation. The sedimentation rates on the low marsh are sufficient to lead to an increase in volume there. As long as the increase in low marsh volume due to sedimentation is larger than the loss in high marsh volume, the net marsh volume will increase. As seen in Figure 7.9 for $T = 200$ years, a tipping point is observed after 100 years of model simulations. The increase of MHW occurs at a faster pace than the sedimentation on the high marsh. For that reason, a relative decrease in high marsh volume is seen. After 100 years of model simulations, the volume losses at the higher marsh have become larger than the volume increase of the low marsh. The net marsh volume decreases from this point onwards.

When comparing Figure 7.9a and 7.9b, it can be seen that the course of the horizontal exchange coefficient δ does not have a turning point. The decrease in marsh volume starting from $T = 100$ years does not lead to a subsequent increase in δ beyond this point. This can be explained by the formulation of δ , which covers the water exchange volume and the inundation frequency. The net marsh volume decrease occurs because the sedimentation at the high marsh is too small to keep up with the increase in MHW, whereas the sedimentation rates on the low marsh are larger than the MHW increase. As a result, the salt marsh profile becomes more uniform in height: it flattens out. This means that the inundation frequency of the low marsh decreases. Even though the net marsh volume decreases and the net water exchange volume could increase, the smaller inundation frequency of the low marsh still causes a decrease in the horizontal exchange coefficient δ from $T = 100$ years onwards for this specific salt marsh.

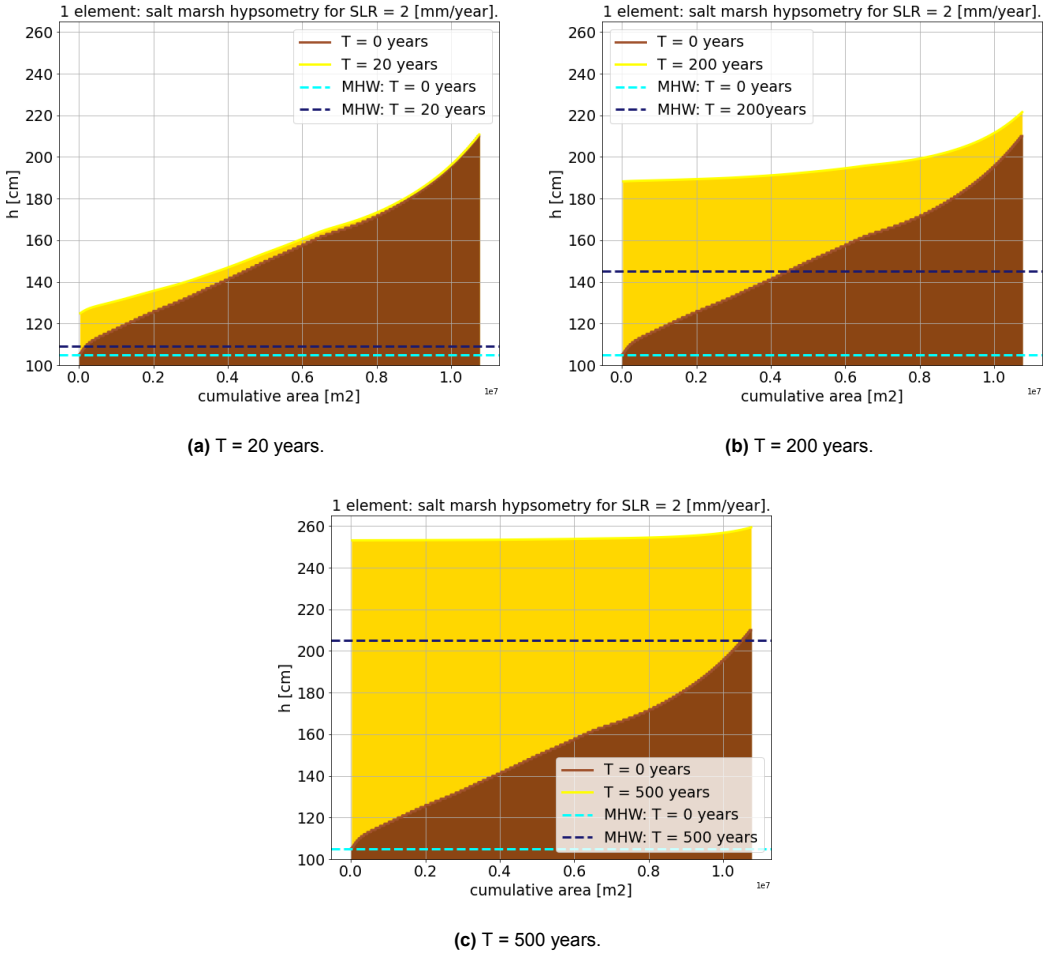


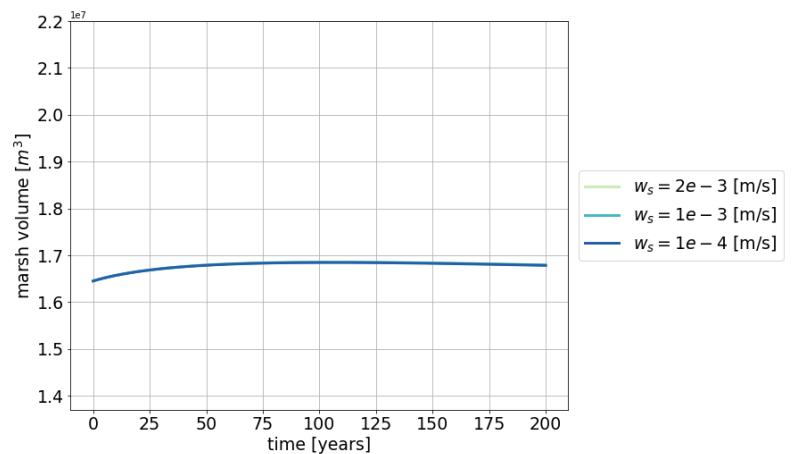
Figure 7.10: Hypsometric curves for different simulation times & SLR = 2 mm/year.

7.3 Sensitivity Analysis

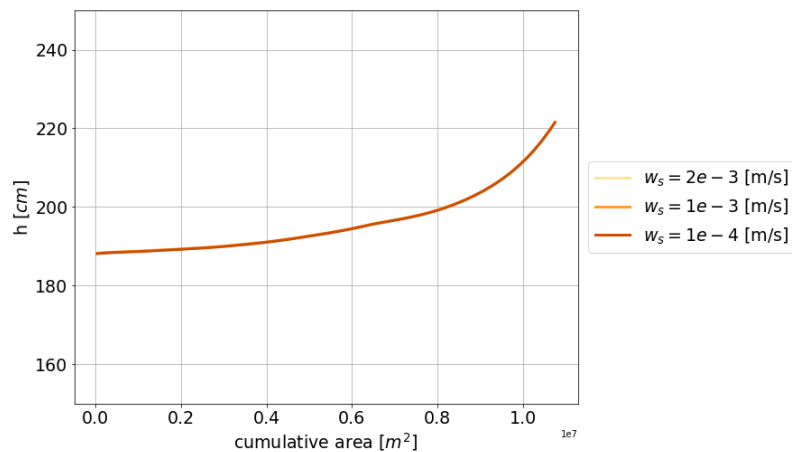
A sensitivity analysis for the one-element model will be conducted for the scenario with a SLR rate of 2 mm/year. The objective of conducting a sensitivity analysis is to examine the impact of parameter choice on the model outcome and to gain insight into the model sensitivity to different parameter values. The parameters that will be assessed are listed below. Figure 7.11, 7.12 and 7.13 give a qualitative overview of the model sensitivity to different parameter values. During the sensitivity analysis of one specific parameter, the remaining parameters are maintained at a constant value, as shown below.

w_s	fall velocity (vertical exchange coefficient)	0.001	[m/s]
c	sediment concentration at outer boundary (= the tidal flat)	0.5	[g/L]
n	porosity	0.8	[-]

The one-element salt marsh model is insensitive to the fall velocity w_s . The insensitivity of w_s can be explained by studying Equation 6.3, which describes the marsh sedimentation, where w_s is present in both the numerator and denominator. The different w_s values in Figure 7.11 are within the range that was discussed in section 6.5. The model results exhibited significant divergence for extreme parameter values beyond this predefined range. However, as these values are not deemed realistic and relevant, they have been excluded from the findings presented here.



(a) Marsh volume change.



(b) Hypsometric curve after simulation.

Figure 7.11: Model simulation for different w_s values, $T = 200$ years & SLR = 2 mm/year.

A large sensitivity is observed for the suspended sediment concentration at the outer boundary of the one-element model, which is depicted as c in this section. This concentration is implemented in the ASMITA model by means of the global equilibrium concentration c_E , which was explained in section 3.6. The range of parameters was chosen according to section 6.6. A significant difference is observed between the different values for c . This implies that the chosen sediment concentration greatly impacts the model results and can be explained by Equation 6.3 and 3.15.

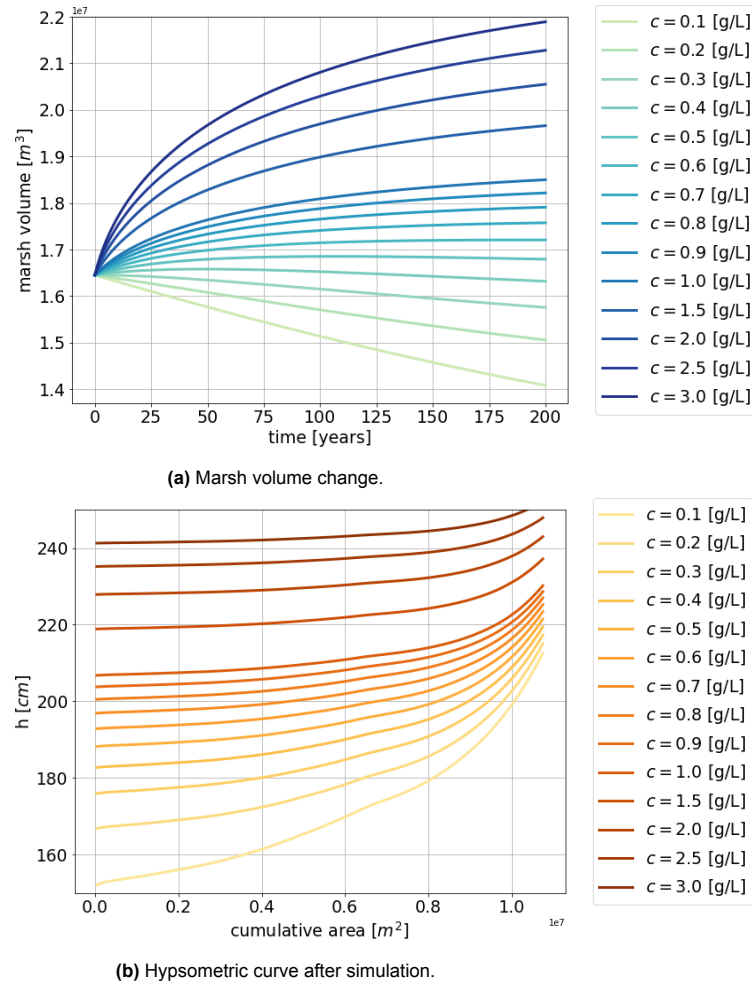
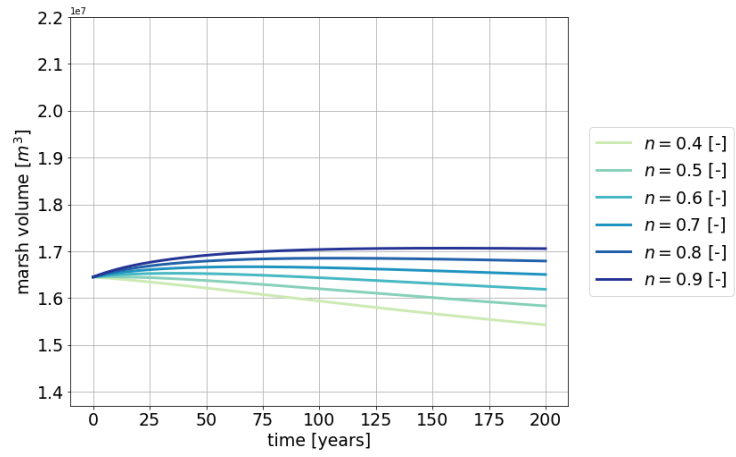


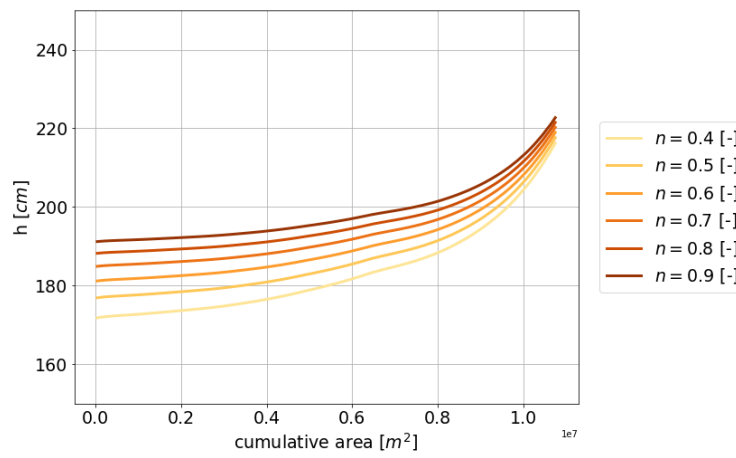
Figure 7.12: Model simulation for different c values, $T = 200$ years & $SLR = 2$ mm/year.

Finally, a sensitivity analysis for the porosity n is conducted. Similar to the sediment concentration c , this parameter is also embedded in ASMITA via the global equilibrium concentration c_E . It can be seen that varying the porosity gives the same sensitivity as the concentration, which can be explained by studying Equation 6.3 and 3.15. The range of varied porosity values is smaller compared to the different concentration values that were modelled. The smallest porosity value $n = 0.40$ corresponds to sandy sediment, whereas $n = 0.90$ indicates a large amount of pore space and corresponds to freshly deposited silty sediment.

Two extreme situations are combined in Figure 7.14, which gives the range of model outcomes within the plausible parameter range.

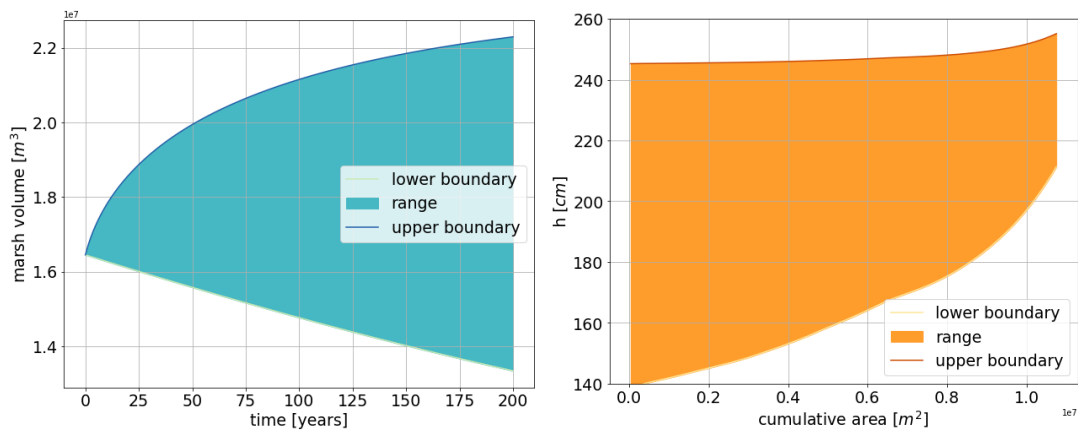


(a) Marsh volume change.



(b) Hypsometric curve after simulation.

Figure 7.13: Model simulation for different n values, $T = 200$ years & $SLR = 2$ mm/year.



(a) Marsh volume.

(b) Hypsometric curve.

Figure 7.14: Range of model outcomes for different parameter settings.

Lower boundary: $w_s = 1e-4$, $c = 0.1$, $n = 0.4$.

Upper boundary: $w_s = 2e-3$, $c = 3.0$, $n = 0.9$.

7.4 Four Elements Model: Zero SLR

Subsequent to the one-element salt marsh model, an extension of the existing 3 elements model is created. This is accomplished by implementing the formulations that were derived for the one-element salt marsh model into the 3 elements model, additional explanation can be found in section 6.7. Accordingly, a 4 elements ASMITA model is obtained that includes an ebb-tidal delta, channels, tidal flats and salt marsh element. The 4 elements model contains a sand and mud fraction. However, it is assumed that no deposition of sand occurs on the salt marsh. The modelled salt marsh sedimentation consists of mud only. The remaining elements contain a sand and mud fraction.

The 4 elements model results for SLR = 0 mm/year can be observed in Figure 7.15, where the dashed line represents the equilibrium volume and the solid line represents the actual moving volume of the element. It is important to acknowledge that the salt marsh element does not have an equilibrium volume. Instead, the growth is limited by a decreasing horizontal exchange coefficient δ for an increasing marsh volume. Moreover, the volumes of the ebb-tidal delta, flats and salt marsh are expressed as dry (sediment) volumes. Whereas the channel volume is a wet volume (previously explained in Chapter 3). A larger channel volume means that the channels eroded and a smaller channel volume indicates sedimentation.

It can be perceived that the ebb-tidal delta, channels and tidal flats reach their equilibrium volume after 75 years. For the channels, a decrease in volume is observed. As the channel volume is expressed as wet volume, a decrease signifies that sedimentation occurred. For the tidal flats, an increase in volume is recognized. This also means that sedimentation occurred since the tidal flats are expressed in dry volume. A decrease of the ebb-tidal delta is visible, which indicates that erosion occurred.

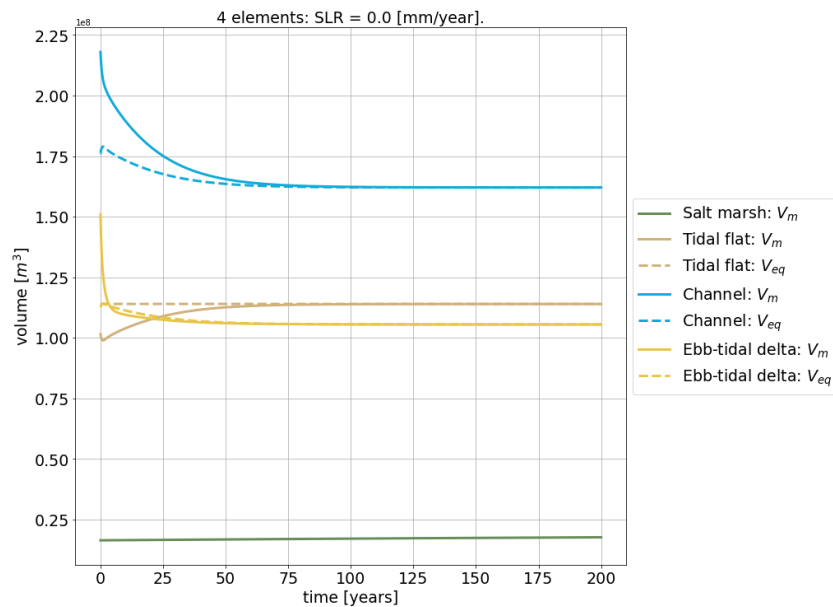


Figure 7.15: Volume change for all four elements over time $T = 200$ years & SLR = 0 mm/year, where the ebb-tidal delta, tidal flats & salt marsh are expressed in dry volume and the channels in wet volume.

The salt marsh volume is one order of magnitude smaller than the other elements, which is why the marsh volume change is not clearly visible in Figure 7.15. A more detailed overview for the course of δ and V_{marsh} is shown in Figure 7.16. The marsh volume slightly increases and the horizontal exchange coefficient has been reduced by almost 50% after 200 years.

A comparison between the height change for the salt marsh element in the one-element and 4 elements model during a simulation of 200 years is shown in Figure 7.17. It can be observed that for the same parameters, the average height change in the one-element model is twice the size of the average salt marsh height change in the 4 elements model. This finding can be attributed to the fact that the suspended sediment concentration was calibrated in the one-element model, to attain comparable model outcomes to the field measurements. However, the concentration that determines the sedimentation for the salt marsh in the 4 elements model is based on the modelled sediment concentration for the tidal flats. This is an aggregated value, which means it represents average conditions. As previously mentioned, salt marsh development does not occur under average conditions but for extreme events, such as storm surges. Figure 7.18 shows the salt marsh hypsometry for the one-element and 4 elements model. The hypsometric curve obtained from the 4 elements model underestimates the sedimentation and is positioned at a lower level compared to the one-element model. The global equilibrium concentration $c_E = 4e-5$ in the 4 elements model, whereas $c_E = 9e-5$ in the one-element model for zero SLR.

The 4 elements model results for SLR = 2 mm/year are shown in Appendix D. In this case, the salt marsh receives an insufficient amount of sediment in order to keep up with SLR. As a result, an immediate reduction in net salt marsh volume is observed. However, the salt marsh did not drown over the simulation time of 200 years. A relatively small marsh volume remains situated above MHW.

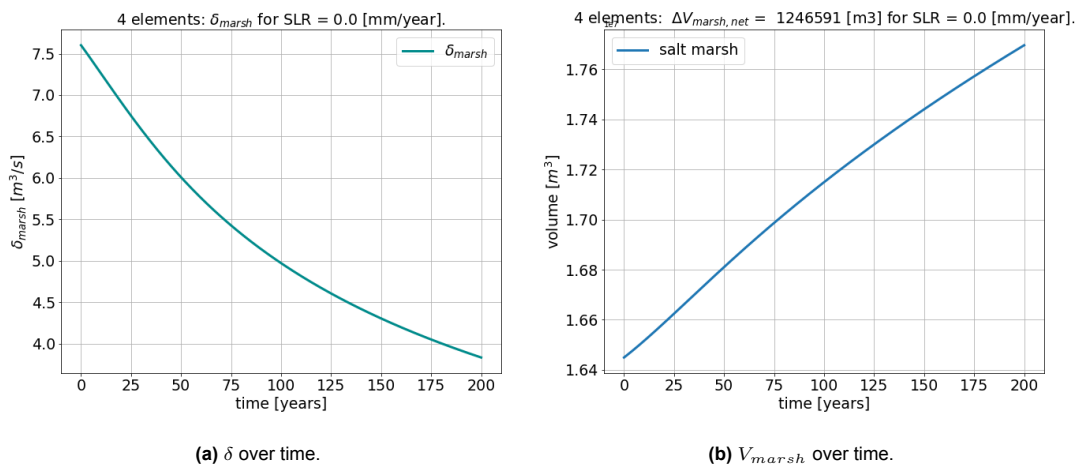


Figure 7.16: 4 elements model simulation for T = 200 years & SLR = 0 mm/year.

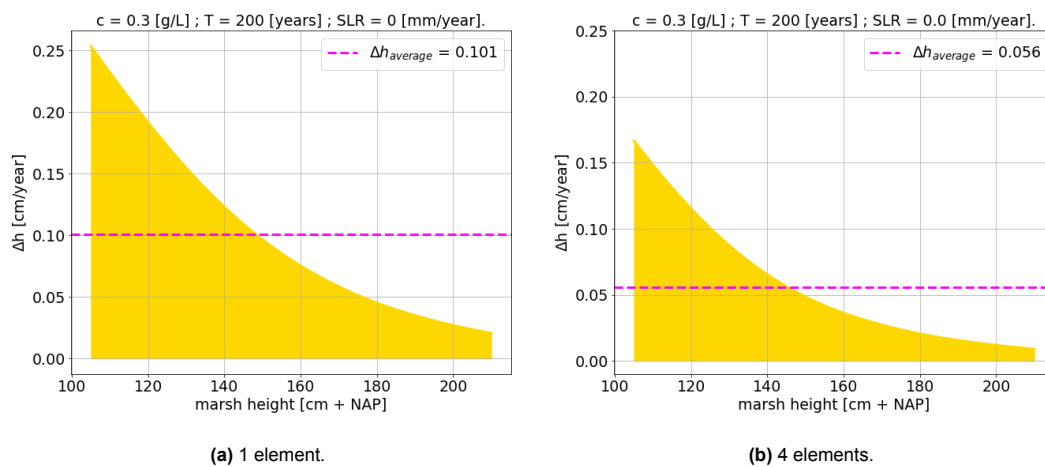


Figure 7.17: Modelled salt marsh height change Δh for SLR = 0 mm/year and a simulation time of T = 200 years.

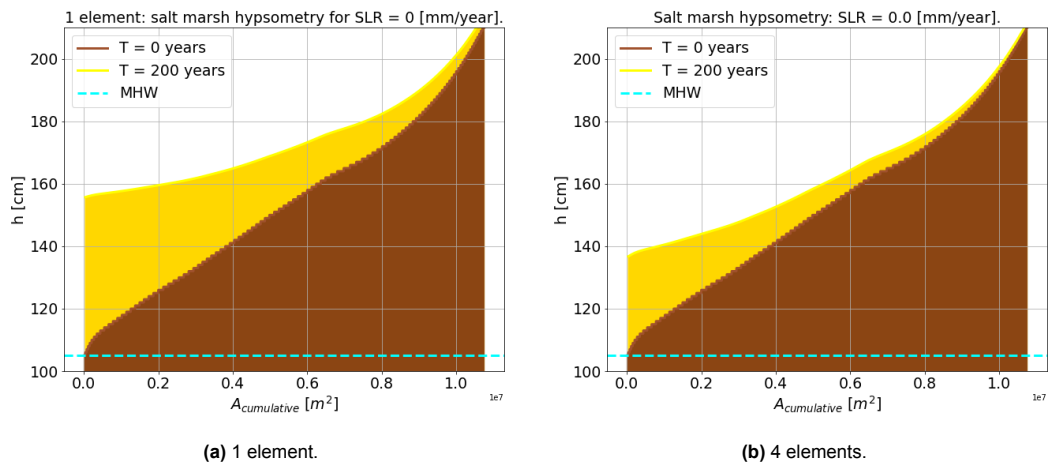


Figure 7.18: Salt marsh hypsometry for SLR = 0 mm/year and a simulation time of T = 200 years.

7.5 Three + One Elements Model

As mentioned in the previous section, the 4 elements model underestimates salt marsh development. It is hypothesized that this arises from incorporating the average sediment concentration in the model, instead of the extreme sediment concentration. To overcome this problem, the one-element salt marsh model is coupled to the existing 3 elements model. Using this method, the extreme scenario for the salt marsh element is matched with the conventional aggregated ASMITA set-up for the other three elements.

In essence, the only adjustment in this new model set-up is found in the equation for the tidal flat element. An outgoing sediment flux is introduced in the sedimentation equation, see Equation 7.1. This outgoing sediment flux is equal to the sedimentation volume that takes place on the salt marsh in the 1-element model.

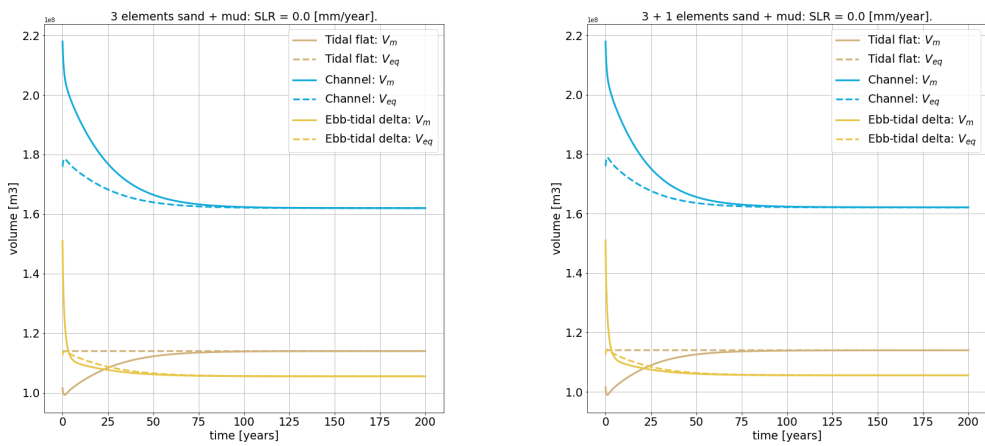
$$\frac{\Delta V}{\Delta t} = B\gamma + d - \frac{\Delta S}{\Delta t} \quad (7.1)$$

Figure 7.19 shows the outcomes for the 3 elements model with and without the outgoing sediment flux. The former will be referred to as the 3 + 1 elements model, while the latter will be labeled the 3 elements model. When comparing Figure 7.19a and 7.19b, no visual differences can be observed. The tidal flat volume for both models is shown in Figure 7.19c. It is evident that the presence or absence of an outgoing sediment flux in the 3 elements model results in negligible differences.

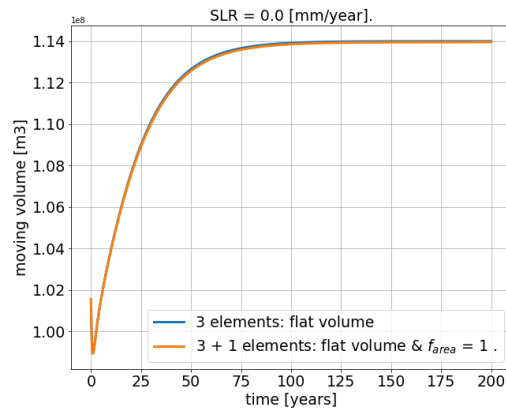
The minor variance between the 3 elements model and the 3 + 1 elements model can be appointed to the difference in initial element volume for the three existing elements and the added salt marsh. The new salt marsh element is one order of magnitude smaller than the other components. Therefore, the marsh sedimentation values are considerably smaller. The minimal size of the outgoing sediment flux makes its influence on the primary elements negligible.

To prove that the element size is important for the outgoing sediment flux, a variation in salt marsh element area (and thus volume) is made. Figure 7.20 shows the course of the tidal flat volumes for scenarios with a salt marsh area that is amplified by a factor of 1, 20 and 100 compared to the initial marsh area as specified in Table 6.9. The tidal flat volume follows the same course for an area that is 20 times larger than the original salt marsh, but ends up at a somewhat lower value after a simulation of 200 years. For a factor of 100, a significant difference is seen. The curve is less steep, which indicates that the tidal flat volume is changing at a slower rate. Moreover, the final flat volume is significantly lower than for the case with the original area of salt marsh Oosterkwelder.

The response of all three elements for the larger salt marshes is shown in Figure 7.21. All elements in Figure 7.21a approach equilibrium after a simulation of 200 years. However, a different outcome is visible in Figure 7.21b. For a salt marsh that is 100 times bigger than the original marsh, the tidal flats and channels are still out of equilibrium after 200 years of modelling. The ebb-tidal delta element did approach morphological equilibrium. However, the approach is less close compared to Figure 7.21a.



(a) Volume change per element for the 3 elements model, where the ebb-tidal delta & tidal flats are expressed in dry volume and the channels in wet volume. (b) Volume change per element for the 3 + 1 elements model, where the ebb-tidal delta & tidal flats are expressed in dry volume and the channels in wet volume.



(c) Comparison of the flat volume.

Figure 7.19: Comparison between the 3 elements model and the 3 + 1 elements model.

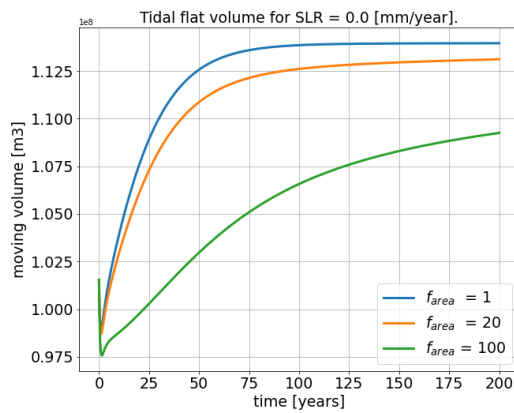
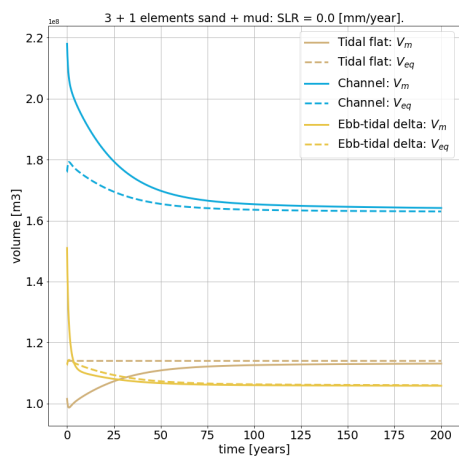
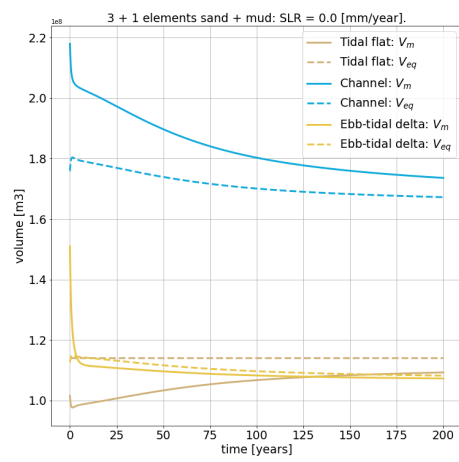


Figure 7.20: 3 + 1 elements model simulation: tidal flat volume for different salt marsh sizes.



(a) $f_{area} = 20$



(b) $f_{area} = 100$

Figure 7.21: 3 + 1 elements model simulations for a salt marsh that is a factor 20 and 100 larger than Oosterkwelder, where the ebb-tidal delta & tidal flats are expressed in dry volume and the channels in wet volume.

7.6 Salt Marsh Development for Different Rates of SLR

This chapter will discuss the results of different SLR scenarios. Section 7.6.1 elaborates on the response of the salt marsh by analyzing the model results of the one-element model. The entire tidal inlet system development is discussed in subsection 7.6.2 by looking at the 3 + 1 elements model.

7.6.1 One-Element Model

The net yearly marsh height change for different rates of SLR and a simulation time of $T = 200$ years are portrayed in Figure 7.22a. The dashed grey line indicates a yearly net marsh height change rate of zero. Values above this line indicate a positive salt marsh development, i.e. the marsh height will increase. If the net marsh height change rates fall below the dashed grey line, a decrease in marsh height is seen. For a SLR rate of 16 mm/year, the net salt marsh height change is below zero for every marsh height. This means that the sedimentation on the salt marsh cannot keep up with SLR. As a result, the salt marsh will drown.

This behaviour is also observed when looking at the course of the horizontal exchange coefficient δ over time in Figure 7.22b. Initially, δ decreases due to the fact that sedimentation happens more quickly than sea level rise. At some point, the rate of SLR is larger than the sedimentation rate and δ starts to increase again. It can be observed that this turning point is crossed at an earlier point in time for a larger rate of SLR.

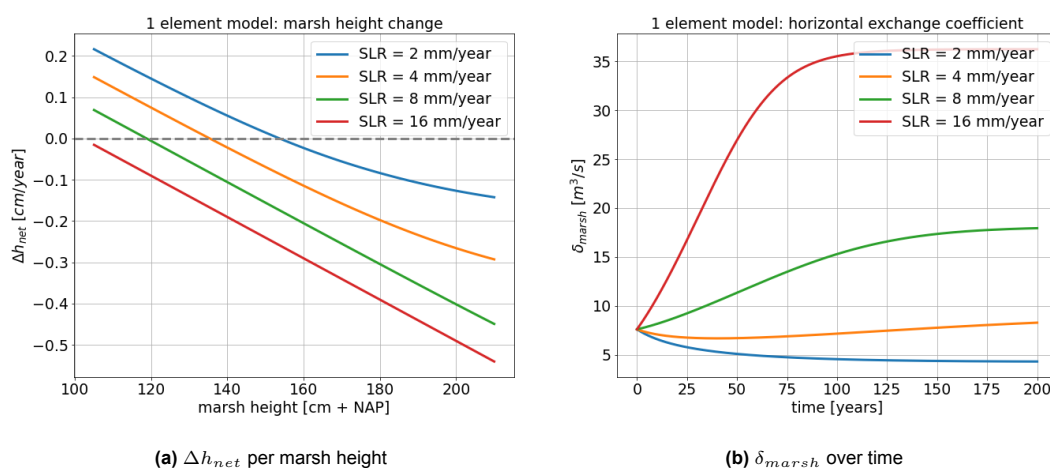


Figure 7.22: One-element salt marsh model results for different SLR scenarios, $T = 200$ years and $c = 0.5$ g/L.

7.6.2 3 + 1 Elements Model

The results for the 3 + 1 elements model including SLR are illustrated in Figure 7.23. The moving and equilibrium volumes over time are shown in respectively the left and right plots. Moving from top to bottom, the results for the ebb-tidal delta, channels and tidal flats are shown. The SLR scenarios from 2 - 16 mm/year are recognized by the varying colours.

A similar trend is observed for the SLR scenarios of 2 - 8 mm/year, with different magnitudes. The ebb-tidal delta experiences a volume reduction, which means that erosion happened. The tidal channels show a decrease in wet volume, which corresponds to sedimentation in the channels. For the tidal flats, a volume increase is observed meaning that sedimentation occurred here as well. For larger rates of SLR, the net volume changes decrease.

For the extreme SLR scenario of 16 mm/year, the trend in all elements reversed. The ebb-tidal delta shows a net increase in volume, which means sedimentation took place at that location. A net increase in wet channel volume is seen. This corresponds to either erosion and deepening of the channels or the sedimentation rates being smaller than the rate of SLR. The tidal flat volume is reduced, which also points to erosion or smaller sedimentation rates than the rate of SLR.

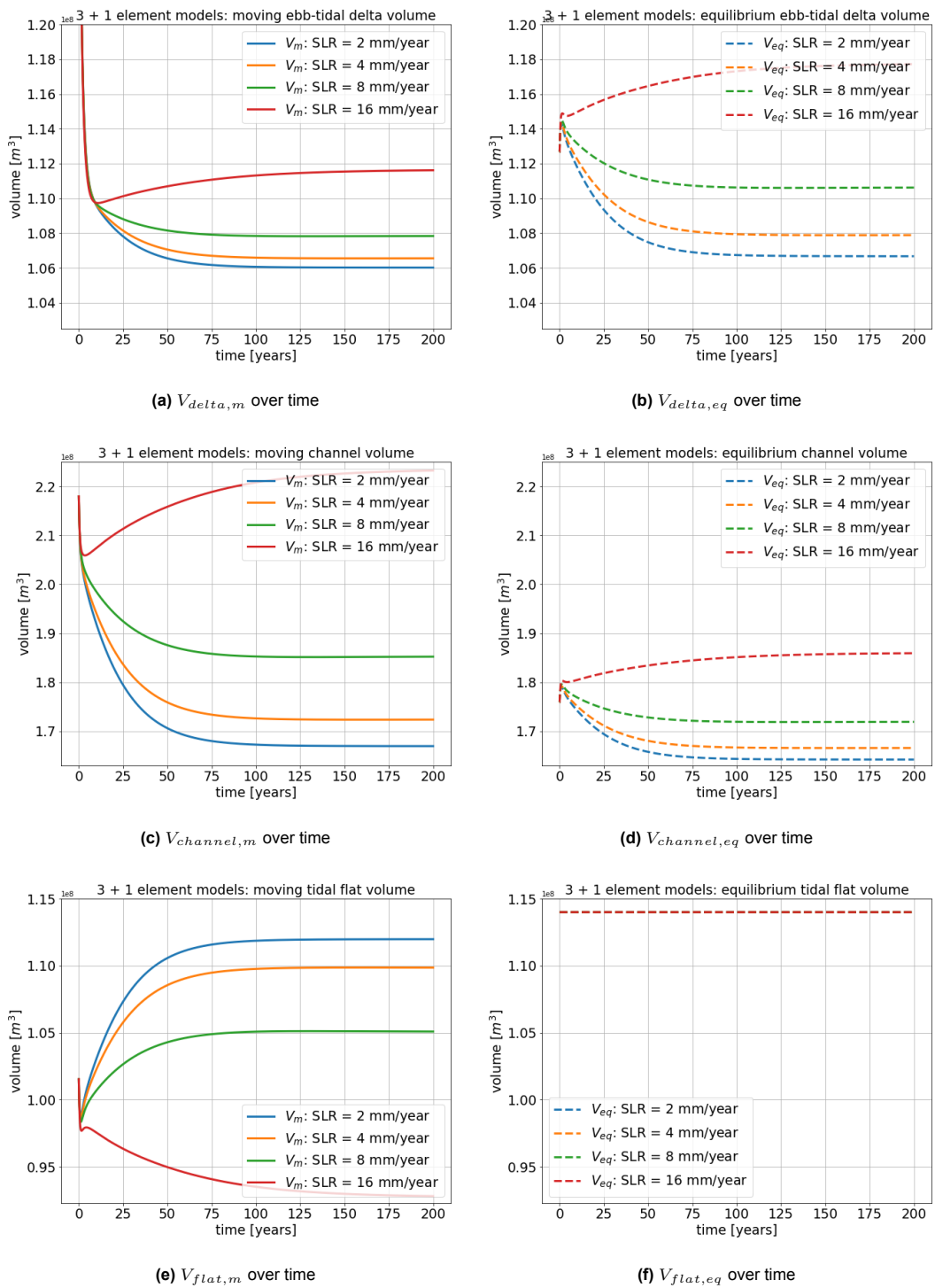


Figure 7.23: 3 + 1 model results for different SLR scenarios, where the ebb-tidal delta & tidal flats are expressed in dry volume and the channels in wet volume.

7.7 3 + 1 Model: Sand-Mud Distribution

Next to the element volumes, a change in the distribution of sand and mud over the elements is observed. The results for the existing 3 elements model under a SLR rate of 2 mm/year excluding a salt marsh are given in Figure 7.24. Figure 7.25 displays the sand and mud content for the channels and flats per marsh size in the 3 + 1 elements model. The total element volumes in the different 3 + 1 model simulations under a SLR rate of 2 mm/year are shown in Appendix E. It is important to highlight that in this context, all volume plots are expressed in sediment volumes, in contrast to the previous sections where the channel volume was presented as wet volume.

When comparing the sand-mud distribution in the 3 elements model (Figure 7.24) and the 3 + 1 elements model with a salt marsh element that is equal to the size of the Oosterkwelder on Schiermonnikoog (Figure 7.25a & 7.25b), a small difference is observed. All volume change that occurs on the salt marsh is extracted from the tidal flats in the 3 + 1 elements model. This outgoing mud flux on the tidal flats is compensated by a larger sedimentation of sand. For the channels, no significant changes are observed.

The effect on the sand-mud distribution is more pronounced when implementing a larger salt marsh element. For a salt marsh element that is 20 times the size of the Oosterkwelder, the sand-mud distribution for the channel and tidal flat elements is shown in respectively Figure 7.25c and 7.25d. Over time, the tidal flats have a notable increase in sand volume and decrease in mud volume. This can be attributed to the extraction of a larger amount of mud by the salt marsh element from the tidal flats. As for the channels, an increase in mud volume is also observed over time. Initially, the sand volume increases as well, but a decline is observed after 100 years. It is hypothesized that extensive extraction of mud from the tidal flats leads to a general rise in mud demand within the system. Consequently, a larger quantity of mud is imported compared to sand. The channels experience an increase in mud volume. However, due to the direct sediment flux, the tidal flats do not witness a rise in mud volume; instead, an increase in sand volume is observed.

The results for an even larger salt marsh element of 100 times the size of the Oosterkwelder is depicted in Figure 7.25e and 7.25f. The channels have an increase in both sand and mud volume. The tidal flats exhibit comparable behaviour to the scenario with a salt marsh element of 20 times the size as the Oosterkwelder. However, in this case the impact is more pronounced.

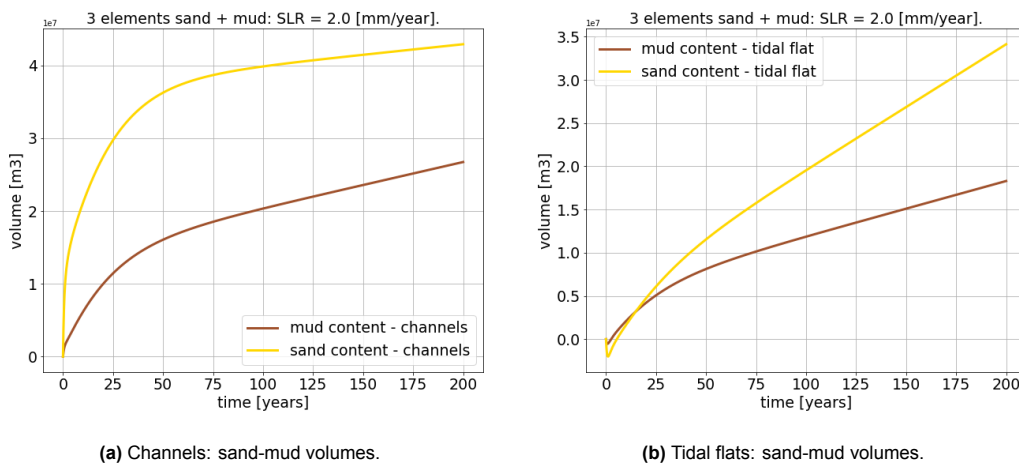
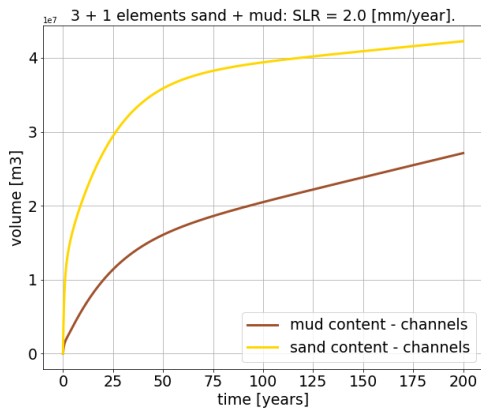
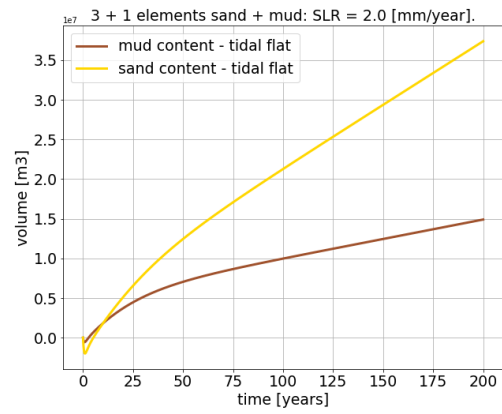


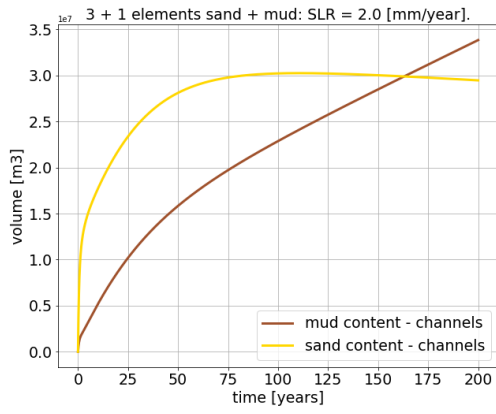
Figure 7.24: 3 elements model: comparison of sand-mud distribution for different salt marsh areas & SLR = 2 mm/year & T = 200 years.



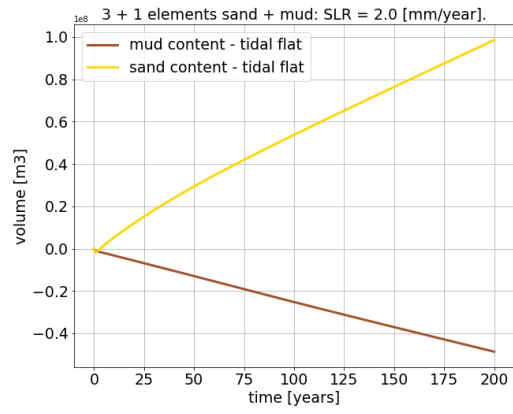
(a) $f_{area} = 1.$



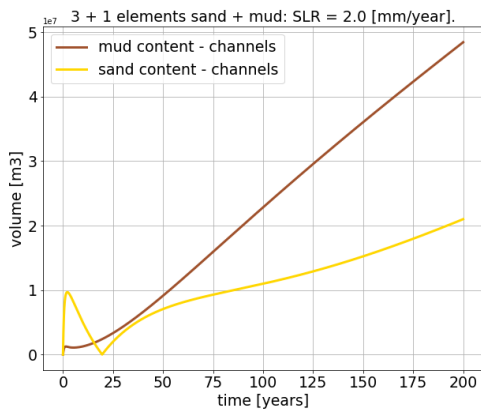
(b) $f_{area} = 1.$



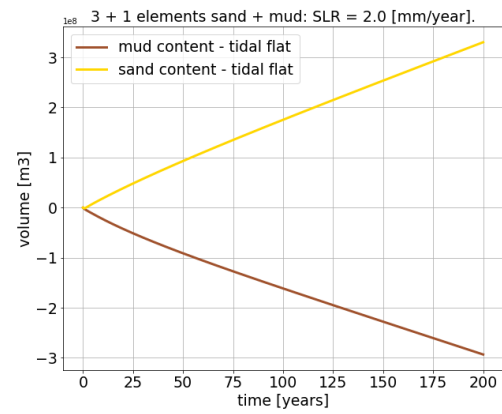
(c) $f_{area} = 20.$



(d) $f_{area} = 20.$



(e) $f_{area} = 100.$



(f) $f_{area} = 100.$

Figure 7.25: 3 + 1 elements model: comparison of sand-mud distribution for different salt marsh areas & SLR = 2 mm/year & T = 200 years.



Discussion

In this research data analysis on salt marsh development in the Dutch Wadden Sea was carried out and salt marshes were implemented in the long-term morphological ASMITA model. This chapter will evaluate the methods and results that follow from the executed research. The salt marsh implementation will be reflected in section 8.1. Discussion of the model results will be given in section 8.2. Finally, implications for coastal management strategies are touched upon in section 8.3.

8.1 Salt Marsh Implementation in ASMITA

The salt marsh implementation in ASMITA is based on a set of underlying assumptions. The implications of these assumptions will be discussed in this section.

Salt marsh extent

In this study, one of the first focus points was to determine the salt marsh extent. As mentioned in section 5.3, the salt marsh extent runs from 350 (~ MHW) to 5 inundations per year. However, as stated in Chapter 2, the salt marsh development begins in the pioneer zone: an area below MHW with an inundation time of approximately 3 hours per tidal cycle. This means that the salt marsh implementation excludes the pioneer zone of the salt marsh. The pioneer zone is now included in the tidal flat element, which is situated between MLW and MHW in the ASMITA model.

The inclusion of the pioneer zone in the salt marsh element could be particularly important for implementing lateral salt marsh development. This process is initiated in the pioneer zone, where the tidal flat experiences a significant amount of sedimentation until it reaches a sufficient height to be classified as part of the salt marsh. Moreover, the pioneer zone could become part of the tidal flats again when cliff erosion occurs. Due to the fixed boundaries between the elements in ASMITA, these dynamics could not be modelled. The pioneer zone could affect the sedimentation volume distribution in the ASMITA model. The sedimentation in the pioneer zone is possibly underestimated in the current model, where the pioneer zone is included in the tidal flats element. However, the results revealed that a relatively small salt marsh element does not have a significant impact on the other tidal inlet elements. Similar outcomes are expected for the pioneer zone, thereby implying that implementing the pioneer zone in the salt marsh element instead of the tidal flat element will not generate entirely different results.

Exclusion of lateral salt marsh development

The salt marsh implementation in ASMITA includes a fixed surface area. This means that the ASMITA model extension does not include lateral regression or transgression of the salt marsh. The main focus of this thesis was directed towards vertical salt marsh development. The literature review argued that lateral transgression allowed for salt marsh establishment during periods of continuous SLR in the past and increases the resilience of salt marshes. However, because it is a cyclic process, the significance of the impact on the aggregated spatial and temporal ASMITA scales is unknown. Therefore, it was excluded from the current model extension.

Additionally, the boundaries of the existing ASMITA elements are based on the vertical limits of MLW and MHW. When lateral transgression and regression are included, the element volumes should be adjusted accordingly, as a shift of element areas will have to be included. This was outside of this research scope. However, in the field, the boundary between the salt marsh and the tidal flat is dynamic. Specifically with accelerating SLR, the boundary is prone to shifting. The current ASMITA salt marsh implementation is unable to model this phenomenon, which may lead to incorrect predictions of the element's behaviour over time. This will be further elaborated on in section 8.2.

Derivation of δ

The horizontal exchange coefficient δ plays a crucial role in determining the amount of sedimentation that occurs on the salt marsh in the ASMITA model. The parameter was derived based on hydrodynamic data and the hypsometric curves of the salt marsh study areas. Uncertainties with respect to the derivation of δ will be discussed here.

Hydrodynamics

The hydrodynamic data analysis that was carried out in Chapter 5 is based on water level data obtained from the Schiermonnikoog measurement station. A transformation was not performed for converting the water level measurements taken at the Schiermonnikoog station to corresponding levels on the salt marsh, because it was assumed that the water levels at both locations are identical.

However, water levels on the salt marsh will most likely be different due to factors such as wave attenuation, tidal propagation and wind set-up (Hijuelos et al., 2019). Moreover, the hydroperiod of a salt marsh exhibits lags with the normal tidal cycle, which could affect the water levels. This is not accounted for in the derivation of δ . As a result, the value for the horizontal exchange coefficient may deviate from what it should be.

The location of the Schiermonnikoog water level measurement station is relatively close to salt marshes Het Rif and Oosterkwelder. However, it is located further away from the Ameland salt marshes. For the ASMITA model application of the Ameland salt marshes, a consideration in the derivation of δ was to apply the Schiermonnikoog water level data or to employ the water level data from the Ameland measurement station. An implication for the latter is that, even though the measurement station is located closer to the Ameland salt marshes, it is positioned in a different tidal inlet system: the Ameland inlet. The salt marshes on Ameland are located in the Frisian inlet. However, Neerlandsreid is situated very close to the tidal watershed between the Ameland and Frisian inlets. The Oosterkwelder on Schiermonnikoog is also located across a tidal watershed.

In this research, it was assumed that the tidal watersheds are closed boundaries. Therefore, it was decided to utilize the Schiermonnikoog data for both the Ameland and Schiermonnikoog salt marshes. In reality, a certain amount of water is exchanged over tidal watersheds, especially for extreme water levels during high wind events. It is important to keep this in mind for the derivation of the horizontal exchange coefficient δ in future research. The influence of the additional tidal inlets was not considered in this research.

Lastly, the 18.6-year tidal cycle was not entirely incorporated in the derivation of δ in this research. Only 10 years of hydrodynamic data were analyzed: 2012 - 2022. Therefore, not all minima and maxima that occur due to the 18.6-year tidal cycle were included in the derivation in δ . This could have led to slight under- or overestimations of the horizontal exchange coefficient.

Salt marsh hypsometry

The hypsometric curves that were extracted from the DTMs of the AHN data were used in the derivation for δ , as they represent the salt marsh bathymetry. However, in Chapter 5 it was discovered that the AHN data contains a certain mismatch with the local SEB measurements. The salt marsh surface heights obtained from the AHN data were structurally higher than the surface heights measured by the local SEBs.

It is important to acknowledge that the surface height difference between the AHN and SEB data varied per study area: an overview is shown in Table 8.1. The hypsometry correction that was applied for the derivation of δ is based on this range of height differences. However, the SEBs mostly contain measurements on the lower part of the salt marsh. Therefore, the height correction could be inaccurate for salt marsh locations where no SEB measurements were taken. Furthermore, the height variation of the Oosterkwelder on Schiermonnikoog was excessive, which made it challenging to implement a precise height correction. A uniform correction was carried out for simplicity. The actual hypsometry is likely to deviate from the corrected hypsometric curve, especially for the Oosterkwelder.

barrier island	salt marsh	$\Delta h_{AHN-SEB}$ [cm]	AHN correction [cm]
Ameland	Neerlandsreid	5 - 15	- 5 / - 15
Ameland	De Hon	~ 10	- 10
Schiermonnikoog	Oosterkwelder	2 - 55	- 20

Table 8.1: Overview of the difference between surface heights obtained from AHN and SEB data for the different study areas in the Dutch Wadden Sea.

Several potential reasons for the surface height difference between the AHN and SEBs were explored. The first cause of the mismatch between the two data types could be measurement uncertainties in either or both datasets, which will be explained below. The second reason for the structurally higher AHN data may be attributed to the transformation of the LiDAR point clouds to the Digital Terrain Model (DTM).

The AHN data contains a systematic measurement uncertainty of 10 cm (Actueel Hoogtebestand Nederland, 2022). This is a significant value for salt marsh development, as the characteristic vertical surface height change is usually in the order mm/year. Furthermore, a stochastic measurement uncertainty of 5 - 15 cm is present in the AHN data.

Moreover, the AHN interpolation could give some unexpected results. Originally, a point cloud layer is obtained from the LiDAR laser altimetry. The points are interpolated to a raster layer, which is the datatype that was used in this research. The interpolation from the point cloud to the raster layer could result in some additional uncertainties. For example, when one point is sampled in a marsh creek and the other point on the marsh platform, the resulting interpolated surface would not contain the steep gradient that is present. The average height is implemented in the raster layer. When comparing this value with the local SEB measurement, this may cause the AHN to give a (substantially) different surface height. Table 8.2 gives an overview of the points per m² in each AHN dataset. The issue of interpolation is likely to pose a problem for the oldest dataset: AHN 1. The newer datasets seem to contain enough points per m² for the transformation from point cloud to raster layer.

dataset	points per m ²
AHN 1	0.3 - 0.6
AHN 2	6 - 10
AHN 3	6 - 10
AHN 4	10 - 14

Table 8.2: Number of points per m² for each AHN dataset (Actueel Hoogtebestand Nederland, 2022).

It was already suggested in subsection 5.5.3 that the surface heights obtained from the AHN data may include a certain quantity of vegetation. The extracted AHN data used in this thesis were DTMs, which means that vegetation should have been eliminated, as opposed to DSMs (subsection 5.5.1). The fact that the AHN data is structurally higher than the SEBs may imply that the filtering method for transforming a DSM into a DTM was not carried out entirely correctly. On the other hand, the salt marsh vegetation may have been too dense which would make it impossible for the filtering to be conducted correctly.

In addition to the systematic difference between the AHN data and SEBs, it was noticed that the AHN 4 dataset showed inconsistencies with respect to the AHN 1, 2 and 3 datasets. Specifically, the AHN 4 dataset exhibited smaller marsh surface heights than anticipated. A possible explanation for this disparity could be attributed to the timing of data extraction. If the AHN data includes the vegetation height, the moment of data collection could give varying results. When the height maps are extracted in summer, taller and denser vegetation will be incorporated in the data, whereas in winter, the vegetation appears less dense and is lower in height. It should be noted that this explanation remains a hypothesis due to the lack of precise information regarding the exact time of data collection.

Next to the AHN data, the SEB measurements also contain some uncertainties. The SEBs on the Ameland salt marshes Neerlandsreid and De Hon are closely managed and maintained by the Dutch oil and gas company NAM. The measurements are precise and expected to contain relatively small errors only. The SEB locations are determined by using laser spirit levels (RTK - DGPS).

However, the measurements of the SEB coordinates on Schiermonnikoog are less precise and contain uncertainties in the order of 5 - 10 m in the horizontal direction (De Groot, personal communication, March 6, 2023). This is significant and could mean the difference between a creek and an elevated platform. Moreover, the NAP references on Schiermonnikoog are not maintained. Observations by De Groot et al. (2015) state that some of the reference levels are skewed. This could have a significant impact on the surface heights that were obtained from the Schiermonnikoog SEBs. Thus, the Schiermonnikoog SEBs have quite some uncertainties whereas the Ameland SEBs appear to be more reliable. This could possibly relate to the large range in Table 8.1 for Schiermonnikoog.

Soil porosity

In this research, the parameter setting for the porosity is chosen at a value of $n = 0.80$. This means that 80% of the soil consists of pores and the remaining 20% consists of sediment particles. The value for $n = 0.80$ corresponds to silty sediments that have just been deposited. Consequently, large pore space is present. However, the ASMITA model should contain the average porosity over the entire model simulation. It is likely that the value of $n = 0.80$ overestimates the porosity. The freshly deposited silty sediment experiences autocompaction over time, as explained in section 5.4. As a result, the average porosity value is expected to be somewhat smaller than $n = 0.80$. The porosity value $n = 0.40$ corresponds to coarse sediments, such as sand. The average porosity value is expected to be in between these two values. When a smaller value for the porosity is implemented in the ASMITA model, the results will depict a reduced salt marsh height change.

8.2 ASMITA Model Results

The ASMITA model results will be interpreted in this section. Furthermore, this section will explore the correspondence between the model results and reality.

One-Element Model

The results for the one-element model suggest that a large cliff forms at the salt marsh boundary. This can be seen in for example Figure 7.6 and 7.10. At the lower salt marsh boundary, a vertical straight line is visible after the model simulations, which indicates a steep cliff. It is crucial to realize that this process is forced because no lateral salt marsh development is included in the model. In practice, the cliff will not grow as large as the long-term one-element simulations imply. A higher cliff becomes more unstable and experiences an increased vulnerability to wave attacks. This results in cliff retreat before it can grow to significant heights, as explained more extensively in section 2.4. At the point of cliff erosion, the amount of sediment volume that belonged to the eroded cliff will be transferred from the salt marsh to the tidal flat. If the model would include cliff erosion, this volume shift from element to element should be visible. The volume change on the lower part of the salt marsh would be somewhat smaller than currently simulated.

Moreover, the one-element salt marsh model does not depict the vertical growth of the adjacent tidal flats. Tidal flats are prone to drowning, which in turn leads to less sediment supply on the salt marsh (Van der Wegen & Roelvink, 2008). A study by Huismans et al. (2022) states that the tidal flats will not be fully able to keep up with SLR for large rates (> 4 mm/year): either a decrease in area or height is observed. This has consequences for the salt marsh cliff formation, which should be considered when the lateral salt marsh development is included in the ASMITA model extension. For a SLR scenario of 2 mm/year, the tidal flats will grow at the same rate as SLR. In that case, the cliff formation is not expected to be enhanced by additional height differences due to the loss of tidal flats.

The comparison between the model outcomes and SEB sedimentation rates implies that the model shows an excessive reduction in sedimentation rate per marsh height. This can be observed in Figure 7.7, as the right half of the blue SEB points are not represented in the model which is shown by the yellow area. This seems to imply an overly pronounced decrease in sedimentation per marsh height. The difference between the model results and the SEBs can be partially explained by studying the locations of the SEB measurements. The SEBs are located relatively close to marsh edges and creeks, which corresponds to relatively high sedimentation values. As a result, the accretion measured by the SEBs may be an overestimation and may not be representative for the entire salt marsh development: lower sedimentation values on the higher parts of the salt marsh are expected to occur.

However, an additional explanation for the excessive reduction in sedimentation per marsh height is possibly found in the fact that the current model extension does not consider a relation between the water level and the SSC. During spring tides and during storms, the high marsh is inundated. These periods are characterised by highly energetic conditions, which means the SSC attains relatively large values. Conversely, the low salt marsh experiences daily flooding, predominantly under low energy conditions. This corresponds to smaller SSCs. The current model extension uses only one value for the SSC, which is embedded in the global equilibrium concentration c_E . Consequently, the average SSC on the low marsh is likely to be overestimated and the average SSC on the high marsh is potentially underestimated. As a result, the hypsometric curve after the model simulation now shows uniformity in height whereas a salt marsh hypsometry should contain some slope. The Oosterkwelder salt marsh on Schiermonnikoog is relatively far in succession and the hypsometric curve is thus expected to be close to an 'equilibrium' shape. This means that the model simulations should yield a somewhat similar shape, which is currently not evident.

Furthermore, the calibration of the model with the SEB measurements is not entirely accurate. The SEBs measure the change in surface height: accretion. As explained in section 2.4, this includes mineral sedimentation, accumulation by plant biomass and autocompaction. The ASMITA salt marsh model formulations are set up to only represent the mineral sedimentation. No extra formulations for accumulation by plant biomass and autocompaction are included. When calibrating the parameters against the accretion rates instead of sedimentation rates, this could lead to a mismatch. However, there was no available data on sedimentation rates for calibration. As a result, the accretion measurements were the only possible calibration dataset for this thesis.

Finally, the model results are very sensitive to the sediment concentration. Since the parameter setting in this research was not based on field measurements, but instead relied on a literature review and calibration, it introduces significant uncertainties for the model outcomes. Mainly the SSC is an important predictor of the ability of salt marsh survival under accelerated SLR. For precise model calibration, field measurements on the SSC close to the boundary between the tidal flat and salt marsh are needed.

Course of the tidal flat volume

At the beginning of the ASMITA simulations for the multiple element models, a dip in the tidal flat volume can be observed in both the 3 elements, 4 elements, and 3 + 1 elements model. This is clearly visible in for example Figure 7.19. The model set-up and elements are based on the Zoutkamperlaag tidal inlet system, where the Lauwerszee reclamation was carried out in 1969. As a result, significant morphological changes occurred (Wang et al., 1995). It is plausible that there exists a correlation between the dip in tidal flat volume and this human intervention.

Due to the Lauwerszee closure, the tidal prism significantly decreased. As a result, the equilibrium volumes of the ebb-tidal delta and tidal channels were reduced. The channels were demanding sediment from the system, whereas the ebb-tidal delta supplied sediment to the system. However, a time lag was present between this sediment demand by the channels and the sediment supply by the delta. Therefore, the channels temporarily extracted sediment from the tidal flats to meet their stronger demand for sediment (which is represented by a strong concentration gradient). This can be observed by the dip in tidal flat volume. After some time, the concentration gradient tilts again due to the increased amount of sediment availability from the ebb-tidal delta and/or the fact that the channels extracted a sufficient amount of sediment from the tidal flats such that the concentration gradient decreased. From this moment onwards, both the channels and tidal flats extract sediment from the system.

3 + 1 Elements Model

Currently, the 3 + 1 elements model is based on an 'offline' method. Initially, the one-element salt marsh simulation is performed, followed by the 3 + 1 elements model simulations. The 3 + 1 model uses the outgoing sediment flux obtained from the previously executed one-element salt marsh model simulations. The one-element model contains a constant value for the global equilibrium concentration c_E . In other words, the boundary condition, that is the SSC on the adjacent tidal flat, remains constant. The 3 + 1 model does not include any feedback from the 3 elements model towards the one-element model. The one-element model runs independently from the conditions in the 3 elements model. This could have some implications, as the salt marsh is presumed to consistently receive the amount of sediment specified by the constant value for c_E . However, the marsh could come short of sediment when for example the tidal flat demands more sediment or when less sediment is available in the entire tidal inlet system. As a result, the salt marsh development would be altered. Two recommendations for improving the communication between the salt marsh element and the rest of the tidal inlet system will be elaborated on in Chapter 9.

Another implication of the outgoing sediment flux on the tidal flat is the lack of a concentration gradient. The salt marsh sedimentation volume is now directly extracted from the tidal flat element by the outgoing sediment flux, as opposed to the methodology between the remaining three elements where the concentration gradient determines the sediment transport. If the 3 + 1 model would contain a sediment concentration gradient between the salt marsh element and tidal flat element, the alterations in sand-mud distribution (Figure 7.25) are expected to be less significant. This problem is not present in the 4 elements model, which does contain a concentration gradient between the salt marsh and tidal flat elements on which the sediment transport is based. A recommendation for improving this model will be given in Chapter 9.

The 3 + 1 model results revealed that the salt marsh element based on the Oosterkwelder on Schiermonnikoog has a negligible effect on the morphological development of the remaining elements in the Zoutkamperlaag tidal inlet. Nevertheless, there exist additional salt marshes in the Zoutkamperlaag inlet apart from the Oosterkwelder. Figure 7.20 shows that a larger salt marsh element could have a significant effect on the remaining tidal inlet system elements provided that the element is at least 20 to 100 times as large as the Oosterkwelder. For the Dutch Wadden Sea, specifically the Zoutkamperlaag tidal inlet, the total salt marsh area is small compared to the size of the remaining tidal inlet elements and the effect of the salt marsh is indeed assumed to be minor. Tidal inlet systems with a larger salt marsh component are expected to be affected more heavily by the salt marsh element.

Prediction of salt marsh development under accelerated SLR

This section will discuss how the model results relate to the predicted future response of salt marshes to accelerated SLR.

The first point of attention for predictions of salt marsh survival under accelerated SLR is the model parameter setting. The ASMITA model results depict a large sensitivity to the parameter setting. Chapter 7 revealed that the global equilibrium concentration c_E has the largest impact on the model outcomes by means of the porosity n and sediment concentration c . Implications with respect to the parameter setting were previously addressed in section 8.1 & 8.2 and should be duly considered when establishing a correlation between the model results to the predicted future response of salt marshes to accelerated SLR since it gives a large uncertainty in the predictions of salt marsh survival under accelerated SLR.

A feared consequence of accelerated SLR is the large-scale loss of salt marshes. However, previous research shows that the loss of salt marshes under accelerated SLR may not be imminent. A study by Kirwan et al. (2016) argues that cases of complete salt marsh loss are rare and usually only occur at locations with human interference in sediment availability or subsidence. For 19 - 36 % of the studied salt marshes, a certain amount of submergence takes place. This is derived from studying accretion or elevation measurements on the marshes, which is a common standard for the evaluation of salt marsh development under accelerated SLR. Kirwan et al. (2016) state that the accretion rates measured in the historical data analysis may be inapplicable, since the number of inundations significantly (non-linearly) increases for accelerated SLR. When only low marsh measurements are included, that do have a higher sedimentation rate, less than 5% of the studied salt marsh experience submergence. The ASMITA model extension presented in this thesis includes the increased amount of salt marsh inundations by means of the horizontal exchange coefficient δ .

Besides the increased number of floods, Kirwan et al. (2016) emphasize that the biogeomorphic feedback mechanisms, as explained in section 2.5, are important in assessing the response of salt marshes to accelerated SLR. The vulnerability of salt marshes is possibly overestimated when the biogeomorphic feedback mechanisms are excluded from analyses. While salt marshes become progressively more flooded, the productivity of various plant species increases (Morris et al., 2002; Kirwan and Guntenspergen, 2012). A denser vegetation canopy leads to enhanced mineral sediment trapping efficiency since the flow and waves are attenuated. Moreover, the deposition of organic material increases for a more productive environment. Kirwan et al. (2016) also mention that there are other effects of climate change that may enhance salt marsh survival. Specifically, raised global temperatures and elevated atmospheric CO₂ concentrations are shown to boost the productivity of marsh plant species and could thus increase the marsh survival rates (Mudd et al., 2010). This ASMITA model lacks the incorporation of biogeomorphic feedback mechanisms. This process was not included in the ASMITA salt marsh model extension because the contribution by plant biomass is relatively small compared to the mineral sedimentation (Figure 2.12) for the study areas in the Dutch Wadden Sea. This process could be more important for the survival of tidal inlet systems with limited sediment availability, transport capacity, or accommodation space.

Dynamic salt marsh models that include biogeomorphic feedback mechanisms were employed by Kirwan et al. (2010) and predict salt marsh survival for rates of SLR up to 10 - 50 mm/year. The threshold range largely depends on the SSC, the tidal range and the distance to the nearest sediment source. These components are mostly related to the mineral sedimentation. Based on the chosen parameter configuration, the ASMITA model predicts complete drowning of the salt marsh for a SLR rate larger than 16 mm/year. The difference between these two survival rates is expected to mainly arise from the parameter setting of the ASMITA model, as the accumulation by plant biomass is expected to be of a different order of magnitude, even under the possible increase of plant productivity under accelerated SLR.

Saintilan et al. (2022) state that autocompaction increases non-linearly with sedimentation. This means that the larger sedimentation rates due to accelerated SLR go hand in hand with more autocompaction. As a result, deficits emerge and the elevation gain is constrained which corresponds to a larger salt marsh vulnerability. This is not included in the ASMITA model extension.

Another important implication of the ASMITA extension with respect to predicting the survival of salt marshes under accelerated SLR is the exclusion of lateral salt marsh development. The change in salt marsh size essentially consists of horizontal and vertical changes. As discussed in section 8.1, the vertical changes are incorporated in the ASMITA model extension whereas the horizontal changes are disregarded. This affects the predictions of salt marsh development under accelerating SLR. Kirwan et al. (2016) declare that lateral salt marsh development is prone to SLR. Lateral salt marsh development can respond quickly to decreasing inundation frequencies, but react more slowly to increasing inundation frequencies (Balke et al., 2016). It is expected that only salt marshes near large sediment sources, such as rivers, are able to keep generating the lateral cycle of regression and transgression. For salt marshes with a smaller sediment supply, transgression is estimated to become dominant. The survival of salt marshes under accelerated SLR will then depend on the ability to transgress landwards in adjacent terrain.

A limitation in accommodation space by anthropogenic barriers, such as flood protection, may pose a larger threat to salt marshes than drowning by SLR (Schuerch et al., 2018; Bouma et al., 2016). This is because these barriers can restrict the salt marsh's ability to expand, as it becomes confined within rigid boundaries. The ASMITA salt marsh model contains a constant marsh surface area, which means that a reduction in accommodation space was not incorporated. This could mean that the marsh volumes obtained from the model extension overestimate the actual marsh survival rate for cases where the lateral accommodation space is limited. Surprisingly, even an overall gain in salt marsh area can occur under accelerating SLR at locations with a significant amount of accommodation space (Schuerch et al., 2018; Enwright et al., 2016). For small SLR scenarios, the overall gain in salt marsh surface area is also seen at locations with a limited accommodation space provided that the sediment availability is sufficient. Schuerch et al. (2018) concludes that, even for high SLR scenarios, an increase in areal salt marsh extent can be observed when a significant amount of accommodation space is granted. This phenomenon is not represented in the ASMITA salt marsh extension presented in this thesis, which could affect the model predictions for salt marsh survival under accelerated SLR.

8.3 Implications for Management Strategies

Chapter 1 argued that salt marshes act as important flood protection for the hinterland, have significant ecological importance and play a role in carbon sequestering. Management strategies are designed to ensure the preservation of these functions, for instance by Rijkswaterstaat. This section will shortly elaborate on the implications of the model outcomes on management strategies, and how the model can be employed in practice.

The model predicts the survival of the Oosterkwelder salt marsh for SLR rates smaller than 16 mm/year. This value highly depends on the model parameter setting but is within the same range as previous research conducted by for example Kirwan et al. (2010). For lower rates of SLR, the salt marsh is modelled to become more uniform in height, which leads to a decrease in biodiversity. Even though the current model results may overestimate the flattening of the hypsometric curve (section 8.2), still a decrease in biodiversity under accelerated SLR is expected. Including landward migration zones and sustainable land use in coastal management strategies could have a beneficial impact on the survival of salt marshes under accelerated SLR. For the salt marshes on Ameland, a reduction of gas extraction would lead to a decrease in rSLR and significantly increase the chances of salt marsh survival in the coming decades.

The ASMITA model uses a high degree of temporal and spatial aggregation. As a result, detailed processes are not included in the salt marsh extension. The model extension could prove to be very useful to get an expeditious first impression of long-term morphological salt marsh development under accelerated SLR. Nevertheless, the model should not be employed for in-depth analyses of salt marsh development due to its lack of incorporation of detailed processes. The ASMITA salt marsh extension can be used in a complementary manner next to process-based models, such as Delft3D. It should be noted that hindcast data on the hydrodynamics, salt marsh bathymetry and salt marsh development is necessary for the calibration of the ASMITA salt marsh extension and for the derivation of model parameters.

Conclusions & Recommendations

This thesis assessed how salt marshes can be implemented in a long-term morphological model for tidal inlet systems and it analyzed the long-term morphological response of salt marshes and other tidal inlet components to accelerated SLR. The main conclusions and recommendations for further research are summarized in respectively section 9.1 and 9.2.

9.1 Conclusions

The conclusions of this thesis are presented by answering the research questions. First, the sub-questions are elaborated on. Hereafter, the main research question is answered.

The main research question is:

How can long-term salt marsh development be modelled on a temporally and spatially aggregated scale?

The sub-questions are answered below.

1. What are the governing processes for salt marsh development?

The change in salt marsh volume depends on horizontal and vertical processes. The horizontal salt marsh development is characterized by cyclic behaviour. A larger sediment trapping efficiency on the salt marsh compared to the tidal flat leads to an increased salt marsh area: the salt marsh extends onto the tidal flat. The height gradient between the marsh and the flat becomes steeper over time. A cliff starts to form at the marsh's edge. Consequently, the marsh edge experiences more wave attacks. This will eventually degrade the marsh cliff, which will lead to a decrease in the salt marsh area. The cycle then starts over again.

Vertical salt marsh accretion consists of three components: mineral sedimentation, accumulation by plant biomass and autocompaction. The first two terms lead to an increase in salt marsh surface height, whereas the latter causes a decrease in marsh surface height. Mineral sedimentation occurs when water carrying an SSC flows onto the salt marsh. It is the primary contributor to accretion and ranges from the order mm/year to cm/year. Accumulation by plant biomass is especially important at locations with a limited supply of mineral sediment since its contribution to accretion is only in the order mm/year. Autocompaction occurs due to salt marsh aging and can be enhanced by the presence of cattle. Autocompaction is typically in the order of mm/year. However, for salt marshes that contain a large organic component, older and thicker sediment layers, and are subject to grazing, the rate could increase to cm/year.

The vertical salt marsh development highly differentiates based on the distance to the nearest sediment source. For locations close to sediment sources, such as creeks and the adjacent sea, relatively large sedimentation rates are observed. However, further away from these locations, the sedimentation rates are evidently lower.

Salt marsh development is forced by three factors: sediment availability, transport capacity and accommodation space. If the tidal inlet system has a larger demand for sediment than the amount that is supplied, the morphological development will be limited. When the available sediment volume in the tidal inlet is sufficient but the sediment transport capacity of the tidal inlet is too small, the morphological development of the salt marsh would also not be able to reach its full potential. Finally, the accommodation space on the salt marsh can increase as a result of rSLR and decreases due to sedimentation.

2. How can these processes be captured in a temporally and spatially aggregated way to implement them in the ASMITA model?

For the salt marsh implementation in ASMITA, the governing processes for salt marsh development have to be aggregated in space (from 3D into 0D) and time (tidally averaged). Moreover, the existing ASMITA formulations do not allow for a varying surface area. Thus, solely the vertical component of salt marsh development is considered in the model extension of this research. Additionally, the implementation of salt marshes in ASMITA is based on a mineral sediment input only. The accumulation due to plant biomass and the decrease in marsh height due to autocompaction are excluded from the model extension due to their relatively small contribution to salt marsh accretion.

As opposed to the existing ASMITA model, the formulations in the salt marsh extension are not based on the tidally averaged hydrodynamic conditions and the morphological equilibrium condition because not every tidal cycle contributes to the morphological development. Instead, it is imposed that all sediment that flows onto the marsh is captured. Consequently, the local equilibrium concentration on the marsh is equal to zero, since the water column no longer contains any sediment. The remaining model steps are similar to the existing ASMITA model and are based on the aggregated advection-diffusion equation.

The spatial and temporal aggregation of the governing processes for salt marsh development is conducted by deriving the ASMITA parameters, which are needed in the formulations for modelling the vertical change in marsh surface height. The horizontal exchange coefficient δ expresses the water volume exchange with the adjacent boundary or adjacent element in m^3/s . It is derived from ten years of hydrodynamic data and represents the average volume of water exchanged per time unit (for instance the tidal cycle). Together with the SSC, δ can be used to describe the horizontal exchange of sediment. Vertical exchange coefficient w_s represents the vertical exchange of sediment between the water column and the bottom in m/s . The parameter indicates how fast sedimentation occurs. The value can be determined based on field measurements or a literature review. For sediment with a sufficient value for w_s , the formulation of $c_e = 0$ implies that all sediment deposits on the salt marsh. The global equilibrium concentration c_E represents the sediment availability by translating the sediment concentrations at the boundary into a deposited sediment volume. The sediment concentration can also be chosen based on field measurements or a literature review. The amount of rSLR that is introduced in the model represents the change in accommodation space.

3. To what extent can salt marsh development be modelled by ASMITA?

The sedimentation rates computed by the ASMITA model are calibrated against field data. This means that a hindcast of previous salt marsh development can be realized quite accurately by calibrating the model parameters. However, the prediction of future salt marsh development seems to be more complicated. The parameter setting has a large influence on the model outcomes and is deemed vital for predictions of future salt marsh development. The sediment concentration and soil porosity that are included in the c_E boundary condition have the largest influence on the model outcomes (section 7.3). The parameter setting in this research was not based on field measurements, but instead relied on a literature review and calibration. This introduces significant uncertainties for the model outcomes. Mainly the SSC is an important predictor of the ability of salt marsh survival under accelerated SLR. For precise model calibration, field measurements on the SSC close to the boundary between the tidal flat and salt marsh are needed. It can be concluded that ASMITA is capable of modelling the mineral sedimentation on a salt marsh, provided that model calibration is conducted. The modelled sedimentation rates in Chapter 7 demonstrate consistency in magnitude compared to the data analysis that was conducted in Chapter 5. The incorporation of organic accumulation and autocompaction in the ASMITA model poses substantial challenges but is deemed less important due to their smaller contributions to salt marsh accretion. However, especially autocompaction could become more important under accelerating SLR, as it increases non-linearly with increased marsh elevation.

4. How do salt marshes interact with the other components of a tidal inlet system?

The forcing mechanisms for the existing ASMITA elements, the ebb-tidal delta, channels and tidal flats, depend on average conditions. However, salt marshes development occurs under extreme conditions. In this research, the interaction between the salt marsh element and the other tidal inlet components was not reproduced correctly in the 4 elements ASMITA model due to the mismatch between average and extreme forcing conditions. A suggestion for improving the 4 elements model is given in section 9.2.

Instead, the salt marsh was implemented in the existing ASMITA model by means of an outgoing sediment flux in the 3 + 1 elements model. The interaction between the salt marsh and other tidal inlet system components highly depends on the size of the salt marsh compared to the size of the other components. When the salt marsh element size is an order of magnitude smaller than the other system components, the outgoing sediment flux is relatively small and no substantial effect of the salt marsh on the other system components is observed. However, when the salt marsh element is comparable in size, the other elements experience a sediment deficit.

The salt marsh element is modelled to have mud sedimentation only. The sand-mud distribution in the remaining elements is affected by this demand for mud from the salt marsh element. It is hypothesized that the system starts to import a larger amount of mud due to the added salt marsh element: an increased demand causes an increased supply, provided that there is sufficient mud availability. The direct extraction of mud flux from the tidal flats is compensated by an increased amount of sand sedimentation there. For the channels, a larger amount of mud sedimentation occurs for a larger salt marsh element. This is likely due to the increased amount of mud in the entire tidal inlet system.

5. How do salt marshes respond to accelerated SLR?

Based on the chosen parameter configuration, the Oosterkwelder salt marsh is able to grow along with SLR rates smaller than 16 mm/year. However, the profile becomes more uniform in height. The higher parts of a salt marsh become lower relative to MHW, whereas the low marsh areas increase in height and are situated higher relative to MHW after simulations than before simulations. The model simulations may overestimate the uniformity of the salt marsh hypsometry due to the SEB calibration and the lack of a relation between SSC and water level. For SLR scenarios that depict a rate of SLR larger than 16 mm/year, the salt marsh is expected to drown according to the ASMITA model extension. This threshold highly depends on the parameter setting of the sediment concentration and availability, which is based on a literature review and calibration with local accretion data. Hence, significant uncertainties in the model predictions are present.

Considering the above answers to the sub-questions posed in this thesis, the main research question can now be answered:

How can long-term salt marsh development be modelled on a temporally and spatially aggregated scale?

From this thesis, it can be concluded that long-term salt marsh development can be modelled on a temporally and spatially aggregated scale by applying simplifications. The ASMITA salt marsh model that was created is based on a mineral sediment input and considers vertical salt marsh development only. Organic processes, autocompaction and cliff erosion are excluded from the model formulations due to their smaller contribution to salt marsh development compared to mineral sedimentation. The current model extension is able to model mineral sedimentation but depicts a large sensitivity to the parameter setting.

Salt marsh development is modelled by the aggregated advection-diffusion equation and the governing processes are included in the spatially and temporally aggregated model parameters δ , w_s and c_E . For the derivation and calibration of the model parameters, a hindcast dataset on the decadal time scale of hydrodynamics and salt marsh hypsometry & development should be available. For the salt marsh development, preferably full coverage measurements over the entire marsh should be present. If point measurements are used, they should be obtained in the different salt marsh zones to account for the spatial variation over the marsh. Moreover, data on suspended sediment concentrations on the salt marsh and tidal flat - salt marsh boundary is needed for precise model calibration.

The ASMITA salt marsh extension can be employed to obtain an expeditious first impression of long-term morphological salt marsh development. However, due to the lack of incorporation of detailed processes, the model should not be employed for in-depth analyses of salt marsh development. The interaction between the salt marsh element and the remaining tidal inlet system components requires further model improvements.

9.2 Recommendations

The ASMITA model extension of salt marshes presented in this thesis can be improved by further research. This section provides five recommendations for further research on the long-term morphological modelling of salt marshes in ASMITA.

1. Study the correlation between water level and SSC

The ASMITA model extension that was developed in this research includes a constant SSC for any water level. Consequently, the average SSC on the low marsh is most likely overestimated whereas the average SSC on the high marsh is expected to be underestimated. Further elaboration on this was given in Chapter 8. It is recommended to create a formulation that considers the correlation between the water level, or inundation depth, and the SSC. This can be obtained by conducting data analysis on water levels and doing field measurements. Earlier research by for instance Van de Kreeke et al. (1997) and Ridderinkhof et al. (2000) revealed that the varying contributions of different tidal constituents and storms lead to SSC fluctuations. A similar analysis is recommended to be executed for salt marshes. Water level and SSC measurements should be obtained close to the salt marsh edge, where the model boundary condition is implied and frequent inundation occurs, and at the higher salt marsh to gain insight into the SSC during extreme water levels.

2. Improve the implementation of the salt marsh in the existing ASMITA model

Two methods were explored for implementing salt marshes in the existing ASMITA model: the 4 elements model and the 3 + 1 elements model. Establishing effective communication between the salt marsh element and the remaining components of the tidal inlet system posed a significant challenge. Accordingly, the acquired model outcomes exhibit certain deficiencies that demand the need for recommendations to enhance the existing model.

The 4 elements ASMITA model employs the average sediment concentration for calculating the element volume changes. Salt marsh development takes place under extreme scenarios with sediment concentrations that are above average. Hence, the salt marsh sedimentation was structurally lower in the 4 elements model than in the one-element salt marsh model. Similar to the first recommendation, it is recommended to study the relationship between the average SSC that determines the sedimentation for the existing ASMITA elements and the peak SSC that governs salt marsh development. If such a relation between the average and peak SSC exists, it can be implemented in the 4 elements model to enhance the communication between the salt marsh element and the remaining tidal inlet system components. This can possibly be done by deriving a factor that grasps the relation between the sediment concentration during average conditions and the sediment concentration during peak conditions, such as storms.

The 3 + 1 ASMITA model was created to overcome the problem of the average SSC governing salt marsh development in the 4 elements model by separating the salt marsh element from the existing 3 elements model. As such, the peak SSC was used for the marsh development. It was introduced as an outgoing sediment flux in the tidal flat element of the 3 elements model. However, no feedback from the tidal flats towards the salt marsh is implemented in this 3 + 1 model. Thus, it is assumed that the salt marsh element does not experience any limitations in terms of sediment availability. This means that ideal conditions prevail and the salt marsh development is only bound by SLR. As a result, the outgoing sediment flux from the tidal flat to the salt marsh suggests that irrespective of the circumstances, the sediment demand of the salt marsh is more dominant than the tidal flat. It is recommended to conduct further research on the source of the peak SSC that prevails for salt marsh development. If this peak concentration is caused solely by the amount of sediment that is brought into suspension on the tidal flats, it is recommended to incorporate feedback between the 3 elements model and the one-element salt marsh model. When it appears that there exists some relation between the peak SSC and the average SSC, it is advised to implement the recommended improvement for the 4 elements model and to use this for modelling the long-term morphological development of tidal inlet systems. The 3 + 1 model can then be disregarded.

3. Include lateral salt marsh development

It is recommended to further research the inclusion of lateral salt marsh development in the ASMITA model. Lateral salt marsh development could be especially important for assessing salt marsh survival under accelerated SLR. The process could possibly be included by means of a probabilistic method. The model would then consider the height difference between the salt marsh and adjacent tidal flats. A certain probability distribution for the collapse of a cliff should be created, where a larger height difference between marsh and flats corresponds to a higher chance of the occurrence of cliff erosion. The cliff erosion itself can then be implemented in the model by means of an outgoing sediment flux from the salt marsh element towards the tidal flat element and adjustment of the salt marsh volume and hypsometric curve.

4. Perform a more detailed data analysis on salt marsh development

It is recommended to carry out the data analysis for the derivation and calibration of the model parameters in more detail. The difference in data obtained from the AHN and SEBs complicated the derivation and calibration of the model parameters in this thesis. Due to a lack of time, it was not possible to conduct a detailed analysis on the spatial differences between the AHN and SEB data, which is advised to compute a more accurate correction on the hypsometric curves. This is relevant because the derivation of the horizontal exchange coefficient δ directly depends on the salt marsh hypsometry, which in turn determines the amount of sedimentation that occurs on the salt marsh. A uniform hypsometry correction of 20 cm was applied for the Oosterkwelder, despite variations in height differences ranging from 2 to 55 cm between the AHN and SEBs (depending on the measurement location). Hence, the applied hypsometry correction lacks accuracy and may have caused deviating results. Analyzing possible spatial patterns in the height difference between the AHN and SEB measurements could improve the hypsometry correction and subsequently enhance the derivation of δ .

For the calibration of the model parameters, data on sedimentation only should be obtained. The current model extension calibrated sedimentation rates against accretion data, which includes accumulation by plant biomass and autocompaction. However, no formulations for these processes are incorporated in the model. Further research into either including accumulation by plant biomass and autocompaction or obtaining data on salt marsh sedimentation is recommended to improve the model calibration for better predictions of salt marsh development under accelerating SLR.

5. Study the sand-mud distribution of salt marsh sedimentation

Currently, the ASMITA model extension implies that only mud sedimentation occurs on the salt marsh. However, in reality, a certain quantity of sand is expected to be deposited at the salt marsh. Data analysis on the sand-mud distribution on salt marshes could be used as an indication for the applicable sand-mud distribution in the model implementation. When two fractions are included in the salt marsh model, a more realistic prediction of the mud deficiencies can be obtained. The major increase in mud demand that was observed in Chapter 7 is expected to become smaller. Still, it should be noted that the mud sedimentation is expected to be larger than the sand sedimentation for the salt marsh element.

References

- Actueel Hoogtebestand Nederland. (2022). Kwaliteitsbeschrijving: tijdverschil/inwinperiode. <https://www.ahn.nl/kwaliteitsbeschrijving>
- Allen, J. (2000a). Holocene coastal lowlands in nw europe: Autocompaction and the uncertain ground. *Geological Society, London, Special Publications*, 175(1), 239–252.
- Allen, J. (2000b). Morphodynamics of Holocene salt marshes: a review sketch from the Atlantic and Southern North Sea coasts of Europe. *Quaternary Science Reviews*, 19(12), 1155–1231.
- Bakker, J. (2014). *Ecology of salt marshes: 40 years of research in the Wadden Sea*. Waddenacademie.
- Bakker, J., Leeuw, J. d., Dijkema, K., Leendertse, P., Prins, H. T., & Rozema, J. (1993). Salt marshes along the coast of the Netherlands. In *Netherlands-wetlands* (pp. 73–95). Springer.
- Balke, T., Stock, M., Jensen, K., Bouma, T. J., & Kleyer, M. (2016). A global analysis of the seaward salt marsh extent: The importance of tidal range. *Water Resources Research*, 52(5), 3775–3786.
- Barbier, E. B., Hacker, S. D., Kennedy, C., Koch, E. W., Stier, A. C., & Silliman, B. R. (2011). The value of estuarine and coastal ecosystem services. *Ecological monographs*, 81(2), 169–193.
- Bartholdy, J. (2012). Salt marsh sedimentation. In *Principles of tidal sedimentology* (pp. 151–185). Springer.
- Beets, D. J., & van der Spek, A. J. (2000). The Holocene evolution of the barrier and the back-barrier basins of Belgium and the Netherlands as a function of late Weichselian morphology, relative sea-level rise and sediment supply. *Netherlands Journal of Geosciences*, 79(1), 3–16.
- Best, Ü. S., Van der Wegen, M., Dijkstra, J., Willemsen, P., Borsje, B., & Roelvink, D. J. (2018). Do salt marshes survive sea level rise? Modelling wave action, morphodynamics and vegetation dynamics. *Environmental modelling & software*, 109, 152–166.
- Bosboom, J., & Stive, M. (2021). Coastal Dynamics.
- Bouma, T., Van Belzen, J., Balke, T., Van Dalen, J., Klaassen, P., Hartog, A., Callaghan, D., Hu, Z., Stive, M., Temmerman, S., et al. (2016). Short-term mudflat dynamics drive long-term cyclic salt marsh dynamics. *Limnology and oceanography*, 61(6), 2261–2275.
- Buijsman, M. (1997). The impact of gas extraction and sea level rise on the morphology of the Wadden Sea: Extension and application of the model ASMITA.
- Buzzards Bay Coalition. (2016). *Scientists work to solve Westport River's eroding salt marsh mystery*. Retrieved September 28, 2022, from <https://www.savebuzzardsbay.org/news/scientists-work-to-solve-westport-rivers-eroding-salt-marsh-mystery/>
- Chen, Z., Gao, B., & Devereux, B. (2017). State-of-the-art: DTM generation using airborne LIDAR data. *Sensors*, 17(1), 150.
- Christiansen, T., Wiberg, P., & Milligan, T. (2000). Flow and sediment transport on a tidal salt marsh surface. *Estuarine, Coastal and Shelf Science*, 50(3), 315–331.
- Cleveringa, J. (2018). *Slibsedimentatie in de kwelders van de Waddenzee*. Arcadis.
- Coleman, D. J., Schuerch, M., Temmerman, S., Guntenspergen, G., Smith, C. G., & Kirwan, M. L. (2022). Reconciling models and measurements of marsh vulnerability to sea level rise. *Limnology and Oceanography Letters*, 7(2), 140–149.
- Colosimo, I., de Vet, P. L., van Maren, D. S., Reniers, A. J., Winterwerp, J. C., & van Prooijen, B. C. (2020). The impact of wind on flow and sediment transport over intertidal flats. *Journal of Marine Science and Engineering*, 8(11), 910.
- Crooks, S., Schutten, J., Sheern, G. D., Pye, K., & Davy, A. J. (2002). Drainage and elevation as factors in the restoration of salt marsh in britain. *Restoration ecology*, 10(3), 591–602.
- De Groot, A., Oost, A., Veeneklaas, R. M., Lammerts, E. J., van Duin, W., van Wesenbeeck, B., Dijkman, E., & Koppenaal, E. (2015). *Ontwikkeling van eilandstaarten: Geomorfologie, waterhuishouding en vegetatie* (tech. rep.). VBNE, Vereniging van Bos-en Natuurterreineigenaren.
- De Groot, A. (2009). Salt-marsh sediment: Natural gamma-radioactivity and spatial patterns.
- De Groot, A., Veeneklaas, R. M., & Bakker, J. P. (2011). Sand in the salt marsh: Contribution of high-energy conditions to salt-marsh accretion. *Marine Geology*, 282(3-4), 240–254.
- Elias, E. (2006). *Morphodynamics of texel inlet*. IOS Press.

- Elschot, K. (2015). *Effects of vegetation patterns and grazers on tidal marshes*. University of Groningen.
- Elschot, K., De Groot, A., Dijkema, K., Sonneveld, C., van der Wal, J. T., de Vries, P., Brinkman, A., van Duin, W., Molenaar, W., Krol, J., et al. (2017). 4. Ontwikkeling kwelder Ameland-Oost: Evaluatie bodemdalingsonderzoek 1986-2016. In *Monitoring effecten van bodemdaling op oost-ameland* (pp. 185–328).
- Engelund, F., & Hansen, E. (1967). A monograph on sediment transport in alluvial streams. *Technical University of Denmark Ostervoldgade 10, Copenhagen K*.
- Enwright, N. M., Griffith, K. T., & Osland, M. J. (2016). Barriers to and opportunities for landward migration of coastal wetlands with sea-level rise. *Frontiers in Ecology and the Environment*, 14(6), 307–316.
- Eysink, W. (1990). Morphologic response of tidal basins to changes. *Coastal Engineering Proceedings*, (22).
- Eysink, W., & Biegel, E. (1992). Impact of sea level rise on the morphology of the Wadden Sea in the scope of its ecological function (phase 2): Investigations on empirical morphological relations. *H1300*.
- FitzGerald, D. M., Fenster, M. S., Argow, B. A., & Buynevich, I. V. (2008). Coastal impacts due to sea-level rise. *Annual review of earth and planetary sciences*, 36(1), 601–647.
- Friedrichs, C., & Perry, J. (2001). Tidal salt marsh morphodynamics: A synthesis. *Journal of Coastal Research*, 7–37.
- Hartig, E. K., Gornitz, V., Kolker, A., Mushacke, F., & Fallon, D. (2002). Anthropogenic and climate-change impacts on salt marshes of Jamaica Bay, New York City. *Wetlands*, 22(1), 71–89.
- Hijuelos, A., Dijkstra, J., Carruthers, T., Heynert, K., Reed, D., & Van Wesenbeeck, B. (2019). Linking management planning for coastal wetlands to potential future wave attenuation under a range of relative sea-level rise scenarios. *Plos one*, 14(5), e0216695.
- Huisman, Y., van der Spek, A., Lodder, Q., Zijlstra, R., Elias, E., & Wang, Z. B. (2022). Development of intertidal flats in the Dutch Wadden Sea in response to a rising sea level: Spatial differentiation and sensitivity to the rate of sea level rise. *Ocean & Coastal Management*, 216, 105969.
- IPCC. (2023). *Climate change 2023: Synthesis report* (Core Writing Team and Lee, H. and Romero, J., Ed.; Contribution to the Sixth Assessment Report of the Intergovernmental Panel on Climate Change) [(in press)]. IPCC. Geneva, Switzerland.
- Kers, B. (2012). Schiermonnikoog 2011, 3e slenk. <https://www.flickr.com/photos/21933510@N07/7008663189/in/photostream/>
- Kirwan, M. L., & Guntenspergen, G. R. (2012). Feedbacks between inundation, root production, and shoot growth in a rapidly submerging brackish marsh. *Journal of Ecology*, 100(3), 764–770.
- Kirwan, M. L., Guntenspergen, G. R., d'Alpaos, A., Morris, J. T., Mudd, S. M., & Temmerman, S. (2010). Limits on the adaptability of coastal marshes to rising sea level. *Geophysical research letters*, 37(23).
- Kirwan, M. L., Temmerman, S., Skeehan, E. E., Guntenspergen, G. R., & Fagherazzi, S. (2016). Over-estimation of marsh vulnerability to sea level rise. *Nature Climate Change*, 6(3), 253–260.
- Koppel, J. v. d., Wal, D. v. d., Bakker, J. P., & Herman, P. M. (2005). Self-organization and vegetation collapse in salt marsh ecosystems. *The American Naturalist*, 165(1), E1–E12.
- Kragtwijk, N., Zitman, T., Stive, M., & Wang, Z. B. (2004). Morphological response of tidal basins to human interventions. *Coastal engineering*, 51(3), 207–221.
- Kuiters, A., & Wegman, R. (2020). *Veranderingen in morfologie kwelderrand en kwelderdrainage op Oost-Ameland in relatie tot bodemdaling*. Wageningen Environmental Research.
- Lodder, Q., Wang, Z. B., Elias, E., Van der Spek, A., de Looff, H., & Townend, I. (2019). Future response of the Wadden Sea Tidal Basins to relative sea-level rise—An aggregated modelling approach. *Water*, 11(10), 2198.
- Luijendijk, A., Ranasinghe, R., de Schipper, M., Huisman, B., Swinkels, C., Walstra, D., & Stive, M. (2017). The initial morphological response of the Sand Engine: A process-based modelling study. *Coastal engineering*, 119, 1–14.
- Marin-Diaz, B., Govers, L. L., van Der Wal, D., Olf, H., & Bouma, T. J. (2021). How grazing management can maximize erosion resistance of salt marshes. *Journal of applied ecology*, 58(7), 1533–1544.
- Mcleod, E., Chmura, G. L., Bouillon, S., Salm, R., Björk, M., Duarte, C. M., Lovelock, C. E., Schlesinger, W. H., & Silliman, B. R. (2011). A blueprint for blue carbon: Toward an improved understanding

- of the role of vegetated coastal habitats in sequestering co₂. *Frontiers in Ecology and the Environment*, 9(10), 552–560.
- Morris, J. T., Sundareshwar, P., Nietch, C. T., Kjerfve, B., & Cahoon, D. R. (2002). Responses of coastal wetlands to rising sea level. *Ecology*, 83(10), 2869–2877.
- Moskalski, S. M., & Sommerfield, C. K. (2012). Suspended sediment deposition and trapping efficiency in a delaware salt marsh. *Geomorphology*, 139, 195–204.
- Mudd, S., D'Alpaos, A., & Morris, J. (2010). How does vegetation affect sedimentation on tidal marshes? Investigating particle capture and hydrodynamic controls on biologically mediated sedimentation. *Journal of Geophysical Research: Earth Surface*, 115(F3).
- Nederlands Centrum voor Geodesie en Geo-informatica (NCG). (2022). *De Bodemdalingskaart van Nederland*. Retrieved December 12, 2022, from <https://bodemdalingskaart.portal.skygeo.com/portal/bodemdalingskaart/u2/viewers/basic/>
- Nolte, S., Esselink, P., Bakker, J. P., & Smit, C. (2015). Effects of livestock species and stocking density on accretion rates in grazed salt marshes. *Estuarine, Coastal and Shelf Science*, 152, 109–115.
- Oenema, O., & DeLaune, R. D. (1988). Accretion rates in salt marshes in the eastern scheldt, south-west netherlands. *Estuarine, Coastal and Shelf Science*, 26(4), 379–394.
- Olf, H. d., De Leeuw, J., Bakker, J., Platerink, R., & Van Wijnen, H. (1997). Vegetation succession and herbivory in a salt marsh: Changes induced by sea level rise and silt deposition along an elevational gradient. *Journal of Ecology*, 799–814.
- Oost, A., & Cleveringa, J. (2017). *Morfologie Kombergingsgebied Borndiep: KPP 2017 BO03 Waddenzee Kennisontwikkeling morfologie en baggerhoeveelheden*. Deltares.
- Oost, A., Cleveringa, J., & Taal, M. (2020). *Kombergingsrapport Friesche Zeegat - Pinkegat en Zoutkamperlaag*. Deltares.
- Piening, H., van der Veen, W., & van Eijs, R. (2017). *Bodemdeling. Monitoring Efecten van Bodemdaling op Oost-Ameland*, ed. J. de Vlas, 9–25. Retrieved September 24, 2022, from https://waddenzee.nl/fileadmin/content/Bodemdeling/2017/Hoofdstuk_1_Bodemdeling.pdf
- Poirier, E., van Proosdij, D., & Milligan, T. G. (2017). The effect of source suspended sediment concentration on the sediment dynamics of a macrotidal creek and salt marsh. *Continental Shelf Research*, 148, 130–138.
- Pont, D., Day, J. W., Hensel, P., Franquet, E., Torre, F., Rioual, P., Ibàñez, C., & Coulet, E. (2002). Response scenarios for the deltaic plain of the rhone in the face of an acceleration in the rate of sea-level rise with special attention to salicornia-type environments. *Estuaries*, 25(3), 337–358.
- Reed, D., van Wesenbeeck, B., Herman, P. M., & Meselhe, E. (2018). Tidal flat-wetland systems as flood defenses: Understanding biogeomorphic controls. *Estuarine, Coastal and Shelf Science*, 213, 269–282.
- Reef, R., Spencer, T., Möller, I., Lovelock, C. E., Christie, E. K., McIvor, A. L., Evans, B. R., & Tempest, J. A. (2017). The effects of elevated CO₂ and eutrophication on surface elevation gain in a European salt marsh. *Global Change Biology*, 23(2), 881–890.
- Renger, E., & Partenscky, H.-W. (1974). Stability criteria for tidal basins. *Coastal Engineering Proceedings*, (14), 93–93.
- Ridderinkhof, H., van der Ham, R., & van der Lee, W. (2000). Temporal variations in concentration and transport of suspended sediments in a channel–flat system in the ems-dollard estuary. *Continental Shelf Research*, 20(12-13), 1479–1493.
- Rijkswaterstaat. (2016). *Vegetatiezonering kwelders Schiermonnikoog*. <https://maps.rijkswaterstaat.nl/dataregister/srv/dut/catalog.search#/metadata/0bb7f390-7761-41da-b341-828c1bc74b5c> (accessed: 14.09.22)
- Rijkswaterstaat. (2020). *Vegetatiezonering kwelders Ameland*. <https://maps.rijkswaterstaat.nl/dataregister/srv/dut/catalog.search#/metadata/0bb7f390-7761-41da-b341-828c1bc74b5c%7D> (accessed: 14.09.22)
- Rijkswaterstaat. (2022a). *Rijkswaterstaat Waterinfo*. Retrieved September 26, 2022, from <https://waterinfo.rws.nl/#!/kaart/waterhoogte/>
- Rijkswaterstaat. (2022b). *Waterinfo Extra. Vegetatie: Kwelders inwinning- en monitoring*. <https://waterinfo-extra.rws.nl/monitoring/biologie/vegetatie/kwelders/inwinning-monitoring/>

- Rijkswaterstaat Publicatie Platform. (2012). *Toelichting bij de vegetatiekartering Schiermonnikoog 2010 : op basis van false colour-luchtfoto's 1:10.000*. Retrieved April 6, 2022, from <https://open.rws.nl/open-overheid/onderzoeksrapporten/@170356/toelichting-vegetatiekartering/>
- Rijkswaterstaat Publicatie Platform. (2016). *Toelichting bij de vegetatiekartering Ameland 2014 : op basis van false colour-luchtfoto's 1:5:000*. Retrieved April 6, 2022, from <https://open.rws.nl/open-overheid/onderzoeksrapporten/@145941/toelichting-vegetatiekartering-ameland/>
- Saintilan, N., Kovalenko, K. E., Guntenspergen, G., Rogers, K., Lynch, J. C., Cahoon, D. R., Lovelock, C. E., Friess, D. A., Ashe, E., Krauss, K. W., et al. (2022). Constraints on the adjustment of tidal marshes to accelerating sea level rise. *Science*, 377(6605), 523–527.
- Schuerch, M., Spencer, T., Temmerman, S., Kirwan, M. L., Wolff, C., Lincke, D., McOwen, C. J., Pickering, M. D., Reef, R., Vafeidis, A. T., et al. (2018). Future response of global coastal wetlands to sea-level rise. *Nature*, 561(7722), 231–234.
- Slim, P., Wegman, R., Sanders, M., Huiskes, H., & Van Dobben, H. (2011). Monitoring kwelderrand Oerderduinen: onderzoek naar de effecten van bodemdaling door gaswinning op de morfologie en vegetatie van de kuststrook ten zuiden van Het Oerd en de Oerderduinen op Oost-Ameland. In *Monitoring effecten van bodemdaling op ameland-oost* (pp. 125–176). Begeleidingscommissie Monitoring Bodemdaling Ameland.
- Stive, M., & Wang, Z. B. (2003). Morphodynamic modeling of tidal basins and coastal inlets. In *Elsevier oceanography series* (pp. 367–392). Elsevier.
- Stive, M., Wang, Z. B., Ruol, P., & Buijsman, M. (1998). Morphodynamics of a tidal lagoon and adjacent coast. *8th International Biennial Conference on Physics of Estuaries and coastal Seas, The Hague, The Netherlands, 1998*.
- Stolte, W., Vroom, J., Santinelli, G., Veenstra, J., van Oeveren, C., & van Zelst and. Jasper Dijkstra, V. (2022). *Systeemrapportage Abiotiek Wadden, concept 0.61*. Retrieved October 10, 2022, from <https://www.teststysteemrapportage.nl/wadden/index.html>
- Swart, S. (2014). *Kwelders of schorren doorsneden door slenken. Waddenzee met Ameland in het verschieft*. Retrieved September 26, 2022, from <https://www.siebeswart.nl/image/I0000b6.nj0YI78>
- Temmerman, S., Govers, G., Wartel, S., & Meire, P. (2004). Modelling estuarine variations in tidal marsh sedimentation: Response to changing sea level and suspended sediment concentrations. *Marine Geology*, 212(1-4), 1–19.
- Townend, I., Wang, Z. B., Stive, M., & Zhou, Z. (2016a). Development and extension of an aggregated scale model: Part 1—Background to ASMITA. *China Ocean Engineering*, 30(4), 483–504.
- Townend, I., Wang, Z. B., Stive, M., & Zhou, Z. (2016b). Development and extension of an aggregated scale model: Part 2—Extensions to ASMITA. *China Ocean Engineering*, 30(5), 651–670.
- Van de Kreeke, J., Day, C., & Mulder, H. (1997). Tidal variations in suspended sediment concentration in the ems estuary: Origin and resulting sediment flux. *Journal of Sea Research*, 38(1-2), 1–16.
- Van der Lugt, M., Cleveringa, J., & Wang, Z. B. (2020). *Integrale analyse morfologische effecten van bodemdaling door gaswinning Ameland-Oost*. Deltares.
- Van der Wegen, M., & Roelvink, J. (2008). Long-term morphodynamic evolution of a tidal embayment using a two-dimensional, process-based model. *Journal of Geophysical Research: Oceans*, 113(C3).
- Van Dobben, H. F., De Groot, A., & Bakker, J. P. (2022). Salt marsh accretion with and without deep soil subsidence as a proxy for sea-level rise. *Estuaries and coasts*, 1–21.
- Van Maren, D., & Winterwerp, J. (2013). The role of flow asymmetry and mud properties on tidal flat sedimentation. *Continental Shelf Research*, 60, S71–S84.
- Van Natijne, A. (2021). *Geotiles NL: ready-made geodata with a focus on the Netherlands*. Retrieved September 27, 2022, from <https://geotiles.nl/>
- Van Puijenbroek, M., Sonneveld, C., & Elschoot, K. (2022). *Vegetatieverandering op Ameland-Oost: jaarrapportage 2021*.
- Van Puijenbroek, M., & Sonneveld, C. (2021). *Opslibbing en kleilaagdikte op Ameland Oost: Jaarrapportage veldwerk 2020* (tech. rep.). Wageningen Marine Research.
- Van Rijn, L. C., et al. (1993). Principles of sediment transport in rivers. *Estuaries and Coastal Seas. Aqua Publications*.

- Van Weerdenburg, R., Pearson, S., van Prooijen, B., Laan, S., Elias, E., Tonnon, P. K., & Wang, Z. B. (2021). Field measurements and numerical modelling of wind-driven exchange flows in a tidal inlet system in the Dutch Wadden Sea. *Ocean & Coastal Management*, 215, 105941.
- Van Wijnen, H., & Bakker, J. (2001). Long-term surface elevation change in salt marshes: A prediction of marsh response to future sea-level rise. *Estuarine, Coastal and Shelf Science*, 52(3), 381–390.
- Walton Jr, T. L., & Adams, W. D. (1976). Capacity of inlet outer bars to store sand. In *Coastal engineering 1976* (pp. 1919–1937).
- Wang, Y., Yu, Q., Jiao, J., Tonnon, P., Wang, Z. B., & Gao, S. (2016). Coupling bedform roughness and sediment grain-size sorting in modelling of tidal inlet incision. *Marine Geology*, 381, 128–141.
- Wang, Z., Louters, T., & de Vriend, H. J. (1995). Morphodynamic modelling for a tidal inlet in the wadden sea. *Marine geology*, 126(1-4), 289–300.
- Wang, Z. B. (2022). Shore protection of Neerlandsreid salt marsh (Ameland).
- Wang, Z. B., De Vriend, H., Stive, M., Townend, I., Dohmen-Jansen, C., & Hulscher, S. (2008). On the parameter setting of semi-empirical long-term morphological models for estuaries and tidal lagoons.
- Wang, Z. B., Elias, E., Van der Spek, A., & Lodder, Q. (2018). Sediment budget and morphological development of the Dutch Wadden Sea: impact of accelerated sea-level rise and subsidence until 2100. *Netherlands Journal of Geosciences*, 97(3), 183–214.
- Wang, Z. B., & Lodder, Q. (2019). *Sediment exchange between the Wadden Sea and North Sea Coast: Modelling based on ASMITA*. Deltares.
- Wang, Z. B., Townend, I., & Stive, M. (2020). Aggregated morphodynamic modelling of tidal inlets and estuaries. *Water Science and Engineering*, 13(1), 1–13.
- Warren, R., Price, J., Fischlin, A., de la Nava Santos, S., & Midgley, G. (2011). Increasing impacts of climate change upon ecosystems with increasing global mean temperature rise. *Climatic Change*, 106(2), 141–177.
- Zhao, Y., Yu, Q., Wang, D., Wang, Y. P., Wang, Y., & Gao, S. (2017). Rapid formation of marsh-edge cliffs, Jiangsu coast, China. *Marine Geology*, 385, 260–273.

AHN Hypsometric Curves without Correction for rSLR

An overview of the hypsometric curves obtained from the different AHN datasets for Neerlandsreid & De Hon on Ameland and Het Rif & Oosterkwelder on Schiermonnikoog can be observed in respectively Figure A.1a, A.1b, A.2a and A.2b. Typically, a salt marsh is expected to have a positive vertical development, i.e. an increase in height. This means that an older hypsometric curve is situated lower in the profile than a more recent hypsometric curve. In general, this behaviour is apparent in the salt marshes on Schiermonnikoog. However, when a significant rSLR rate is present on a salt marsh, a negative development occurs which corresponds to a decrease in height. Consequently, the hypsometric curve of an older dataset is situated higher in the profile than a recently acquired hypsometric curve. The latter is predominantly the case for the Ameland salt marshes Neerlandsreid and De Hon.

Figure A.1 shows that Neerlandsreid and De Hon have a similar hypsometry shape. For both salt marshes, the highest hypsometric curve corresponds to the oldest dataset: AHN 1. The consecutive datasets AHN 2 and AHN 3 are following the course of negative salt marsh development: a decrease in height is observed. The decrease in height of the Ameland salt marshes can be attributed to a significant rSLR rate due to gas mining, as previously discussed in section 4.3. An outlier is found in the most recent dataset: AHN 4. For salt marsh Neerlandsreid, the hypsometric curve for AHN 4 coincides with the AHN 2 data. The AHN 4 data for De Hon is situated in between the hypsometric curves of AHN 2 and AHN 3. The hypsometric curves were presumed to decrease in height as the data became younger in age. However, AHN 4 does not conform to the expected pattern.

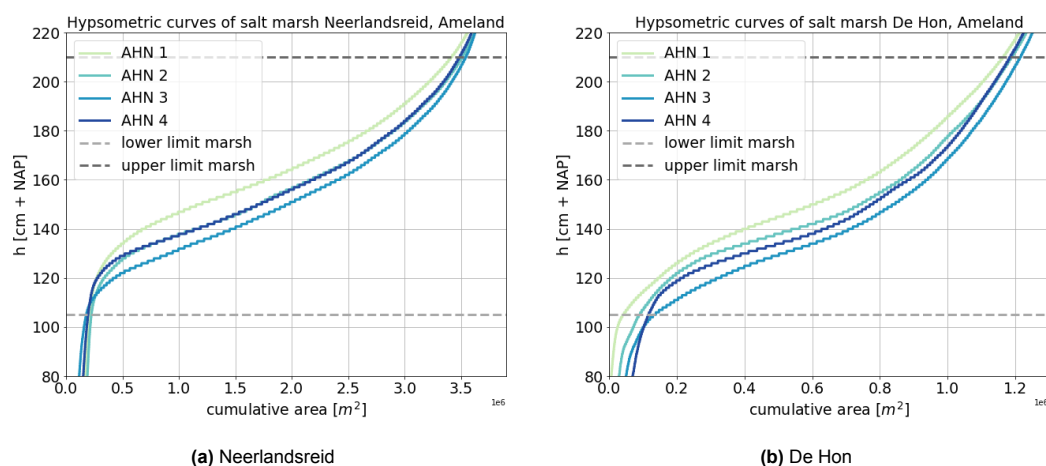


Figure A.1: Hypsometric curves for salt marshes on Ameland over the years.

The salt marshes of Schiermonnikoog are expected to have a positive salt marsh development since no significant rSLR rate is present for this barrier island. This means that the height of the hypsometric curves is expected to increase with increasing age. Figure A.2a shows that this is indeed the observed behaviour for salt marsh Het Rif. The lowest hypsometric curve belongs to AHN 1 data. The hypsometric curves for respectively AHN 2, 3 and 4 increase in consecutive order. For the salt marsh Oosterkwelder, a similar observation is identified for the hypsometric curves corresponding to AHN 1 up to and including AHN 3, see Figure A.2b. This means that the newer data has a higher hypsometric curve, which conforms to the positive salt marsh development. Nevertheless, an unexpected observation is that the hypsometric curve for AHN 4 is situated lower than both AHN 2 and AHN 3. AHN 4 was also an outlier for the Ameland salt marshes.

A major difference in hypsometry shape is observed between the Schiermonnikoog salt marshes. Het Rif has a very flat course on the lower marsh and suddenly a very steep increase. This can be explained by the fact that it is a very young marsh. The higher marsh is not yet developed and therefore only a very small part of the marsh surface area contains levels above 140 cm. For Oosterkwelder, the hypsometry shape is much more gradual. This salt marsh is much older compared to Het Rif. As a result, the marsh has evolved to a more advanced stage leading to a smoother hypsometric curve. Since Oosterkwelder is already quite old, the low marsh only covers a relatively small part.

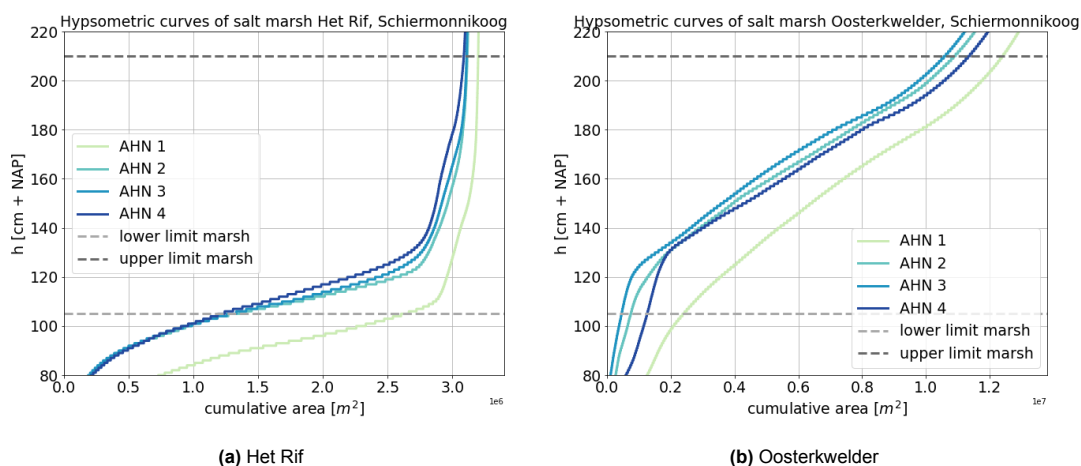


Figure A.2: Hypsometric curves for salt marshes on Schiermonnikoog over the years.

AHN Sampled at Locations of SEBs

The AHN data was sampled at the SEB locations in order to do a comparative analysis between the two datatypes. This appendix gives an overview of the surface heights per AHN dataset at each SEB location. The sampled values for the Ameland salt marshes Neerlandsreid and De Hon are given in Figure B.1. For Schiermonnikoog, there is a distinction between SCH1 and SCH2 samples, which can be observed in respectively Figure B.2 and B.3.

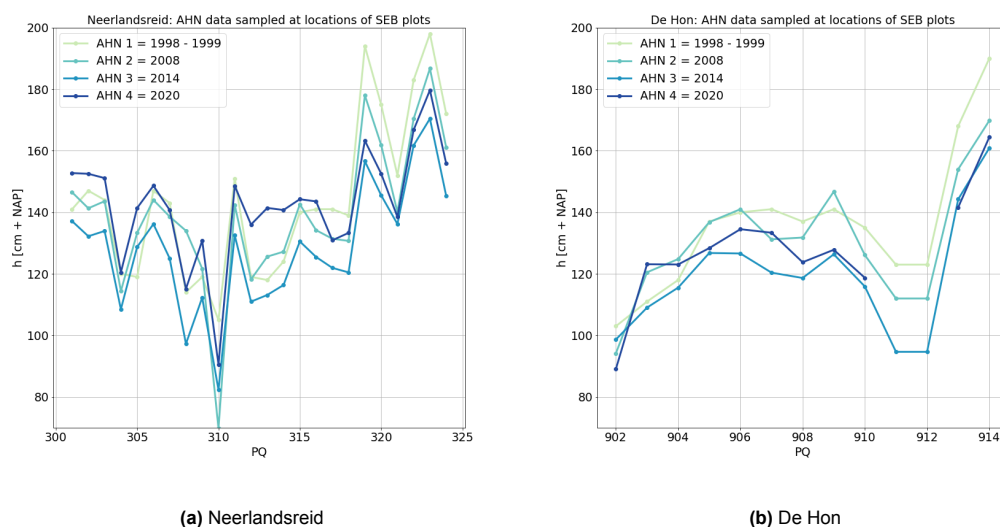
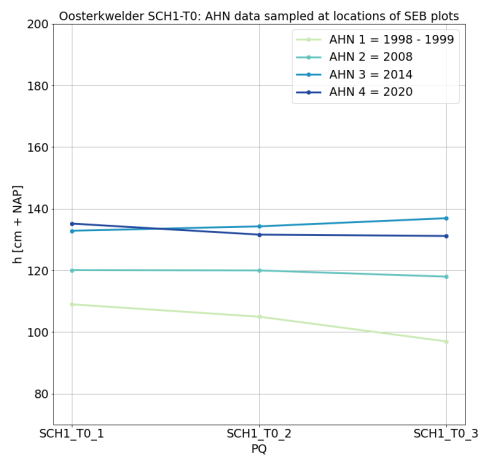
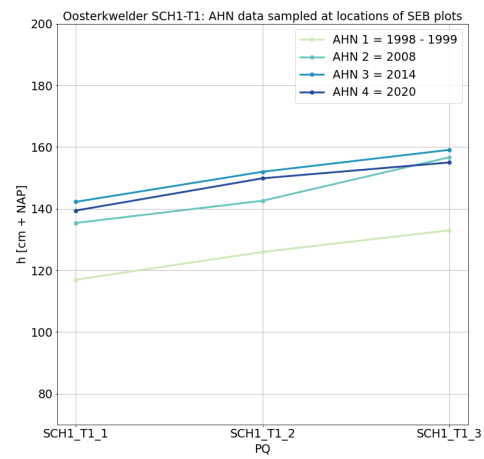


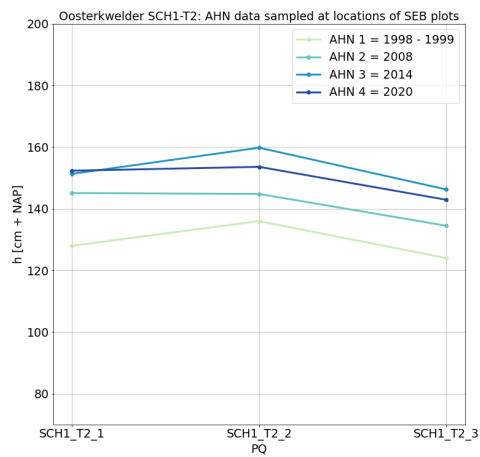
Figure B.1: AHN data sampled at locations of SEBs for the Ameland salt marshes.



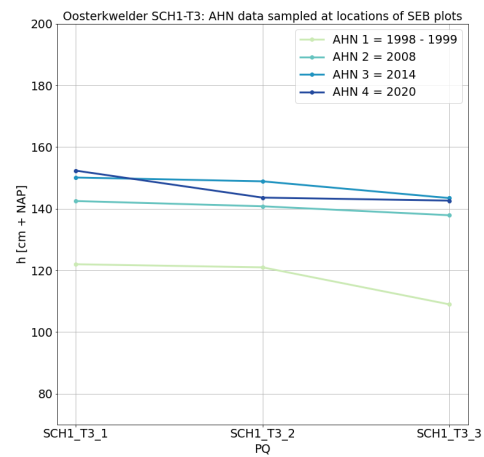
(a) Oosterkwelder: SCH1-T0.



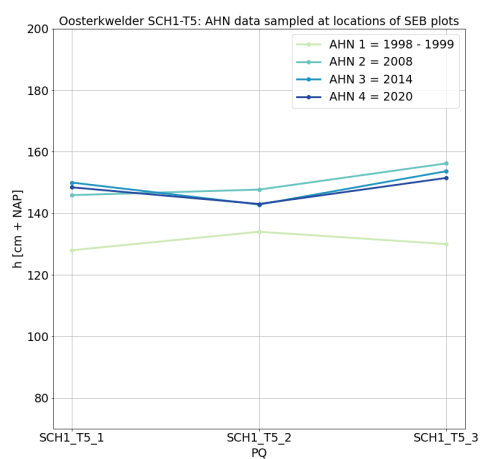
(b) Oosterkwelder: SCH1-T1.



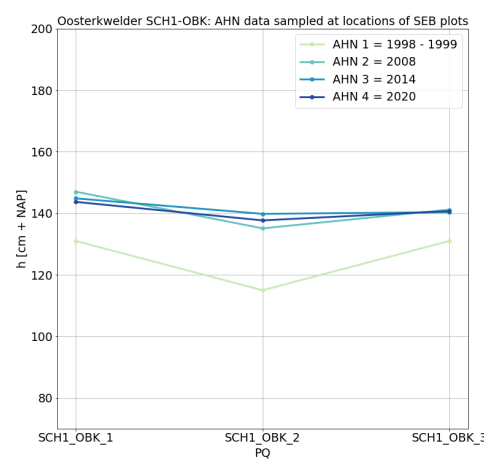
(c) Oosterkwelder: SCH1-T2.



(d) Oosterkwelder: SCH1-T3.

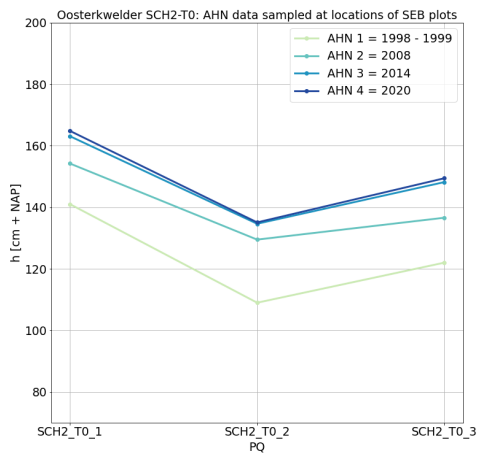


(e) Oosterkwelder: SCH1-T5.

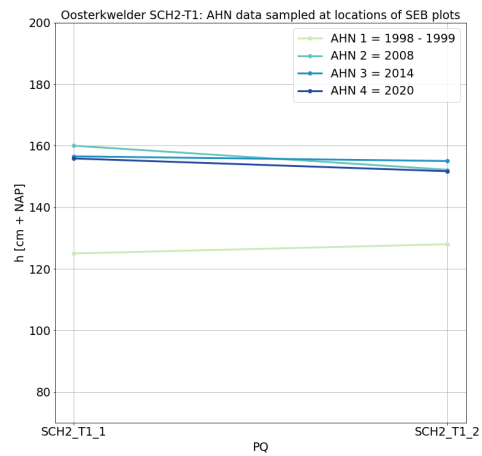


(f) Oosterkwelder: SCH1-OBK.

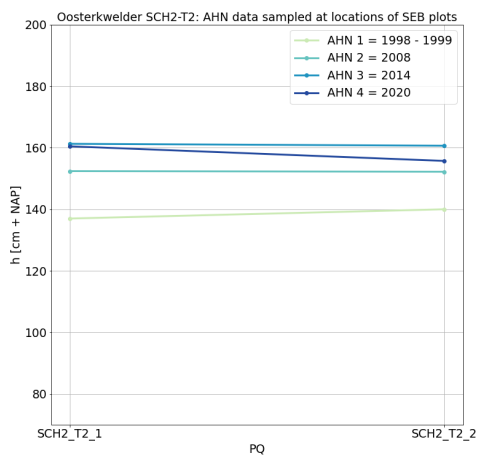
Figure B.2: AHN data sampled at SCH1 locations of the different SEB clusters for the Oosterkwelder, Schiermonnikoog.



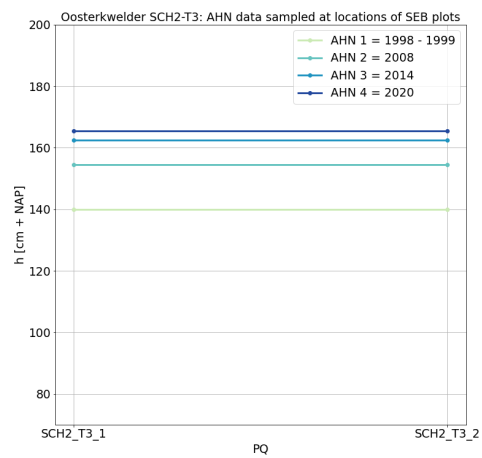
(a) Oosterkwelder: SCH2-T0.



(b) Oosterkwelder: SCH2-T1.



(c) Oosterkwelder: SCH2-T2.



(d) Oosterkwelder: SCH2-T3.

Figure B.3: AHN data sampled at SCH2 locations of the different SEB clusters for the Oosterkwelder, Schiermonnikoog.

One-Element Results for Remaining Salt Marshes

This appendix shows the results when the one-element is applied for the remaining study areas: Neerlandsreid (Ameland), De Hon (Ameland) and Het Rif (Schiermonnikoog).

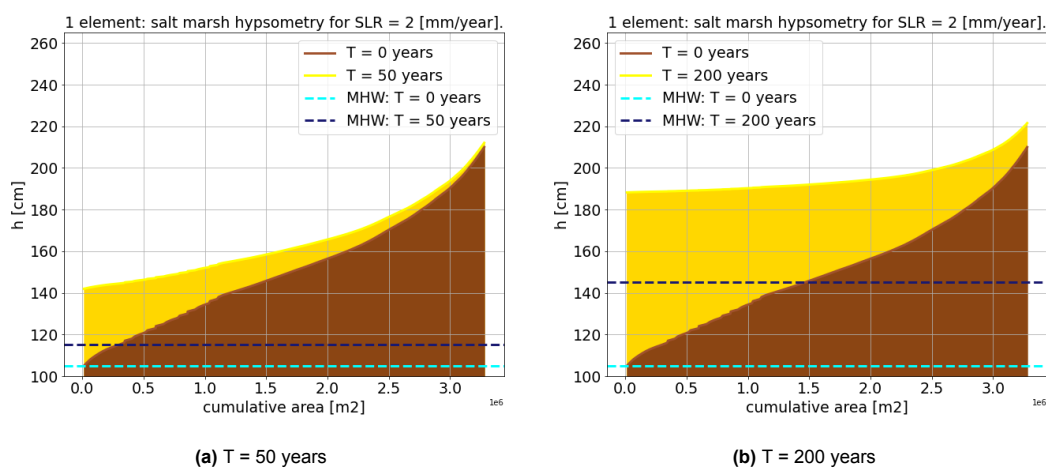


Figure C.1: Hypsometric curve for SLR = 2 mm/year Neerlandsreid, Ameland.

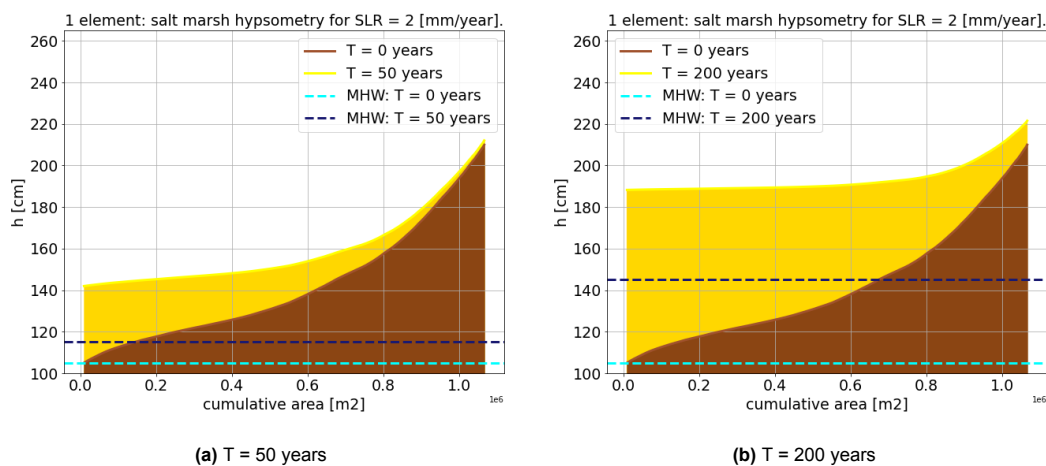
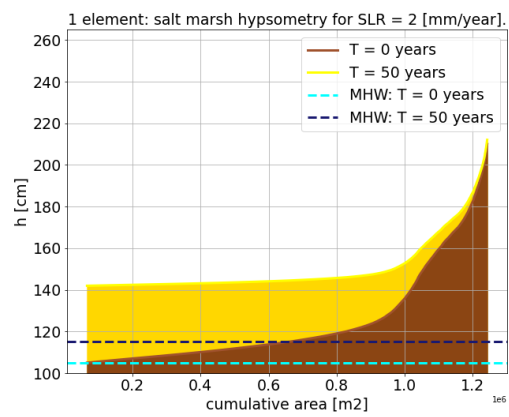
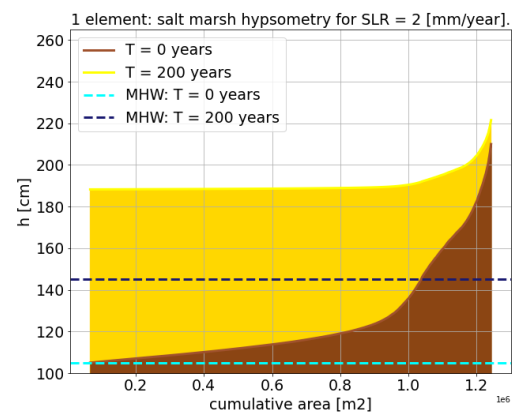


Figure C.2: Hypsometric curve for SLR = 2 mm/year De Hon, Ameland.



(a) T = 50 years



(b) T = 200 years

Four Elements Model: SLR

The 4 elements model results for a SLR scenario of 2 mm/year are depicted in this appendix.

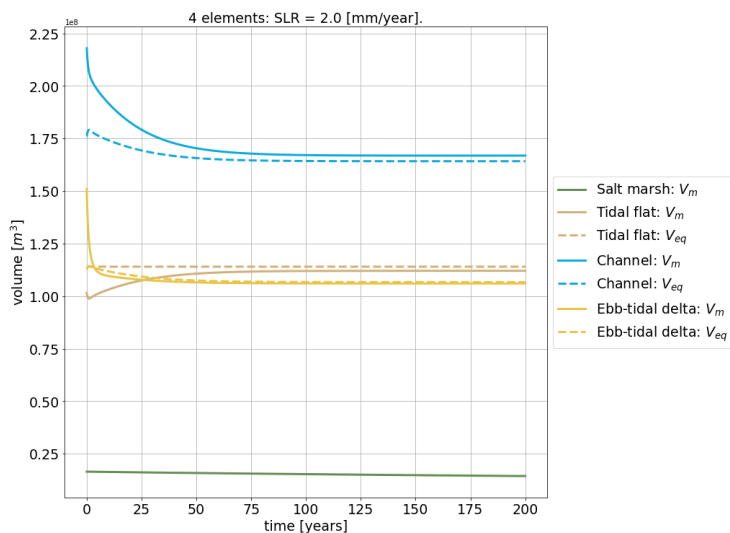
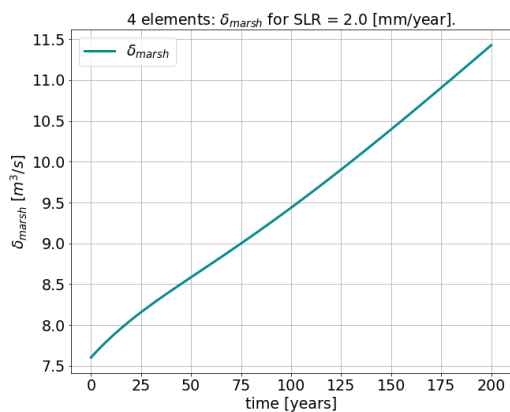
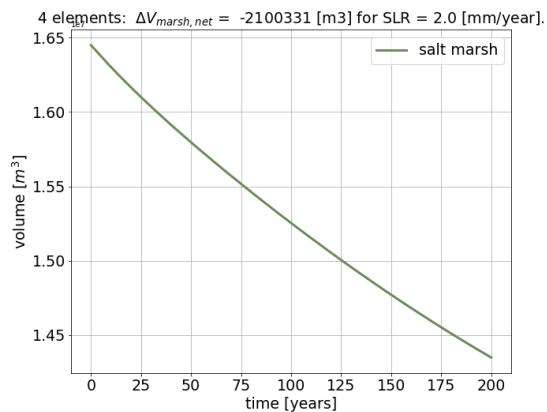


Figure D.1: Volume change for all four elements over time $T = 200$ years & SLR = 2 mm/year, where the ebb-tidal delta, tidal flats & salt marsh are expressed in dry volume and the channels in wet volume.



(a) δ over time.



(b) V_{marsh} over time.

Figure D.2: 4 elements model simulation for $T = 200$ years & SLR = 2 mm/year.

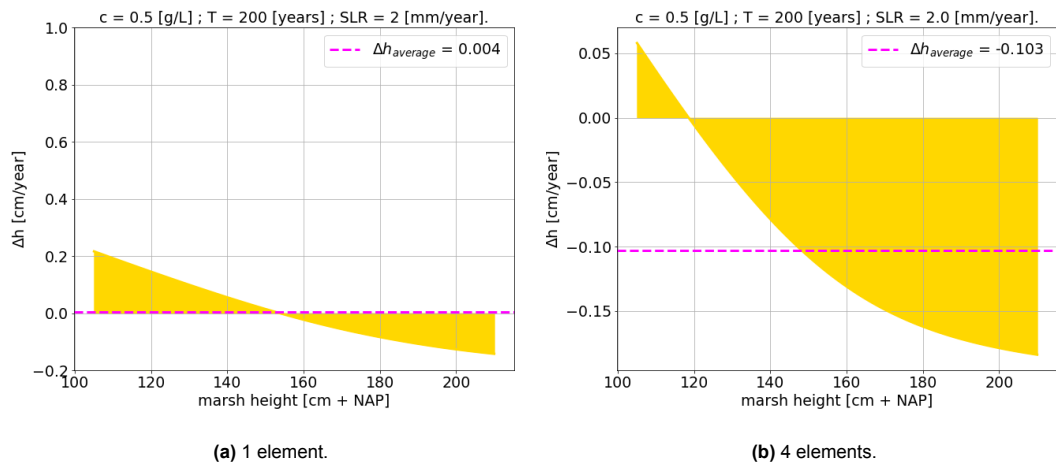


Figure D.3: Modelled salt marsh height change Δh for $SLR = 2$ mm/year and a simulation time of $T = 200$ years.

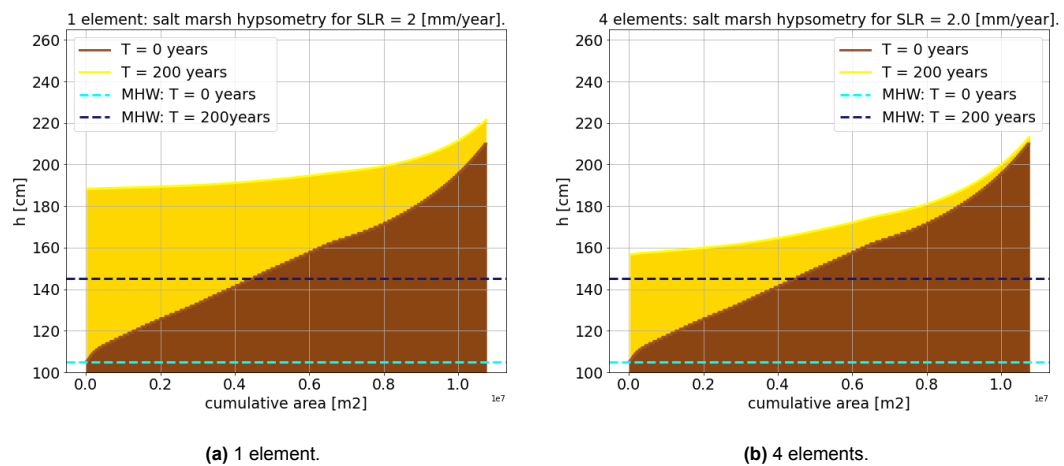


Figure D.4: Salt marsh hypsometry for $SLR = 2$ mm/year and a simulation time of $T = 200$ years.

3 + 1 Model: Element Volumes for SLR

This appendix shows the element volumes during a 3 + 1 ASMITA model simulation of $T = 200$ years for a SLR rate of 2 mm/year, where different sizes of the salt marsh element are introduced.

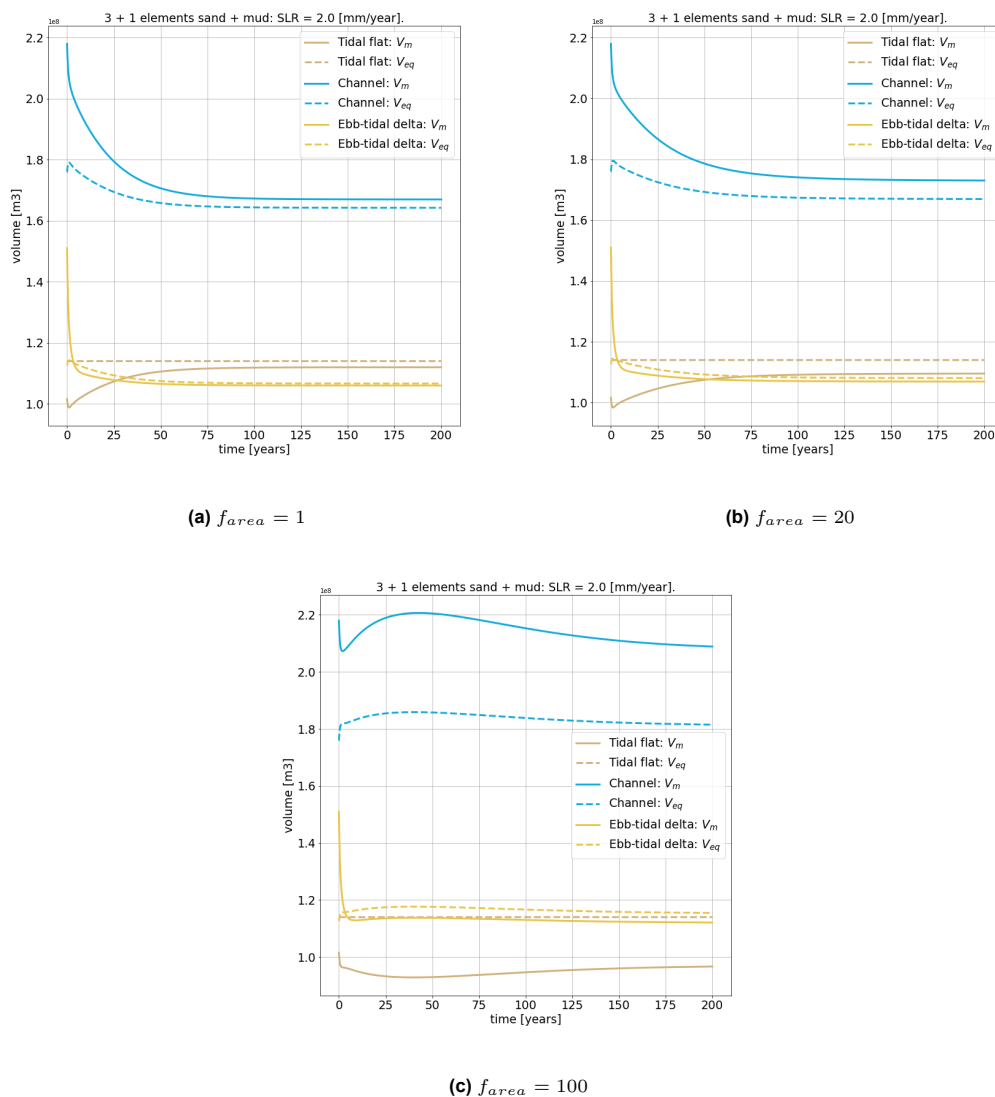


Figure E.1: 3 + 1 elements model simulations for SLR = 2 mm/year & $T = 200$ years for different salt marsh element sizes, where the ebb-tidal delta & tidal flats are expressed in dry volume and the channels in wet volume.